MEDICAL UNIVERSITY
OF VIENNA

Identification of Novel Proteins Required for the DNA Damage Response

Doctoral thesis at the Medical University of Vienna
for obtaining the academic degree

Doctor of Philosophy

Submitted by

MSc, Abdelghani Mazouzi

Supervisor:
PhD, Joanna Loizou
CeMM Research Center for Molecular Medicine
of the Austrian Academy of Sciences
Lazarettgasse 14, AKH BT25.3
1090 Vienna, Austria

Vienna, 02/2017

DECLARATION

This cumulative thesis comprises two chapters of results. The first chapter is published and the second is submitted. The author of this thesis is the first author in the both manuscripts. Moreover, the introduction of this thesis is partially adapted from a review article written by the author (Mazouzi A, Velimezi G, Loizou JI (2014) DNA replication stress: causes, resolution and disease. Exp Cell Res 329: 85-93).

The experimental work of this thesis is mostly performed in the laboratory of Joanna Loizou at the CeMM Research Center for Molecular Medicine of the Austrian Academy of Sciences. Additional experiments were carried out in internal collaboration at CeMM with Mass Spectrometry and Proteomics Laboratory headed by Keiryn L. Bennett, Biomedical Sequencing Facility (BSF) headed by Christoph Bock and Chemical Screening and Platform Austria for Chemical Biology (PLACEBO) directed by Stefan Kubicek. Some experiments were also done externally in collaboration with Sherif F. El-Khamisy laboratory at Krebs Institute, Department of Molecular Biology and Biotechnology, University of Sheffield, Andreas Pichlmair laboratory at Max Planck Institute of Biochemistry and Jürgen Neesen laboratory at the Institute of Medical Genetics, Medical University of Vienna. The author contributions were detailed in the prologue and interlude before each manuscript.

Chapter 2.1 is published in Cell Reports: Mazouzi A, Stukalov A, Muller AC, Chen D, Wiedner M, Prochazkoya J, Chiang SC, Schuster M, Breitwieser FP, Pichlmair A, El-Khamisy S, Bock C, Kralovics R, Colinge J, Bennett K and Loizou JI. (2016). A comprehensive analysis of the dynamic response to aphidicolin-mediated replication stress uncovers targets for ATM and ATMIN. Cell Reports 15: 893-908. (DOI: http://dx.doi.org/10.1016/j.celrep.2016.03.077)

Chapter 2.2 is submitted to Molecular Cell: Mazouzi A, Moser SC, Wiedner M, Lardeau CH, Ringler A, Neesen J, Kubicek S and Loizou JI. UV sensitivity and genomic instability due to defective nucleotide excision repair is alleviated by MUTYH loss. Molecular Cell. submitted.

The review article included in the introduction and chapter 2.1 was published under a Creative Commons License which allows the access of its content.

TABLE OF CONTENTS

LIST OF FIGURES

ABSTRACT

All eukaryotic cells have evolved a network of DNA damage response (DRR) pathways to cope with the deleterious effects of DNA alterations. The DDR signaling is coordinated by the kinases Ataxia Telangiectasia Mutated protein (ATM) and Ataxia Telangiectasia and Rad3 Related protein (ATR). These pathways mediate the repair of the DNA lesions through a compendium of specialized DNA repair pathways. Defects in the DDR machinery (either in the signaling or the repair of DNA damage) may trigger various diseases including cancer, ageing related pathologies, immunodeficiency, developmental defects, growth retardation and neurological disorders. Despite the great progress that has been made in revealing genetic mutations of various diseases associated with DDR, the development of effective therapies has remained a challenge.

In the first chapter of my thesis, we focused on investigating the signaling of replication stress. Although the role of ATM in response to double strand breaks is well investigated, its function in signaling DNA replication stress, via its cofactor ATMIN, is comparatively poorly understood. We therefore combined quantitative mass-spectrometry-based phosphoproteomics with transcriptomics to present the first large-scale investigation depicting the functions of ATM and ATMIN in signaling replication stress. Our data show that replication stress induces time-dependent and widespread changes in the transcriptome and phosphoproteome. Interestingly, these events clustered into early and late responses. Furthermore, we reveal that ATM and ATMIN regulate multiple phosphorylation sites on diverse proteins, many of which have not been involved previously in the DDR. Additionally, we found that ATMIN regulates the phosphorylation of γH2AX, which has well known functions in signaling and engaging DNA repair factors to the sites of DNA lesions. We also identified CRMP2 as a novel replication stress-induced phospho-protein that depends on ATMIN for its function and ensures chromosomal stability and cell survival. Overall, our data present global and comprehensive analyses of replication stress responses and provide a large resource for identifying novel factors involved in this signaling and potentially associated diseases.

In the second chapter of this thesis, we aimed to alleviate the nucleotide excision repair (NER) deficiencies, by searching for synthetic viable interactions via a chemical screen for agents that enhance survival of NER defective cells. We focused on NER because

mutations within this pathway cause several diseases with distinct clinical manifestations, and there are no curative therapies for NER deficient patients. Therefore, we performed a high-throughput drug screen using a library of Food and Drug Administration (FDA) approved compounds to allow for potential drug repurposing. Interestingly, we found that the anti-diabetic drug acetohexamide enhances the ability of NER-defective cells to remove UV-induced DNA damage without the accumulation of chromosomal instability, hence promoting cellular survival. Acetohexamide ensures this protective effect by regulating the stability of the DNA glycosylase, MUTYH, which otherwise leads to toxicity in NER deficient background. This synthetic viable interaction could lead to the development of novel therapies for patients, particularly with inherited diseases caused by defective NER pathway.

Collectively, our data provide a systematic and comprehensive analysis of the replication stress signaling in a time-resolved manner and underline the functions of ATM and ATMIN in this signaling pathway, which may allow the identification of novel players in replication stress signaling and associated diseases. We additionally described CRMP2 as novel replication stress response factor. Furthermore, we identified an FDA-approved drug that could be used to develop novel therapeutic approaches for various diseases associated with NER deficiency.

ZUSAMMENFASSUNG

Zellen lebender Organismen besitzen eine Vielzahl an DNA Überwachungs- und Instandhaltungsmechanismen genannt DNA Schadensreaktion, um verschiedenste Arten von DNA-Schäden zu beseitigen. Diese Signalwege garantieren die erfolgreiche Detektion, Signalweiterleitung und Reparatur der DNA Schäden. Eine wichtige Rolle spielen darin die Kinasen Ataxia Telangiectasia mutated protein (ATM), Ataxia Telangiectasia und Rad3 verwandtes Protein (ATR). Diese Proteine initiieren Signalkaskaden um DNA Schäden mithilfe verschiedenster spezialisierter DNA Reparaturmechanismen zu beseitigen. Defekte in der DNA Schadensreaktion, entweder in der Signalweiterleitung oder in der Reparatur, führen zu Krebs, altersassoziierten Krankheiten, Immundefekten, Entwicklungs- und Wachstumsstörungen und neurologischen Krankheiten. Obwohl schon viele ursächliche genetische Mutationen bekannt sind, bleibt die Entwicklung effektiver Therapien eine Herausforderung.

Das erste Kapitel meiner Doktorarbeit befasst sich mit der Erforschung der Replikationsstressantwort. Der ATM Aktivierungsmechanismus nach einem DNA Doppelstrangbruch ist gut erforscht, dessen Rolle in der Replikationsstressantwort und die Rolle seines Cofaktors ATMIN ist jedoch noch unklar. Wir kombinierten Massenspektrometer-basierte Phosphoproteomics mit Transcriptomics um in einer großangelegten Untersuchung, die Rolle von ATM und ATMIN in der Replikationsstressantwort zu definieren. Unsere Resultate zeigen, dass Replikationsstress die Phosphorylierung von Proteinen und die Genexpression in der Zelle zeitabhängig verändert. Die beobachteten Änderungen lassen sich in frühe und späte Replikationsstressantwort unterteilen. Wir konnten zeigen, dass ATM und ATMIN viele Phosphorylierungen regulieren, deren Rolle in der DNA Schadensreaktion bisher unbekannt war. Darüber hinaus, fanden wir, dass ATMIN die Phosphorylierung von γH2AX beeinflusst, welches eine wichtige Rolle in der Signalweiterleitung und der Rekrutierung anderer DNA Reperaturproteine zu geschädigter DNA besitzt. Weiters fanden wir, dass CRMP2, ein in Alzheimer involviertes Protein, infolge von Replikationsstress phosphoryliert wird und es ATMIN zum Überleben der Zelle benötigt.

Unsere Ergebnisse präsentieren eine globale und umfassende Analyse von Zellantworten auf Replikationsstress und bieten eine große Ressource um neue, in

diese Prozesse involvierte Faktoren und potentielle assoziierte Krankheiten, zu erforschen.

Im zweiten Kapitel meiner Doktorarbeit setzten wir uns zum Ziel NER-Defizite zu kompensieren und mithilfe eines Screening-Verfahrens Chemikalien zu identifizieren, die das Überleben von NER-defizienten Zellen verbessern. Wir spezialisierten uns dabei auf NER, da Mutationen dieses Signalweges zu Krankheiten mit verschiedensten Symptomen führen, und es im Moment keine effektiven Therapien für diese Krankheiten gibt. Wir führten ein Hochdurchsatz-Screening mit einer Sammlung an Chemikalien durch, die von der US-amerikanischen Food and Drug Administration (FDA) zugelassen sind. Hier fanden wir, dass das Antidiabetikum Acetohexamid NER-defizienten Zellen hilft UV-induzierte DNA Schäden zu reparieren ohne dabei chromosomale Instabilität zu verursachen und somit die Zellviabilität verlängert. Acetohexamid verbessert die DNA Reparatur indem es die Stabilität der DNA-Glycosylase MUTYH reguliert, welche ansonsten in Kombination mit defekter NER toxisch wirkt. Diese Interaktion bietet Potential für die Entwicklung neuer Therapien für Patienten mit angeborenen NER-Defekten.

Alles in allem, untersuchten wir systematisch die Zellantwort von Replikationsstress und definierten die Rolle von ATM und ATMIN in diesem Prozess. Darüber hinaus zeigten wir, dass CRMP2 ein in die Replikationsstressantwort involvierter Faktor ist. Außerdem fanden wir ein von der FDA zugelassenes Medikament, das Potential für neue Therapien von Krankheiten bietet, denen DNA Reparaturdefekte zugrunde liegen.

PUBLICATIONS ARISING FROM THIS THESIS

1. **Mazouzi A**, Stukalov A, Muller AC, Chen D, Wiedner M, Prochazkoya J, Chiang SC, Schuster M, Breitwieser FP, Pichlmair A, El-Khamisy S, Bock C, Kralovics R, Colinge J, Bennett K and Loizou JI. (2016). A comprehensive analysis of the dynamic response to aphidicolin-mediated replication stress uncovers targets for ATM and ATMIN. Cell Reports 15:893-908.

2. **Mazouzi A**, Moser SC, Wiedner M, Lardeau CH, Ringler A, Neesen J, Kubicek S and Loizou JI. UV sensitivity and genomic instability due to defective nucleotide excision repair is alleviated by MUTYH loss. Molecular Cell. submitted.

3. **Mazouzi A**, Velimezi G, Loizou JI (2014) DNA replication stress: causes, resolution and disease. Exp Cell Res 329: 85-93.

ABBREVIATIONS

9-1-1	Rad9-Hus1-Rad1
6-4PPs	6-4 pyrimidine-pyrimidone photoproducts
AICDA	Activation-Induced Cytidine Deaminase
AOA1	Apraxia Oculomotor Ataxia 1
AP sites	Apurinic/Apyrimidinic sites
APE1	AP endonuclease 1
APH	Aphidicolin
APTX	Aprataxin
ASCIZ	ASCIZ, ATM/ATR-substrate CHK2-interacting zinc finger protein
ATM	Ataxia Telangiectasia Mutated protein
ATMIN	ATM interactor
ATR	Ataxia Telangiectasia And Rad3-Related Protein;
ATRIP	ATR Interacting Protein
ATRX	Alpha Thalassemia/Mental Retardation Syndrome X-Linked
BARD1	BRCA1 Associated RING Domain 1
BER	Base Excision Repair
BLM	Bloom Syndrome Protein
Bp	Base pair
BRCA1	Breast Cancer 1
BRCA2	Breast Cancer 2
c-Myc	Avian Myelocytomatosis Viral Oncogene Homolog
CAK	CDK-activating kinase
CCR5	C-C Motif Chemokine Receptor 5
cdc25A	Cell Division Cycle 25A
Cdc45	Cell Division Cycle 45
Cdc6	Cell Division Cycle 6
Cdc7	Cell Division Cycle 7
CDKs	Cyclin Dependent Kinases
Cdt1	Cell Division Cycle 10-Dependent Transcript 1
CETN2	Centrin 2
CFSs	Common Fragile Sites
CHK1	Checkpoint Kinase 1
CIN	Chromosomal Instability
CMG	Cdc45.Mcm2-7.GINS
COFS	Like Cerebro-Oculo-Facioskeletal Syndrome
CPDs	Cyclobutane-Pyrimidine Dimers
CRL	Cullin 4A (CUL4A)-Regulator Of Cullins 1 (ROC1) E3 Ubiquitin Ligase
CS	Cockayne Syndrome
CSA	Cockayne Syndrome A
CSB	Cockayne Syndrome B
CSN	Signalosome
CTIP	CTBP-Interacting Protein
DDB1	DNA damage-binding protein 1
DDB2	DNA damage-binding protein 2
DDKs	Dbf Dependent Kinases
DDR	DNA Damage Response
DMD	Dystrophin
dRP	Deoxyribose Phosphate
DSBs	DNA double-strand breaks

E2F1	E2F Transcription Factor 1
EME1	Essential Meiotic Structure-Specific Endonuclease 1
ERCC1	Excision Repair Cross-Complementing 1
ERCC2	Excision Repair Cross-Complementing 2
ERCC3	Excision Repair Cross-Complementing 3
ERCC4	Excision Repair Cross-Complementing 4
ERCC5	Excision Repair Cross-Complementing 5
ERCC6	Excision Repair Cross-Complementing 6
ERCC8	Excision Repair Cross-Complementing 8
ERFSs	Early-Replicating Fragile Sites
EXO1	Exonuclease 1
FA	Fanconi Anaemia
FAAP24	Fanconi Anemia Core Complex Associated Protein 24
FAN1	Fanconi-Associated Nuclease 1
FANCD2	Fanconi Anemia Complementation Group D2
FANCI	Fanconi Anemia Complementation Group I
FANCL	Fanconi Anemia Complementation Group L
FANCM	Fanconi Anemia Complementation Group M
FEN-1	Flap Endonuclease-1
FRA16D	Fragile Site, Aphidicolin Type, Common, Fra(16)(Q23.2)
FRA3B	Fragile Site, Aphidicolin Type, Common, Fra(3)(P14.2)
FRA6E	Fragile Site, Aphidicolin Type, Common, Fra(6)(Q26)
GG-NER	Global Genome Repair Pathway
HGPS	Hutchinson-Gilford Progeria Syndrome
HIV-1	Human Immunodeficiency Virus 1
HR	Homologous Recombination
HRAS	Harvey Rat Sarcoma Viral Oncogene Homolog
ICLs	DNA Interstrand Crosslinks
IDLs	Insertion–Deletion Loops
IR	Ionizing Radiation
LIGI	DNA Ligase I
LIGIII	DNA Ligase III
LIG4	DNA Ligase 4
Mcm 2-7	Minichromosome Maintenance 2-7
MHF1	FANCM Associated Histone Fold Protein 1
MHF2	FANCM Associated Histone Fold Protein 2
MLH1	MutL Homolog 1
MMEJ	Microhomology Mediated End Joining
MMR	Mismatch Repair
MRN	MRE11-RAD50-NBS1
MSH2	MutS Homolog 2
MSH3	MutS Homolog 3
MSH6	MutS Homolog 6
MUS81	MMS And UV-Sensitive Protein 81
NAT10	N-Acetyltransferase 10
NER	Nucleotide Excision Repair
NHEJ	Non-Homologous End Joining
OGG1	8-Oxoguanine DNA Glycosylase
ORC1–6	Recognition Complex 1-6
PARP1	Poly(ADP-Ribose) Polymerase 1
PCNA	Proliferating Cell Nuclear Antigen
PCNT	Pericentrin
PIKK	phosphoinositide 3-kinase (PI3K)-related protein
PMS2	Postmeiotic Segregation Increased (S. Cerevisiae) 2

PNKP	Polynucleotide Kinase Phosphatase
Pol	Polymerase
pol β	Polymerase β
pre-RC	Pre-Replicative Complex
PTIP	PAX Transactivation Activation Domain-Interacting Protein
RAD23B	UV excision repair protein RAD23 homolog B
RFC	Replication Factor C
RNaseH	Ribonuclease H
RPA	Replication protein A
SIOD	Schimke Immune-Osseous Dysplasia
SMARCAL1	SWI/SNF Related, Matrix Associated Subfamily A Like 1
ssDNA	Single-Stranded DNA
T53BP1	Tumor Suppressor P53-Binding Protein 1
TC-NER	Transcription coupled repair pathway
TFIIH	Transcription factor II Human
TopBP1	DNA Topoisomerase 2-Binding Protein 1
TTD	Trichothiodystrophy
UBE2T	Ubiquitin-Conjugating Enzyme E2 T
UHRF1	Ubiquitin-Like With PHD And RING Finger Domains 1
UNG	Uracil DNA Glycosylase
USP7	Ubiquitin-Specific-Processing Protease 7
UV	Ultraviolet Irradiation
UV-DDB	Ultraviolet Radiation-DNA Damage-Binding Protein Complex
UVSSA	UV-Sensitive Syndrome A
WRN	Werner Syndrome Recq Like Helicase
XP	Xeroderma Pigmentosum
XPA	Xeroderma Pigmentosum, Complementation Group A
XPB	Xeroderma Pigmentosum, Complementation Group B
XPC	Xeroderma Pigmentosum, Complementation Group C
XPCS	Xeroderma Pigmentosum And Cockayne Syndrome
XPD	Xeroderma Pigmentosum, Complementation Group D
XPF	Xeroderma Pigmentosum, Complementation Group F
XPG	Xeroderma Pigmentosum, Complementation Group G
XPV	Xeroderma Pigmentosum Variant Type Protein
XRCC1	X-Ray Cross-Complementing Protein 1

ACKNOWLEDGEMENTS

It was a really great pleasure and honor for me to be part of the CeMM family! It has been a wonderful and unique experience personally as well as professionally. Therefore, I would like to show my highest appreciation and it was a great privilege to work and interact with a lot of smart and talented people, that inspired me over the course of my PhD. The time that I spent at CeMM was a fabulous journey that forged and enriched my scientific personality.

First of all, I would like to thank my supervisor Joanna Loizou for giving me the opportunity to do my PhD in her laboratory and always being supportive and enriching me with her fruitful advice. My gratitude goes as well to the members of the Joanna Loizou Laboratory for their great support, continuous feedback and input in particular Michel who was the big brother, always there whenever I needed help or support. Many thanks as well to the other members: Georgia, Marc, Martin, Jana, Lydia, Joana, Luisa, Peter and special thanks and gratitude to Sarah for her great help.

I would also like to express my gratitude to my PhD committee members Jiri Lukas, Sebastian Nijman and Dea Slade for their precious advice, fruitful discussion, supportive ideas, constructive feedback and encouragements that have been absolutely invaluable during my PhD.

Next, I want to thank the members of the Sebastian Nijman laboratory specially Markus, Ferran, Bianca and Barbara for their kindness, support and sharing enjoyable moments together.

I would like to express my deepest appreciation for Alexey Stukalov, André Müller and Doris Chen for their assistance and support during my PhD. I want also to thank all my friends in particular Chris, Bojan and Lindsay.

Finally, I would like to show my deepest gratitude and my special thanks to my mother who supported me all the time, believed in me and gave me all what she could to make me the man who I am today. Many thanks also to my siblings and to my girlfriend who entered my life and made it happier and more interesting.

1. CHAPTER ONE: INTRODUCTION

1.1. DNA repair pathways

The maintenance of our genetic material is an essential process for all living organisms to ensure its accurate transfer to daughter cells. Our genome receives dozens of thousands of DNA lesions every day by endogenous sources like reactive oxygen species (ROS) or by errors during DNA replication. Additionally, several other exogenous sources such as ultraviolet irradiation (UV), tobacco smoke and ionizing radiation (IR) can also generate DNA alterations. These different sources can cause a wide range of DNA lesions including single- and double-stranded DNA breaks, AP (apurinic/apyrimidinic) sites, cyclic nucleotides, intra- and interstrand cross-links and more than 80 different altered DNA bases and as well as alterations to the sugar backbone. If the DNA damage persists or is incorrectly repaired this may cause mutations or DNA aberrations that could threaten the viability of the cell or organism. Therefore, to counteract these threats, cells have evolved several sophisticated mechanisms, that ensure the efficient repair of DNA lesions and preserving the genomic stability. There are multiple specialized DNA repair systems which deal with various types of DNA alterations. In this chapter, we discuss base excision repair (BER) and nucleotide excision repair (NER) in more detail and we review briefly the other DNA repair mechanisms including mismatch repair (MMR), double strand break repair (homologous recombination; HR and non-homologous end-joining: NHEJ) and Fanconi anemia (FA).

1.1.1. Base excision repair (BER)

BER is a very dynamic excision repair pathway responsible for repairing most of the small non-bulky lesions, which do not significantly change the double helix structure such as oxidized bases, apurinic/apyrimidinic sites (AP sites) and DNA single-strand breaks. The first step of BER consists of the recognition of the DNA lesion by 11 known specific DNA glycosylases that use “base-flipping” to excise the damaged base (Jacobs & Schar, 2012). Although many kinds of base lesions are known, only a few DNA glycosylases have been discovered so far. Some of them are characterized by wide substrate specificity, while others are exquisitely specific. There are two classes of DNA glycosylases: monofunctional, having only the DNA glycosylase activity or

bifunctional, possessing the DNA strand excision activities in addition to the ability to remove the damaged base (Demple, Herman et al., 1991). Monofunctional DNA glycosylases usually cleave the N-glycosylic bond between DNA base and the sugar backbone (deoxyribose phosphate), giving rise to an AP site, which is recognized by AP endonuclease 1 (APE1), generating a hydroxyl residue at the 3' end and a 5' deoxyribose phosphate (dRP) terminus (Robson & Hickson, 1991). In the case of bifunctional DNA glycosylases the damaged base is first removed and the DNA backbone is additionally incised generating either 3'α, β unsaturated aldehyde and 5' phosphate residue, through a process called β-elimination, or 3' phosphate and 5' phosphate named β, δ-elimination. The known DNA glycosylases that perform β-elimination are 8-oxoguanine DNA glycosylase (OGG1) and the endonuclease III homologue (NTH1), these enzymes incise the α, β unsaturated aldehyde to create hydroxyl residue at the 3'end . However, in the case of β, δ-elimination the 3' phosphate created by endonuclease VII like proteins 1 to 3 (NEIL1 to -3) is removed by the polynucleotide kinase phosphatase (PNKP) (Wiederhold, Leppard et al., 2004). The DNA glycosylases and APE1 or PNKP activities aim ultimately to create single nucleotide gap consisting of a 3'hydroxyl end which serves as a substrate for a DNA polymerase (Matsumoto & Kim, 1995, Sobol, Horton et al., 1996). In BER, the main DNA polymerase involved in filling the gap is DNA polymerase β (pol β), which removes the 5'dRP through its lyase activity and incorporates the correct undamaged nucleotide, and finally DNA ligase IIIα (Lig III) and X-ray cross-complementing protein 1 (XRCC1) seal the nick in the DNA, restoring the intact sugar-phosphate backbone (Cappelli, Taylor et al., 1997, Nash, Caldecott et al., 1997). This process of BER where one nucleotide is repaired represents 80 % of all the events and it is commonly known as short-patch BER (Dianov, Price et al., 1992). In certain cases, where the 5'dRP for instance is resistant to removal by pol β, the replicative DNA polymerases pol δ/ε take over from pol β and add a flap of 2-12 nucleotides generating a 5' DNA flap structure, which is removed by flap endonuclease-1 (FEN-1), allowing the final ligation by the DNA ligase I (LIGI) and completing the long patch BER pathway (Frosina, Fortini et al., 1996, Podlutsky, Dianova et al., 2001).

1.1.2. Nucleotide excision repair (NER)

Nucleotide excision repair (NER) is a very versatile and flexible pathway because it has the capacity to cope with structurally distinct DNA lesions. This pathway repairs ultraviolet (UV) radiation-induced lesions that are commonly in the form of cyclobutane-pyrimidine dimers (CPDs) but also 6-4 pyrimidine-pyrimidone photoproducts (6-4PPs), as well as other lesions like intrastrand crosslinks and several other bulky adducts such as cyclopurines (Marteijn, Lans et al., 2014). CPDs and 6-4PPs are very toxic lesions if they are left unrepaired and represent roughly 75% and 25% of genomic UV lesions respectively (Mitchell, Adair et al., 1989). These lesions block transcription via RNA polymerase II (RNAPII) and can also promote activity of error-prone translesion polymerases in S phase (Friedberg, 2001), which is highly mutagenic and triggers skin carcinogenesis (Hoeijmakers, 2009). There are approximately 30 proteins involved in the NER pathway, that cooperate together to ensure the appropriate and precise repair of the DNA lesion through four main basic steps: damage recognition, excision of the damaged DNA strand, DNA synthesis and DNA ligation. NER is comprised of two major sub-pathways, based on the recognition and the location of the damage in the genome: global genome repair (GG-NER) that deals with DNA damage through the genome comprising repressed non-coding regions and non-transcribed strands of active genes and transcription coupled repair (TC-NER) that acts on transcribed strands of active genes and engages RNA polymerase II in the recognition of the DNA damage (Fousteri & Mullenders, 2008).

Global genome repair pathway (GG-NER)

As with many other DNA repair pathways, GG-NER is initiated by DNA damage detection and recognition. The former consists of scanning the whole genome for helix distortions and changes in the conformation and the structure of the nucleotides. The major DNA lesion detector in GG-NER is a complex that consists mainly of XPC, UV-excision repair protein RAD23 homolog B (RAD23B) and centrin 2 (CETN2). XPC is known to recognize a variety of DNA structures *in vitro* that cause DNA helix distortion and even nucleotide mismatches that are reported to be repaired by mismatch repair *in vivo* (Sugasawa, Okamoto et al., 2001). Therefore, the recognition of DNA lesions in GG-NER was suggested to require two steps: first the binding of XPC to the single-stranded DNA (ssDNA) gap that is created by the lesion, followed by the lesion

verification step **(Figure 1)** (Marteijn et al., 2014). Even though XPC is the major protein in detecting UV lesions in GG-NER, CPDs are hardly recognized by XPC due to its mild thermodynamic duplex destabilization of the double helix (Jing, Kao et al., 1998). To deal with this type of lesions, recently, XPC was shown to be recruited to chromatin via the ultraviolet radiation-DNA damage-binding protein complex (UV-DDB-associated E3) (Nishi, Alekseev et al., 2009) **(Figure 1)**. This complex consists of DDB1 (DNA damage-binding protein 1), DDB2 (DNA damage-binding protein 2) and CRL complex (Cullin-RING ubiquitin ligase). Under UV irradiation, UV-DDB-associated E3 complex is activated by interaction with NEDD8 leading to its recruitment to the damaged chromatin. UV-DDB-associated E3 complex then targets XPC, DDB2 and cullin 4A for polyubiquitylation, resulting in increase of XPC affinity to DNA lesions and proteolytic degradation of DDB2 causing the loss of UV-DDB complex binding activity and the displacement of UV-DDB by XPC on the damage site (Scrima, Konickova et al., 2008, Sugasawa, Okuda et al., 2005). After the damage is recognized by XPC, this used as a substrate for the transcription initiation factor IIH (TFIIH), which is composed of ten protein subunits, including two helicases XPB and XPD. XPB with its ATPase activity plays crucial role in recruiting TFIIH to the site of the damage (Coin, Oksenych et al., 2007). However, XPD helicase is mostly involved in damage verification through its FeS cluster domains, which structurally has an internal channel allowing the passage of undamaged ssDNA but not the damaged one (Fan, Fuss et al., 2008, Liu, Rudolf et al., 2008, Marteijn et al., 2014).

Subsequently, the damage is excised by XPF-ERCC1 and XPG endonucleases at 5' and 3' respectively at short distances away from the lesion, resulting in a single strand gap of 22 to 30 nucleotides. This step requires a high level of coordination between XPA, XPG and replication protein A (RPA) to prevent the non-modified DNA strand from endonuclease activity of XPF-ERCC1. XPG helps to excise specifically only the damaged strand; avoiding an increase in genomic instability at this site (de Laat, Appeldoorn et al., 1998). XPA is one of the central components of NER due its versatile functions, it is very important in triggering DNA damage verification and presumably it is also involved in detecting and binding to structurally damaged nucleotides in ssDNA (Camenisch, Dip et al., 2006). Furthermore, XPA interacts with most of NER proteins (Scharer, 2013). Next, the single strand gap is filled through the activity DNA polymerases including DNA Pol δ, ε or κ. Finally, the GG-NER is completed by sealing the nick via DNA ligase I or XRCC1-DNA ligase 3 (Marteijn et al., 2014).

Transcription coupled repair pathway (TC-NER)

TC-NER has the ability to detect DNA alterations in the transcribed strand during transcription elongation. The stalling or arrest of RNA polymerase II triggers the localization of CSB to the DNA damage site (Vermeulen & Fousteri, 2013). This protein is highly regulated during this process due to the function of the deubiquitin ligase USP7, which protects CSB from CSA-dependent degradation (Marteijn et al., 2014, Schwertman, Lagarou et al., 2012, Vermeulen & Fousteri, 2013). Furthermore, CSB plays an important function in the $CRL4^{CSA}$ complex engagement and coordinates the events of RNA polymerase stalling and chromatin remodeling via p300 and HMGN1 (Fousteri, Vermeulen et al., 2006) **(Figure 1)**.

To proceed with the incision of the damaged strand by endonucleases, the lesion needs to be first accessible for the NER incision machinery. However, the presence of RNA polymerase II in the damage site represents an obstacle for TC-NER machinery to access. For instance in the case of CPDs lesions, the stalled RNA polymerase II masks around 35 nucleotides on the transcribed strand (Tornaletti, Reines et al., 1999).Therefore, mechanisms dealing with the stalled RNA polymerase II should exist. One of the most believed model is a process called RNA polymerase II backtracking, a well known molecular process in transcription proofreading. CSB protein is probably implicated in this process as well, however, the main factors required for this mechanism remain unknown (Marteijn et al., 2014, Sigurdsson, Dirac-Svejstrup et al., 2010). After the removal of RNA polymerase II from the damaged site the strand can be cleaved and the lesion cleared and repaired as described above in the GG-NER sub-pathway **(Figure 1)**.

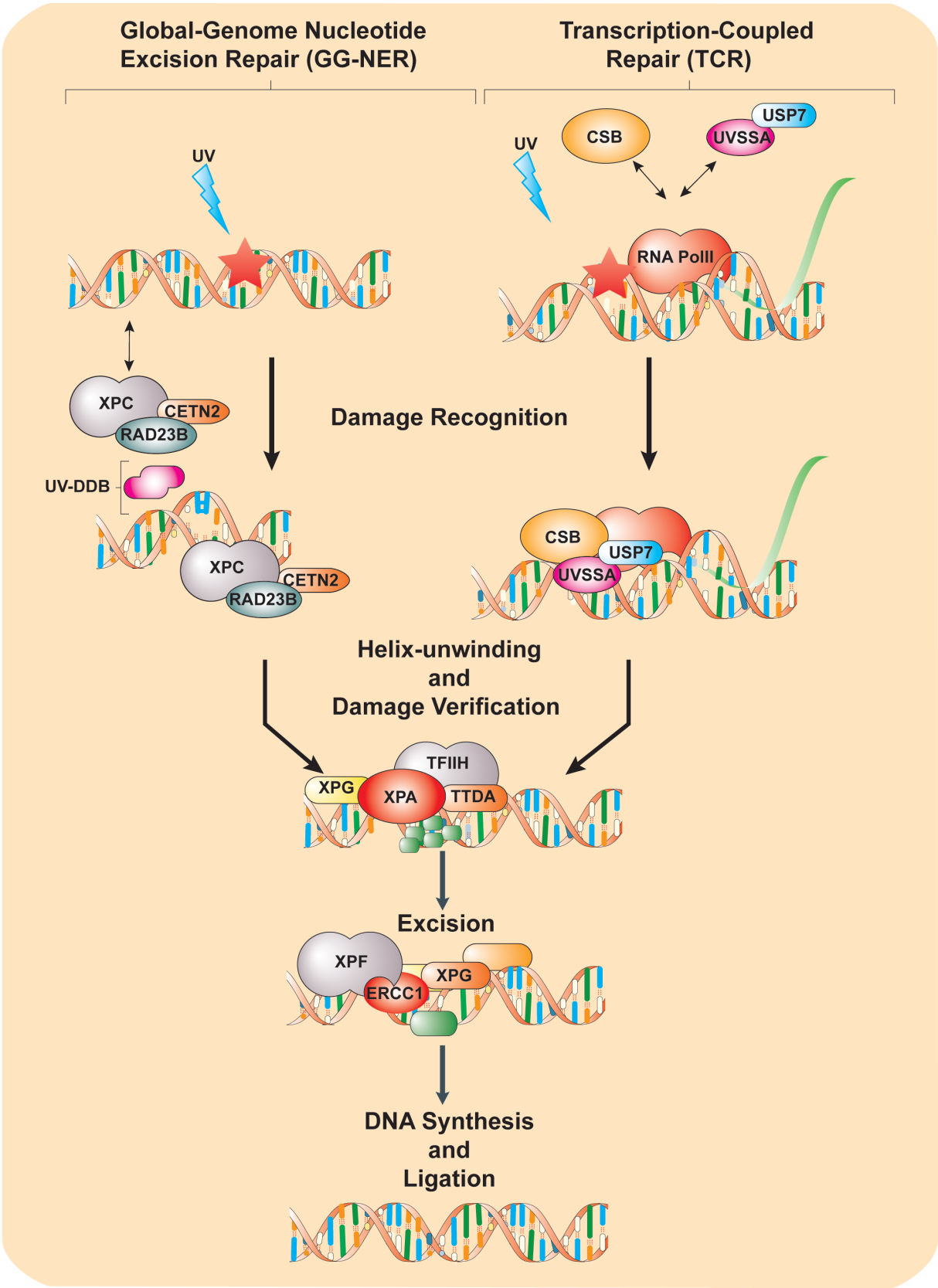

Figure 1: Molecular mechanism of nucleotide excision repair (NER):

NER is comprised of two major sub-pathways: global genome repair (GG-NER) and transcription coupled repair (TC-NER), that cooperate together to ensure the

appropriate and precise repair of damaged DNA through four main basic steps: damage recognition, helix-unwinding and damage verification, excision and DNA synthesis and DNA ligation.

1.1.3. Mismatch Repair (MMR)

MMR is one of the most conserved pathways through evolution due to its important role in protecting against spontaneous mutations. This pathway ensures the correction of errors during DNA replication and faithful genetic recombination. Additionally, it plays crucial function in the initial steps of checkpoint and apoptotic responses to different types of DNA alterations (Modrich, 2006). MMR is initiated by the binding of the heterodimers MSH2–MSH6 (MutSα) to either DNA mismatches or self-complementary insertion–deletion loops (IDLs) of 1-2 base pair (bp). If the IDLs are longer than 2 bp then MSH2–MSH3 (MutSß) initiates this process (Drummond, Li et al., 1995). After the recognition, the MLH1-PMS2 (MutLα) complex is recruited to MutSα or MutSß (Hombauer, Campbell et al., 2011). Subsequently, the proliferating cell nuclear antigen (PCNA) permits the loading of the replication factor C (RFC), allowing the interaction between PCNA and MLH1-PMS2, which enables the endonuclease activity of PMS2 to excise the mismatch at 3'. Next, Exo1 (exonuclease 1) removes the mismatch via its exonuclease activity. Finally, the RPA is recruited to the single stranded DNA and the gap is filled and sealed by DNA polymerase δ and DNA ligase I respectively (Li & Martin, 2016, Modrich, 2006).

1.1.4. Double strand break repair

Of the different forms of DNA alterations, double-stranded breaks (DSBs) are the most toxic and harmful lesions. They can be generated either by exogenous sources like ionizing radiation (IR) and radiomimetic agents, or by endogenous sources, predominantly reactive oxygen species and replication stress (Bensimon, Aebersold et al., 2011, Mazouzi, Stukalov et al., 2016, Mazouzi, Velimezi et al., 2014, Toledo, Altmeyer et al., 2013). DSBs can be also formed during the physiological processes of meiotic and V (D) J recombination (Hartlerode & Scully, 2009). In order to cope with DSBs repair, cells evolved two major mechanisms: non-homologous end joining (NHEJ) and homologous recombination (HR). In the case of NHEJ, DSBs are first recognized by the Ku heterodimer (Ku70–Ku80), which prevents nucleolytic end-

processing and activates the kinase DNA-PKcs, leading to ligation via the hetero-complex LIG4–XRCC4. Another Ku-independent NHEJ pathway also exists known as microhomology mediated end joining (MMEJ). Both NHEJ and MMEJ are error-prone that can act predominantly in G1 phase (Lieber, 2008). In contrast, HR repairs efficiently the DSBs formed in S-G2 phase in an error-free manner. HR starts with ssDNA formation, which is triggered by several proteins including the MRN complex (MRE11–RAD50–NBS1), CTIP and EXO1, leading to 3' single stranded DNA formation (ssDNA). This allow the recruitment of recombination protein A (RPA) to the single stranded DNA, giving rise to RPA-ssDNA filament formation. The RPA-ssDNA filaments are replaced subsequently by Rad51 filaments, ensuring the strand invasion and homology search with the intervention of breast cancer susceptibility proteins BRCA1 and BRCA2. Finally, other enzymes comprising polymerases, nucleases, helicases and DNA ligases ensure the completion of the process (Jackson & Bartek, 2009, Papamichos-Chronakis & Peterson, 2013) .

1.1.5. Fanconi anaemia (FA)

The Fanconi anemia pathway ensures mostly the repair of DNA interstrand crosslinks (ICLs). The repair of these lesions is crucial for cellular survival due to their ability to block transcription and DNA replication (Ceccaldi, Sarangi et al., 2016, Deans & West, 2011). FA pathway involves a network of 19 genes, mutations in which were found to cause a severe genetic disease characterized by enhanced sensitivity to ICLs, bone marrow failure and cancer predisposition (Joenje & Patel, 2001, Kottemann & Smogorzewska, 2013). In vertebrates, the repair of ICLs is mostly linked to DNA replication. The recognition of ICLs in the stalling replication fork is ensured by a complex of four proteins: FANCM, FAAP24, MHF1 and MHF2 (UHRF1 may be implicated as well in ICLs recognition), leading to ATR activation and subsequent phosphorylation of FANCI, triggering mono-ubiquitination of both FANCD2 and FANCI through the ubiquitin ligase activity of FANCL with the help of UBE2T and other members of the core complex of the Fanconi anemia proteins. The presence of ICL in replicating DNA during S phase causes stalling of the replication fork progression and a pause of the leading strand at about 20 nucleotides away from each side of the ICL due to the steric hindrance of the CMG complex (CDC45/MCM2-7/GINS). Next, the CMG complex is removed with the help of BRCA1-BARD1 and ubiquitination events (Long, Raschle et al., 2011), that permit the extension of the leading strand to about

one nucleotide away from the ICL. The ubiquitination of FANCD2 then allows its binding to the ICL site and recruit XPF-ERCC1-SLX4 complex (FAN1 and MUS81 are also likely involved in this process), which ensures the incision of the ICL (Deans & West, 2011), creating a double strand break (DSB) in one sister chromatid and a mono-adduct is left in the other strand, which is by-passed by REV1 and DNA polymerase ζ in an error-free manner. The DSB is then fixed by homologous recombination in a RAD51 dependent manner (Long et al., 2011) and the mono-adduct is probably cleaned by nucleotide excision repair (NER) (Crossan & Patel, 2012).

1.2. Replication stress

Replication stress represents one of the endogenous sources of DNA damage that challenge DNA replication and cause serious threats for the genomic integrity. Replication stress can occur stochastically during normal cell cycle progression in certain regions of the genome or pathologically due to the constitutive activation of some oncogenes such as cyclin E and c-Myc. Moreover, there are several exogenous sources that induce replication stress either by depleting cellular pools of ribonucleosides such as hydroxyurea (HU) or by inhibiting the replicative DNA polymerases by aphidicolin (APH). Multiple signaling pathways, known as DNA damage response (DDR), have been evolved to counteract the genomic instability arising from replication stress. These pathways ensure the efficient repair of DNA damage, regulation of cell cycle progression and restauration of DNA replication after fork stalling. If the DNA lesions persist, this may trigger programmed cell death or cause mutations and chromosomal aberrations. Maintaining genomic stability during DNA replication is a key biological process required for suppressing several pathologies including cancer, developmental and neurological abnormalities and many ageing-related diseases.

In the following review, the predominant sources of replication stress, the signaling pathways that regulate this process and the pathologies related to deficiencies in signaling replication stress are discussed.

EXPERIMENTAL CELL RESEARCH 329 (2014) 85–93

Available online at www.sciencedirect.com

ScienceDirect

journal homepage: www.elsevier.com/locate/yexcr

Review Article

DNA replication stress: Causes, resolution and disease

*Abdelghani Mazouzi, Georgia Velimezi, Joanna I. Loizou**

CeMM Research Center for Molecular Medicine of the Austrian Academy of Sciences, Lazarettgasse 14, AKH BT 25.3, 1090 Vienna, Austria

ARTICLE INFORMATION

Article Chronology:
Received 30 May 2014
Received in revised form
20 September 2014
Accepted 22 September 2014
Available online 30 September 2014

Keywords:
DNA replication
DNA damage signaling
Replication stress
Genome stability
Chromosome fragile sites

ABSTRACT

DNA replication is a fundamental process of the cell that ensures accurate duplication of the genetic information and subsequent transfer to daughter cells. Various pertubations, originating from endogenous or exogenous sources, can interfere with proper progression and completion of the replication process, thus threatening genome integrity. Coordinated regulation of replication and the DNA damage response is therefore fundamental to counteract these challenges and ensure accurate synthesis of the genetic material under conditions of replication stress. In this review, we summarize the main sources of replication stress and the DNA damage signaling pathways that are activated in order to preserve genome integrity during DNA replication. We also discuss the association of replication stress and DNA damage in human disease and future perspectives in the field.

Contents

Abbreviations: pre-RC, pre-replicative complex; CFS, common fragile site; DSB, DNA double strand break; CMG complex, Cdc45.Mcm2–7.GINS; ERFS, early-replicating fragile site; DDR, DNA damage response; ssDNA, single-stranded DNA; IR, ionizing radiation; HGPS, Hutchinson–Gilford progeria syndrome; SIOD, Schimke immune-osseous dysplasia; AOA1, Apraxia Oculomotor Ataxia 1; FA, Fanconi anemia; iPOND, Isolation of protein on nascent DNA; BLESS, direct in situ breaks labeling, enrichment on streptavidin and next-generation sequencing; CRISPR, Clustered regulatory interspaced short palindromic repeats

*Corresponding author. Fax: +43 1 40160 970 000.
E-mail address: jloizou@cemm.oeaw.ac.at (J.I. Loizou).

http://dx.doi.org/10.1016/j.yexcr.2014.09.030
0014-4827/

Introduction

Several exogenous and endogenous sources constantly challenge the integrity of replicating DNA, and can pose a serious threat to chromosomal stability by interfering with progression, stability and proper resumption of replication after fork arrest. DNA damage generated endogenously by errors during DNA replication is often referred to as replication stress and particularly affects genomic loci where progression of replication forks is slow or problematic. Cells have evolved a panoply of mechanisms to deal with different kinds of DNA damage that ensure the integrity of the genome during replication. Various repair mechanisms and different checkpoint machineries exist, which stop or slow down cell cycle progression until the damage is repaired. These DNA replication, repair and checkpoint activation pathways are highly regulated and coordinated. Defects in any of these functions leads to genomic instability and may lead to cancer, premature ageing or disorders associated with loss of genomic integrity.

Overview of DNA replication

DNA replication is initiated at defined loci known as replication origins. In the eukaryotic genome, replication begins at multiple origins, ranging from a few hundred in yeast to thousands in humans. These are distributed along the length of each chromosome [1]. Initiation of replication comprises a two-step process: origin licensing and firing. Origin licensing starts as early as late M or early G1 with the assembly of a pre-replicative complex (pre-RC) at each origin (early or late). The pre-RC consists of the origin recognition complex (ORC1–6 proteins), cell division cycle 6 (Cdc6), cell division cycle 10-dependent transcript 1 (Cdt1) and the core replicative helicase component Mcm2–7, consisting of the minichromosome maintenance proteins 2–7 (Mcm2–Mcm7) [2,3]. The second step, origin firing, involves the activation of the Mcm2–7 complex which is restricted to S phase and culminates in the formation of a pair of oppositely oriented replication forks that contain a single Mcm2–7 helicase hexamer complex at the apex of each fork [4]. Cyclin dependent kinases (CDKs) and Dbf dependent kinases (DDKs) promote the conversion of the pre-RC complex into a pre-initiation complex capable of unwinding DNA and carrying out DNA synthesis [5]. At the G1/S transition, when CDK activity rises, numerous additional factors cooperate to convert the MCM2–7 double hexamer into two CMG (Cdc45. Mcm2–7.GINS) complexes [6]. In particular, Cdc7–Dbf4 protein kinase (DDK) phosphorylates MCM2–7. CDK phosphorylates Sld2 (sharing homology to human RECQ4) and Sld3 (the yeast homolog of Treslin in human), promoting their interaction with Dpb11 (the yeast homolog of TopBP1 in human). The Sld3–Sld2–Dpb11 complex enables the stable binding of Cdc45 and GINS to phosphorylated MCM2–7. Once formed, CMG unwinds the origin, allowing replisome assembly. Replication forks then travel bidirectionally outwards from the origin until the entire genome is replicated [7–10].

Sources of DNA replication stress

Replication stress is defined as slowing or stalling in replication fork progression. It arises from many different sources, which are considered as replication barriers such as telomeres, repetitive sequences, DNA lesions and misincorporation of ribonucleotides, secondary DNA structures, DNA–RNA hybrids, dormant replication origins, collisions between replication and transcription complexes, hypo-acetylation and compaction of chromatin, early-replicating fragile sites (ERFSs) and common fragile sites (CFSs). Finally overexpression or constitutive activation of oncogenes such as HRAS, c-Myc and cyclin E is an emerging source of replication stress. Following, we discuss some of the most relevant sources of replication stress in more detail (see Fig. 1). We refer readers to the following review for an overall picture of agents than induce replication stress [11].

Fragile sites

Certain loci in the human genome are particularly difficult to replicate, hence rendering them prone to fragility. Most prominent amongst these are the so-called fragile site loci. As mentioned above, fragile sites can be classed CFSs or ERFSs. The former have a high A/T content, occur at sequences prone to form secondary structures, possess a condensed chromatin structure and replicate late. In contrast ERFSs are G/C rich, have an open chromatin state and replicate early.

Fragile sites are defined as being either common or rare; the former, CFSs, are present in all individuals, whereas rare fragile sites are found in less than 5% of the population [12]. There are over 200 CFSs in the human genome and these regions are quite large, ranging from just under 1 Mb to over 10 Mb in size. CFSs are prone to replication stress-induced DNA double-strand breaks (DSBs) visible in condensed metaphase chromosomes and their occurrence is dependent on the endonuclease activity of MUS81-EME1, in synergy with the resolving action of the BLM helicase to prevent chromosome breakage [13,14]. The most typical inducer of CFSs used experimentally is aphidicolin, an inhibitor of the replicative DNA polymerases α, δ, and ε [15]. The three most frequently expressed CFSs are FRA3B, FRA16D, and FRA6E [16–18]. Several studies in cell culture models have shown that under conditions that induce replication stress, fragile sites are hotspots for sister chromatid exchange, translocations and deletions [19]. The frequent alterations within these regions in multiple cancers have led to the identification of a number of extremely large genes contained within CFSs. Several of these large genes have

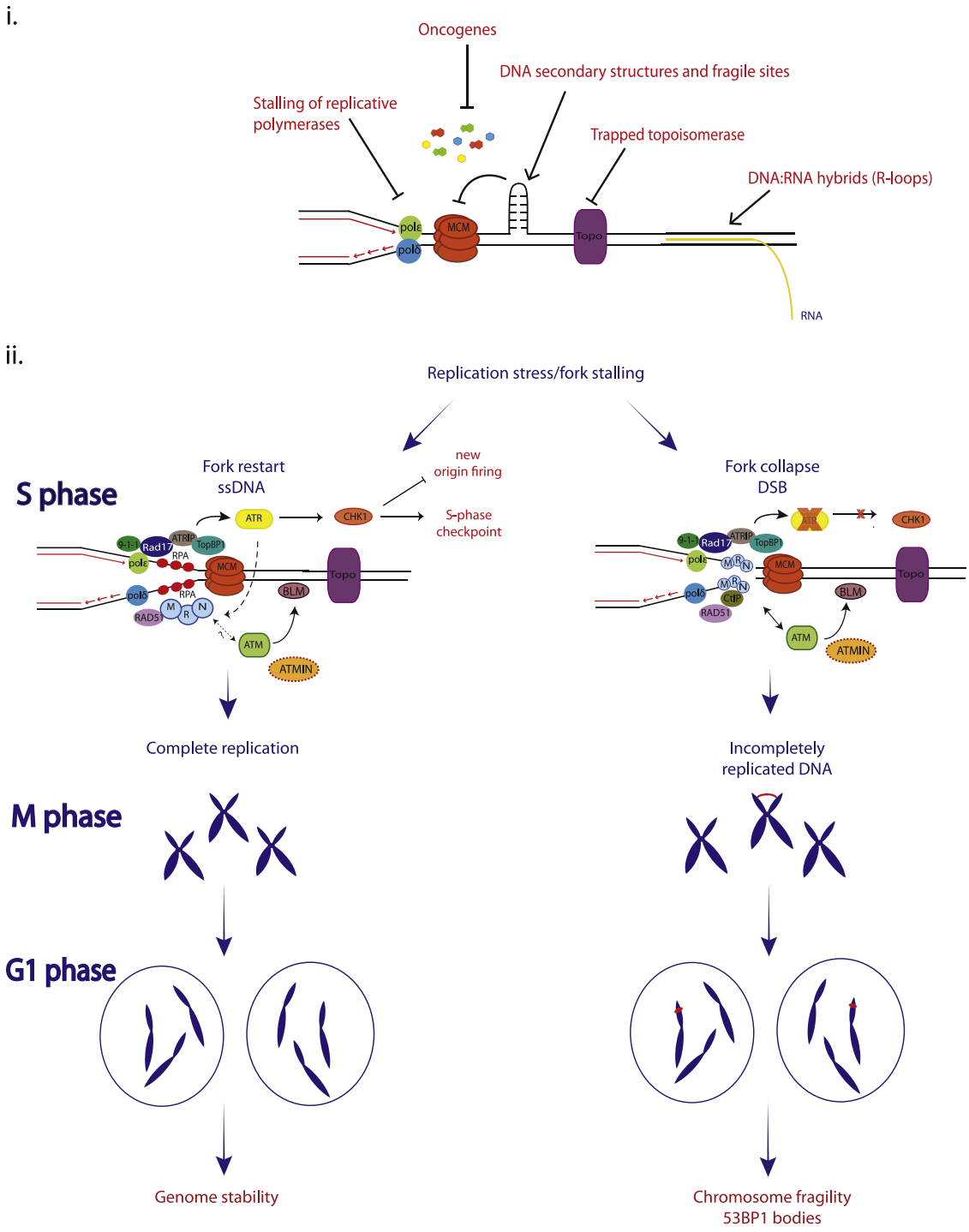

Fig. 1 – Schematic representation of the predominant DNA damage pathways that process replication intermediates. Replication stress induced by various endogenous or exogenous sources results in the generation of single strand DNA bound by RPA protein. RPA recruits ATRIP, Rad17 and 9-1-1 complex which together with TOPBP1 result in the activation of the ATR kinase, which is responsible for phosphorylation of CHK1, suppression of new origin firing and activation of the S phase checkpoint, allowing time for the cell to recover. The MRN complex and RAD51 have also been shown to be recruited at sites of single strand DNA after replication stress and to be required for fork restart. While it is unclear whether ATM has a role in MRN activation under these conditions, ATMIN, which is also an interactor of ATM, may play a role in ATM activation in response to replication stress. ATM can also activate BLM helicase which contributes to the resolution of replication intermediates. When the ATR pathway is compromised, defective checkpoint activation may result to the collapse of the replication fork into double strand breaks which then may be resolved by homologous recombination through recruitment of CtIP and RAD51. However, in the absence of ATR, replication stress can leave regions of the genome incompletely replicated resulting in abnormal DNA structures which if not properly resolved can be transmitted to the next generation in the form of DNA lesions resulting in genome instability.

been demonstrated to function as tumor suppressors involved in the formation of many different cancers including colorectal cancer and oropharyngeal squamous cell carcinomas [20–22]. A recent concept emphasizes the importance of replication origin density in the maintenance of CFS stability [23]. According to this concept, certain common fragile sites are characterized by a reduced number of replication initiation events that limit the number and density of active origins, thus rendering these "initiation-poor" regions susceptible to incomplete replication and fragility.

ERFSs are a new class of fragile sites and have been defined as similar to CFSs. This is because of their susceptibility to chromosome breakage, dependence on ATR signaling and sensitivity to replication stress induced by hydroxyurea, ATR inhibition or deregulated c-Myc expression. Moreover, more than 50% of recurrent amplifications/deletions in human diffuse large B cell lymphoma map to ERFSs [24].

Replication–transcription complex collision

Collisions between transcription machinery and replication forks are an additional source of genome instability. In higher eukaryotes, replication and transcription are coordinated processes, and they occur within spatially and temporally separated domains. Active transcription usually occurs in the G1 phase. When transcription occurs in S phase, it has been suggested to be spatially separated from replication sites [25]. It has been reported that genes of 800 Kb or more in size, often located at CFSs, produce their transcripts over more than one cell cycle, consequently extending transcription into the next S phase, which increases the probability of collisions between replication and transcription complexes and hence formation of DNA–RNA hybrids (R-loops). Multiple strategies are employed to avoid R-loop formation in prokaryotic and eukaryotic cells. Helmrich and colleagues and Wahba and colleagues demonstrate in vivo roles for RNaseH enzymes in maintaining genome integrity, which has potential implications in human disease (see section on diseases associated with defective clearance of replication stress) [26,27]. Interestingly, a recent study showed that BRCA2, a DNA repair protein with tumor suppressive function prevents accumulation of R-loops [28]. Although the exact mechanism is unclear, this important finding further demonstrates the essential role of DNA damage and repair components for efficient dealing with replication stress. Apart from the generation of R-loops transcription can interfere with replication by imposing increased topological stress at sites where newly formed RNA transcripts are tethered to nuclear pore complexes for further processing. Bermejo et al. showed that the ATR-dependent checkpoint counteracts this topological stress by releasing transcribed genes from the nuclear pores, allowing normal progression of the replication fork [29]

Oncogenic stress

Oncogenic stress is a major driving force in the early stages of cancer development [30]. The finding that DNA damage response is activated in hyperplastic tissues and after overexpression of oncogenes such as cyclin E, cdc25A and E2F1 (that deregulate replication) set the ground for linking oncogenes to replication stress-associated DNA damage [31,32]. In studies that followed, further analysis of replication dynamics and the DNA damage response after overexpression of oncogenes confirmed this model, where oncogenes such as cyclin E lead to perturbation of normal replication, activation of the DNA damage response and cell cycle checkpoints that lead to arrest or senescence [33,34]. Cyclin E causes replication stress not only by deregulating cell cycle progression but also by disrupting DNA replication during S phase. Cyclin E overexpression is associated with increased firing of replication origins, impaired replication fork progression and DNA damage. A significant amount of Cyclin E-induced replication slowing is due to decreased nucleotide pools and/or interference between replication and transcription. c-Myc is another oncogene found to directly control DNA synthesis and promotes cell proliferation. Indeed, overexpression studies have indicated that ectopic expression or conditional activation of c-Myc triggers an increase in the percentage of S phase cells in asynchronous populations [35]. The overexpression of c-Myc in a number of in *vitro* cellular systems has been associated with the activation of a DNA damage response (DDR), and increased genomic instability [36,37]. This suggests that elevated c-Myc levels lead to the accumulation of DNA damage, however the molecular mechanism is still not completely defined. One of the suggested mechanisms c-Myc induced genomic instability is its affect on replication fork dynamics [38]. It has been shown that elevated levels of c-Myc increase the number of firing replication origins which are highly asymmetric. This can lead to uneven replication processivity on either side of the replication bubble, which is indicative of replication stress and fork stalling events [35].

DNA structures

It is thought that the accessibility of DNA to replication factors can be influenced by local chromatin structure. Additionally, chromatin structure modulates origin firing time and efficiency [39]. The canonical DNA structure is the right-handed double helix B form of DNA. However, it can adopt several other non-B DNA structures including: cruciforms, hairpins, H DNA, Z DNA and G4. These secondary conformations form in the genome at specific DNA repetitive sequences and present a challenge for progression of DNA replication forks. Impeding normal DNA synthesis, and formation of these alternative forms of DNA structure may threat genome stability and in some instances play a causal role in disease development [40].

The kinases ATR and ATM signal DNA replication stress

In order to cope with the constant challenge of DNA damage encountered by replicating DNA, cells activate a complex network of interacting pathways that lead either to the repair of the damage and resumption of normal cell cycle progression or to programmed cell death. This network coordinates the activation of cell cycle checkpoints, the appropriate DNA repair pathways, and numerous other responses [41]. One of the central components of the DDR is the serine–threonine kinase Ataxia Telangiectasia Mutated protein (ATM), which phosphorylates numerous key players in various branches of the DDR [42,43]. ATM is a member of the phosphoinositide 3-kinase (PI3K)-related protein kinase (PIKK) family, which also includes Ataxia Telangiectasia and Rad3 Related protein (ATR) – refer to Fig. 1. ATM

transduces a response to various stimuli, but most prominently to DNA DSBs. In contrast, ATR is the key kinase in signaling the response to ssDNA, which can occur at persistent DSBs, but more extensively on stalled replication forks [44].

Functions of ATR

ATR is activated by its physical recruitment to the ss-DNA binding protein RPA, which independently brings together the two components of the ATR pathway. On one hand, RPA recruits ATRIP, which is in a complex with ATR and thus brings the kinase to the DNA lesion. On the other hand, RPA recruits Rad17, which loads the Rad9–Hus1–Rad1 (9-1-1) complex. This complex is then essential to recruit and position the allosteric activator TopBP1. Within close proximity, TopBP1 activates ATR. In spite of the numerous substrates of ATR, the key event that translates ATR activity into a checkpoint signal may mostly depend on one single target, which is the phosphorylation and activation of CHK1 [44]. ATR and/or CHK1 inhibition results in checkpoint defects and chromosome breakage, further consolidating the notion that cell-cycle checkpoints somehow prevent uncontrolled fork collapse [45]. However, the mechanism governing global regulation of checkpoints via inhibition of new DNA replication origins from firing by the ATR/CHK1 pathway to maintain local fork stability remains unclear. There are two possible mechanisms, firstly checkpoint signaling locally affects replication fork components, which would contribute directly to fork stabilization. Secondly, ATR signaling regulates recombinational repair, which is necessary to restart collapsed forks. Toledo and colleagues demonstrated another mechanism, which explains how ATR protects replication forks locally and suppresses origin firing globally. When ATR is activated by RPA-coated ssDNA generated ahead of the stalled replication fork, CHK1 diffuses globally through the nucleus, where it inhibits new origin firing [46]. This ensures that RPA remains in excess over ssDNA by limiting the number of stalled forks to those that were originally active at the onset of the replication stress. If ATR signaling fails, dormant origins fire, and the newly generated ssDNA progressively depletes nuclear RPA. When all RPA becomes sequestered, every active replicon generates unprotected ssDNA, which is rapidly converted into DSBs [45,46]. Recently, Yamada et al. showed that in human cells activation of the ATR/CHK1 pathway results in stabilization of chromatin-bound Cdc7–ASK kinase complex (human homolog of cdc7–Dbf4) which is necessary for initiation of normal replication and origin firing [47]. However, upon staling of replication, activation of cdc7/ASK complex by the ATR/CHK1 pathway is required for efficient lesion bypass repair, thus preventing fork collapse under conditions of replication stress.

Functions of ATM

Although ATR is considered to be the major kinase mediating the response to replication stress, mainly due to its ability to activate the intra-S phase checkpoint, evidence exists to support a role for ATM activation in response to replication stress. One aspect of ATM function under these conditions could be the activation of the homologous recombination repair pathway, which is important for restart of collapsed replication forks and recovery of replication after induction of replication stress [48]. This function may require the recruitment of the MRN complex at sites of stalled or collapsed replication forks that promote DNA end-resection, the first important step for homologous recombination. Recruitment of the MRN complex to sites of DNA damage is important for ATM activation in response to ionizing radiation (IR)-induced DSBs. The MRN complex members Mre11 and Nbs1 are required for efficient recovery of replication after treatment with replication stalling agents such as hydroxyurea [49,50]. However, the necessity for an interaction between ATM and Mre11 and Nbs1 at sites of stalled forks remains a matter of controversy. Certain studies indicate that recruitment of the MRN complex following replication stress contributes to activation of ATR rather than ATM signaling [51–53]. However, another study suggests that both ATM and ATR are required for efficient Mre11-dependent fork restart and prevention of DSB accumulation during unperturbed replication and after chemically induced replication stress [54]. Apart from homologous recombination, ATM can also influence replication fork restart by directly regulating the DNA helicases WRN and BLM, which are both required for resolution of replication intermediates and are both substrates of ATM [55,56].

Two independent studies show that activated ATM is recruited to chromatin foci at sites of common fragile sites following mild replication stress induced by aphidicolin [57,58]. In line with this, ATM depletion in addition to ATR loss results in increased fragility at CFS compared to depletion of ATR alone, supporting a role for ATM in the maintenance of chromosome stability after replication stress [59]. According to the proposed model, ATM is activated after formation of DNA DSBs that arise at a later stage as a result of replication fork collapse or chromatin breakage at sites of unreplicated DNA during mitosis. If the role of ATM is restricted solely to the activation of checkpoint and DNA repair in response to DSBs that arise as a result of further processing of replication intermediates remains unclear. Evidence challenging this view is limited, nevertheless intriguing, especially considering the lack of information on the exact nature of the specific DNA lesions that arise at sites of stalled forks and incompletely replicated DNA. For example, induction of replication stress by low doses of the topoisomerase I inhibitor camptothecin results in ATM activation in the absence of detectable DSBs [60]. Furthermore recent data from a large-scale analysis of proteins specifically localized at stalled forks after replication stress showed ATM recruitment at nascent chromatin at an early stage of DNA replication [61]. However, a role for ATM in the early response to replication stress has not been confirmed and more studies will be needed to clarify this. Moreover, the type, intensity and duration of the stimulus might be critical factors determining the relative contribution of each pathway to the final response.

In addition to NBS1, ATM possesses a second cofactor; ATMIN (also known as ASCIZ) that has been described [62,63]. ATMIN interacts with ATM using a motif homologous to that of NBS1 [62]. It has previously been shown using siRNA approaches in human cell lines and using ATMIN-deficient mouse embryonic fibroblasts (MEFs) that ATMIN has a complementary function to NBS1 with respect to ATM activation: ATMIN is dispensable for IR-induced ATM signaling, but ATM activation following replication and hypotonic stress is mediated by ATMIN [62]. Hence, NBS1 and ATMIN are required for ATM activation in a signal dependent manner [64].

Unresolved replication intermediates can occur during S/G2 phases of the cell cycle and can be converted into DNA lesions in

M phase in particular into DSBs. It has been shown that a protein that binds to p53, known as 53BP1 [65], is involved in shielding genomic regions exposed to replication stress and is recruited to such sites in an ATM-dependent manner. 53BP1 forms nuclear bodies at such sites of unrepaired DNA lesions in the subsequent G1 phase to shield these regions against erosion [58].

Defects in resolving DNA replication stress: implications in human disease

Identification of mutations responsible for various genetic syndromes has revealed the direct implication of proteins mediating the response to replication stress in the pathology of human disease [11]. Phenotypic characteristics shared among these syndromes include developmental defects, growth retardation and neurological disorders, suggestive for the importance of efficient regulation of replication during processes that require increased cell proliferation. For example, mutations in the pre-replication factors ORC1, ORC2–6 and cdt1, cdc6 that affect licensing of DNA replication are related to the Meier–Gorlin Syndrome, a disease characterized by severe growth retardation and developmental malformations [66].

Many other mutations involved in genetic syndromes affect proteins that also play an important role in the DDR, which is essential for accurate replication of the genetic material. The most prominent example is the Seckel syndrome caused predominantly by mutations in the ATR gene, which is essential for the activation of the intra-S phase checkpoint during replication stress [67]. Interestingly, a different type of Seckel syndrome is associated with mutations found in the RBBP8 gene encoding CtIP, a protein required for DNA-end resection during S phase [68]. More importantly, CtIP is an ATM substrate and interacts with the MRN complex, which also mediates DNA damage signaling and repair during replication. Mutations affecting members of the MRN complex cause syndromes characterized by growth and developmental defects [69]. Apart from ATR and RBBP8, other types of Seckel syndrome are caused by mutations in genes affecting centrosome structure and function including pericentrin (PCNT) [70].

Another type of heterogeneous human diseases, collectively called laminopathies, are the result of mutations in nuclear lamin genes such as LMNA which lead to abnormal nuclear morphology and alterations in chromatin structure. Interestingly, cells expressing a defective form of Lamin A called progerin are more sensitive to replication stress and recently it has been demonstrated that reorganization of the microtubule network inside the nucleus can rescue the nuclear morphology and fitness of laminopathic cells derived from Hutchinson–Gilford progeria syndrome (HGPS) patients [71,72]. The above examples provide a link between microtubule network organization and replication stress and point out the importance of intact centrosome function and nuclear structure for normal replication.

Mutations in proteins involved in chromatin remodeling during DNA replication have also been associated with human disease. Mutations in the SMARCAL1 and ATRX genes, which are both related to the SWI–SNF chromatin remodeling complex, are mutated in the Schimke immune-osseous dysplasia (SIOD) and the α-thalassemia/mental retardation syndrome, X-linked (ATR-X) respectively [73,74].

Hypomorphic mutations in the RNase H2 gene cause the Aicardi-Goutieres syndrome that is characterized by severe neurological dysfunction and a congenital infection-like phenotype [75]. As RNase H2 cleaves misincorporated ribonucleotides and DNA:RNA hybrids that arise during replication, it is possible that a defective response to increased replication stress may be the cause of the developmental retardation phenotype. Another protein acting in the same pathway, aprataxin (APTX) is mutated in the neurological disorder Apraxia Oculomotor Ataxia 1 (AOA1), characterized by cerebellar degeneration. Aprataxin deadenylates adenylated RNA:DNA hybrids that arise after cleavage by RNase H2, thus preventing S phase checkpoint activation [76].

Mutations in the FA complementation group are responsible for the heterogeneous genetic disorder Fanconi Anemia (FA) which is characterized by skeletal abnormalities, developmental delay, growth retardation and increased incidence of cancer development, especially in tissues with a high proliferation index [77]. FA proteins are components of the interstrand crosslink DNA repair pathway, while FANCD2 is also essential for maintenance of genome stability during replication [78]. Mutations affecting the RECQ family DNA helicases WRN, BLM and RECQL4, which play an important role in the efficient resolution of replication intermediates and arrested forks, are responsible for the genetic syndromes Werner, Bloom and Rothmund–Thomson respectively [79]. In addition to growth retardation, these syndromes are also characterized by premature aging and predisposition to cancer, phenotypes indicative of increased genomic instability. Cancer susceptibility is also a characteristic of FA patients suggesting a causative link between replication stress and cancer. Confirming this link, replication stress has been shown to be a major source of chromosomal instability (CIN) observed in CIN^+ colorectal cancers [80].

Whether replication stress is a driving force of tumourigenesis or a result of oncogenic mutations that allows further genome instability during cancer development remains to be elucidated. Interestingly, extensive crosstalk between different DNA repair pathways is necessary for the coordination of an efficient response to replication stress. For example, FANCD2 has been shown to mediate part of the ATR response to replication stress, while it also interacts with CtIP and BLM to promote restart of stalled replication forks [81–83]. Although the exact mechanism of the pathological phenotype is not entirely understood, common clinical manifestations of mutations in different genes of these pathways clearly indicates the existing crosstalk and the need for efficient coordination of the replication process with the DNA repair machinery through the DNA damage signaling pathway in order to allow normal progression of DNA replication while preserving genome integrity.

Conclusions and perspectives

Elucidating the pathways and interactions governing the response to replication stress will shed light on the molecular mechanisms that ensure genome integrity during replication under endogenous sources of replication stress. Furthermore, we will increase our understanding of how exogenous sources or defects in critical pathway components can lead to increased genome instability. An important challenge for the years to come will be to identify the specific regions of the genome that are particularly affected

during different types of replication stress. To this end, recent advances in technology can be exploited to apply novel methodology such as next generation sequencing, iPOND or BLESS to map specific DNA regions affected by replication stress and the specific protein interactions that mediate their fragility, respectively [84,85]. Moreover, CRISPR-mediated imaging of specific chromatin loci in living cells offers a powerful opportunity to reveal the dynamic interactions at sites of increased fragility following replication stress [86]. Thus, despite the progress that has been achieved during the last years, extensive studies and novel technology will be needed to boost our current understanding of the mechanisms mediating the response to replication stress and the associated genome instability. Advance in current knowledge regarding the response to replication stress will also be an important step towards more specialized therapies and development of new treatments for diseases including cancer.

Conflict of interest

The authors declare that they have no conflict of interest.

Acknowledgments

We thank the Loizou lab for input and discussions. We thank Drs. Slade, Nijman and Schliehe for critical reading of the manuscript. We apologize to those authors whose work was not cited in some instances due to space limitations. Funding from the FWF (Project number P 24766-B20) and from a Marie-Curie Career Integration Grant (Project number: 321602- NonCanATM) support the Loizou lab. GV is funded by an EMBO Long Term fellowship (Fellowship number ALTF 730-2014) CeMM is funded by the Austrian Academy of Sciences.

REFERENCES

[1] E. Sacco, M.M. Hasan, L. Alberghina, M. Vanoni, Comparative analysis of the molecular mechanisms controlling the initiation of chromosomal DNA replication in yeast and in mammalian cells, Biotechnol. Adv. 30 (2012) 73–98.
[2] A. Gambus, G.A. Khoudoli, R.C. Jones, J.J. Blow, MCM2-7 form double hexamers at licensed origins in Xenopus egg extract, J. Biol. Chem. 286 (2011) 11855–11864.
[3] S. Yamazaki, M. Hayano, H. Masai, Replication timing regulation of eukaryotic replicons: Rif1 as a global regulator of replication timing, Trends Genet. TIG 29 (2013) 449–460.
[4] D. Boos, J. Frigola, J.F. Diffley, Activation of the replicative DNA helicase: breaking up is hard to do, Curr. Opin. Cell Biol. 24 (2012) 423–430.
[5] A. Errico, V. Costanzo, Mechanisms of replication fork protection: a safeguard for genome stability, Crit. Rev. Biochem. Mol. Biol. 47 (2012) 222–235.
[6] S.E. Moyer, P.W. Lewis, M.R. Botchan, Isolation of the Cdc45/Mcm2-7/GINS (CMG) complex, a candidate for the eukaryotic DNA replication fork helicase, Proc. Natl. Acad. Sci. USA 103 (2006) 10236–10241.
[7] I. Ilves, T. Petojevic, J.J. Pesavento, M.R. Botchan, Activation of the MCM2-7 helicase by association with Cdc45 and GINS proteins, Mol. Cell 37 (2010) 247–258.
[8] Y.V. Fu, et al., Selective bypass of a lagging strand roadblock by the eukaryotic replicative DNA helicase, Cell 146 (2011) 931–941.
[9] K. Labib, How do Cdc7 and cyclin-dependent kinases trigger the initiation of chromosome replication in eukaryotic cells?, Genes Dev. 24 (2010) 1208–1219.
[10] S. Tanaka, H. Araki, Regulation of the initiation step of DNA replication by cyclin-dependent kinases, Chromosoma 119 (2010) 565–574.
[11] M.K. Zeman, K.A. Cimprich, Causes and consequences of replication stress, Nat. Cell Biol. 16 (2014) 2–9.
[12] S.G. Durkin, T.W. Glover, Chromosome fragile sites, Annu. Rev. Genet. 41 (2007) 169–192.
[13] S. Ying, et al., MUS81 promotes common fragile site expression, Nat. Cell Biol. 15 (2013) 1001–1007.
[14] V. Naim, T. Wilhelm, M. Debatisse, F. Rosselli, ERCC1 and MUS81-EME1 promote sister chromatid separation by processing late replication intermediates at common fragile sites during mitosis, Nat. Cell Biol. 15 (2013) 1008–1015.
[15] T.W. Glover, C. Berger, J. Coyle, B. Echo, DNA polymerase alpha inhibition by aphidicolin induces gaps and breaks at common fragile sites in human chromosomes, Hum. Genet. 67 (1984) 136–142.
[16] N.A. Becker, E.C. Thorland, S.R. Denison, L.A. Phillips, D.I. Smith, Evidence that instability within the FRA3B region extends four megabases, Oncogene 21 (2002) 8713–8722.
[17] A.K. Bednarek, et al., WWOX, the FRA16D gene, behaves as a suppressor of tumor growth, Cancer Res. 61 (2001) 8068–8073.
[18] S.R. Denison, G. Callahan, N.A. Becker, L.A. Phillips, D.I. Smith, Characterization of FRA6E and its potential role in autosomal recessive juvenile parkinsonism and ovarian cancer, Genes Chromosomes Cancer 38 (2003) 40–52.
[19] L. Wang, et al., Aphidicolin-induced FRA3B breakpoints cluster in two distinct regions, Genomics 41 (1997) 485–488.
[20] G. Poulogiannis, et al., PARK2 deletions occur frequently in sporadic colorectal cancer and accelerate adenoma development in Apc mutant mice, Proc. Natl. Acad. Sci. USA 107 (2010) 15145–15150.
[21] G. Gao, et al., A selected group of large common fragile site genes have decreased expression in oropharyngeal squamous cell carcinomas, Genes Chromosomes Cancer 53 (2014) 392–401.
[22] M. Ohta, et al., The FHIT gene, spanning the chromosome 3p14.2 fragile site and renal carcinoma-associated t(3;8) breakpoint, is abnormal in digestive tract cancers, Cell 84 (1996) 587–597.
[23] A. Letessier, et al., Cell-type-specific replication initiation programs set fragility of the FRA3B fragile site, Nature 470 (2011) 120–123.
[24] J.H. Barlow, et al., Identification of early replicating fragile sites that contribute to genome instability, Cell 152 (2013) 620–632.
[25] K.F. Vieira, et al., Recruitment of transcription complexes to the beta-globin gene locus in vivo and in vitro, J. Biol. Chem. 279 (2004) 50350–50357.
[26] A. Helmrich, M. Ballarino, L. Tora, Collisions between replication and transcription complexes cause common fragile site instability at the longest human genes, Mol. Cell 44 (2011) 966–977.
[27] L. Wahba, J.D. Amon, D. Koshland, M. Vuica-Ross, RNase H and multiple RNA biogenesis factors cooperate to prevent RNA:DNA hybrids from generating genome instability, Mol. Cell 44 (2011) 978–988.
[28] V. Bhatia, et al., BRCA2 prevents R-loop accumulation and associates with TREX-2 mRNA export factor PCID2, Nature 511 (2014) 362–365.
[29] R. Bermejo, et al., The replication checkpoint protects fork stability by releasing transcribed genes from nuclear pores, Cell 146 (2011) 233–246.
[30] T.D. Halazonetis, V.G. Gorgoulis, J. Bartek, An oncogene-induced DNA damage model for cancer development, Science 319 (2008) 1352–1355.
[31] J. Bartkova, et al., DNA damage response as a candidate anti-cancer barrier in early human tumorigenesis, Nature 434 (2005) 864–870.

[32] V.G. Gorgoulis, et al., Activation of the DNA damage checkpoint and genomic instability in human precancerous lesions, Nature 434 (2005) 907–913.
[33] J. Bartkova, et al., Oncogene-induced senescence is part of the tumorigenesis barrier imposed by DNA damage checkpoints, Nature 444 (2006) 633–637.
[34] R. Di Micco, et al., Oncogene-induced senescence is a DNA damage response triggered by DNA hyper-replication, Nature 444 (2006) 638–642.
[35] S.V. Srinivasan, D. Dominguez-Sola, L.C. Wang, O. Hyrien, J. Gautier, Cdc45 is a critical effector of myc-dependent DNA replication stress, Cell Rep. 3 (2013) 1629–1639.
[36] M. Reimann, et al., The Myc-evoked DNA damage response accounts for treatment resistance in primary lymphomas in vivo, Blood 110 (2007) 2996–3004.
[37] P.E. Neiman, et al., Genomic instability during Myc-induced lymphomagenesis in the bursa of Fabricius, Oncogene 25 (2006) 6325–6335.
[38] S. Rohban, S. Campaner, Myc induced replicative stress response: How to cope with it and exploit it, Biochim. Biophys. Acta (2014).
[39] J.G. Aparicio, C.J. Viggiani, D.G. Gibson, O.M. Aparicio, The Rpd3-Sin3 histone deacetylase regulates replication timing and enables intra-S origin control in Saccharomyces cerevisiae, Mol. Cell Biol. 24 (2004) 4769–4780.
[40] A.S. Boyer, S. Grgurevic, C. Cazaux, J.S. Hoffmann, The human specialized DNA polymerases and non-B DNA: vital relationships to preserve genome integrity, J. Mol. Biol. 425 (2013) 4767–4781.
[41] A. Ciccia, S.J. Elledge, The DNA damage response: making it safe to play with knives, Mol. Cell 40 (2010) 179–204.
[42] M.F. Lavin, S. Kozlov, ATM activation and DNA damage response, Cell Cycle 6 (2007) 931–942.
[43] F.A. Derheimer, M.B. Kastan, Multiple roles of ATM in monitoring and maintaining DNA integrity, FEBS Lett. 584 (2010) 3675–3681.
[44] A.J. Lopez-Contreras, O. Fernandez-Capetillo, The ATR barrier to replication-born DNA damage, DNA Repair (Amst) 9 (2010) 1249–1255.
[45] O. Fernandez-Capetillo, A. Nussenzweig, Naked replication forks break apRPArt, Cell 155 (2013) 979–980.
[46] L.I. Toledo, et al., ATR prohibits replication catastrophe by preventing global exhaustion of RPA, Cell 155 (2013) 1088–1103.
[47] M. Yamada, et al., ATR-Chk1-APC/CCdh1-dependent stabilization of Cdc7-ASK (Dbf4) kinase is required for DNA lesion bypass under replication stress, Genes Dev. 27 (2013) 2459–2472.
[48] E. Petermann, T. Helleday, Pathways of mammalian replication fork restart. Nature reviews, Mol. Cell Biol. 11 (2010) 683–687.
[49] J. Falck, et al., CDK targeting of NBS1 promotes DNA-end resection, replication restart and homologous recombination, EMBO Rep. 13 (2012) 561–568.
[50] J.G. Robison, J. Elliott, K. Dixon, G.G. Oakley, Replication protein A and the Mre11.Rad50.Nbs1 complex co-localize and interact at sites of stalled replication forks, J. Biol. Chem. 279 (2004) 34802–34810.
[51] A.M. Duursma, R. Driscoll, J.E. Elias, K.A. Cimprich, A role for the MRN complex in ATR activation via TOPBP1 recruitment, Mol. Cell 50 (2013) 116–122.
[52] J. Lee, W.G. Dunphy, The Mre11-Rad50-Nbs1 (MRN) complex has a specific role in the activation of Chk1 in response to stalled replication forks, Mol. Biol. Cell 24 (2013) 1343–1353.
[53] B. Shiotani, et al., Two distinct modes of ATR activation orchestrated by Rad17 and Nbs1, Cell Rep. 3 (2013) 1651–1662.
[54] K. Trenz, E. Smith, S. Smith, V. Costanzo, ATM and ATR promote Mre11 dependent restart of collapsed replication forks and prevent accumulation of DNA breaks, EMBO J. 25 (2006) 1764–1774.
[55] F. Ammazzalorso, L.M. Pirzio, M. Bignami, A. Franchitto, P. Pichierri, ATR and ATM differently regulate WRN to prevent DSBs at stalled replication forks and promote replication fork recovery, EMBO J. 29 (2010) 3156–3169.
[56] A.R. Davalos, P. Kaminker, R.K. Hansen, J. Campisi, ATR and ATM-dependent movement of BLM helicase during replication stress ensures optimal ATM activation and 53BP1 focus formation, Cell Cycle 3 (2004) 1579–1586.
[57] J.A. Harrigan, et al., Replication stress induces 53BP1-containing OPT domains in G1 cells, J. Cell Biol. 193 (2011) 97–108.
[58] C. Lukas, et al., 53BP1 nuclear bodies form around DNA lesions generated by mitotic transmission of chromosomes under replication stress, Nat. Cell Biol. 13 (2011) 243–253.
[59] E. Ozeri-Galai, M. Schwartz, A. Rahat, B. Kerem, Interplay between ATM and ATR in the regulation of common fragile site stability, Oncogene 27 (2008) 2109–2117.
[60] A. Ray Chaudhuri, et al., Topoisomerase I poisoning results in PARP-mediated replication fork reversal, Nat. Struct. Mol. Biol. 19 (2012) 417–423.
[61] C. Alabert, et al., Nascent chromatin capture proteomics determines chromatin dynamics during DNA replication and identifies unknown fork components, Nat. Cell Biol. 16 (2014) 281–293.
[62] N. Kanu, A. Behrens, ATMIN defines an NBS1-independent pathway of ATM signalling, EMBO J. 26 (2007) 2933–2941.
[63] C.J. McNees, L.A. Conlan, N. Tenis, J. Heierhorst, ASCIZ regulates lesion-specific Rad51 focus formation and apoptosis after methylating DNA damage, EMBO J. 24 (2005) 2447–2457.
[64] T. Zhang, et al., Competition between NBS1 and ATMIN controls ATM signaling pathway choice, Cell Rep. 2 (2012) 1498–1504.
[65] K. Iwabuchi, et al., Stimulation of p53-mediated transcriptional activation by the p53-binding proteins, 53BP1 and 53BP2, J. Biol. Chem. 273 (1998) 26061–26068.
[66] L.S. Bicknell, et al., Mutations in the pre-replication complex cause Meier-Gorlin syndrome, Nat. Genet. 43 (2011) 356–359.
[67] M. O'Driscoll, V.L. Ruiz-Perez, C.G. Woods, P.A. Jeggo, J.A. Goodship, A splicing mutation affecting expression of ataxia-telangiectasia and Rad3-related protein (ATR) results in Seckel syndrome, Nat. Genet. 33 (2003) 497–501.
[68] P. Qvist, et al., CtIP Mutations Cause Seckel and Jawad Syndromes, PLoS Genet. 7 (2011) e1002310.
[69] T.H. Stracker, J.H. Petrini, The MRE11 complex: starting from the ends. Nature reviews, Mol. Cell Biol. 12 (2011) 90–103.
[70] E. Griffith, et al., Mutations in pericentrin cause Seckel syndrome with defective ATR-dependent DNA damage signaling, Nat. Genet. 40 (2008) 232–236.
[71] M. Singh, et al., Lamin A/C depletion enhances DNA damage-induced stalled replication fork arrest, Mol. Cell Biol. 33 (2013) 1210–1222.
[72] D. Larrieu, S. Britton, M. Demir, R. Rodriguez, S.P. Jackson, Chemical inhibition of NAT10 corrects defects of laminopathic cells, Science 344 (2014) 527–532.
[73] C.F. Boerkoel, et al., Mutant chromatin remodeling protein SMARCAL1 causes Schimke immuno-osseous dysplasia, Nat. Genet. 30 (2002) 215–220.
[74] D. Clynes, et al., ATRX dysfunction induces replication defects in primary mouse cells, PloS One 9 (2014) e92915.
[75] Y.J. Crow, et al., Mutations in genes encoding ribonuclease H2 subunits cause Aicardi-Goutieres syndrome and mimic congenital viral brain infection, Nat. Genet. 38 (2006) 910–916.
[76] P. Tumbale, J.S. Williams, M.J. Schellenberg, T.A. Kunkel, R.S. Williams, Aprataxin resolves adenylated RNA-DNA junctions to maintain genome integrity, Nature 506 (2014) 111–115.
[77] M. Tischkowitz, I. Dokal, Fanconi anaemia and leukaemia - clinical and molecular aspects, Br. J. Haematol. 126 (2004) 176–191.
[78] N.G. Howlett, T. Taniguchi, S.G. Durkin, A.D. D'Andrea, T.W. Glover, The Fanconi anemia pathway is required for the DNA replication stress response and for the regulation of common fragile site stability, Hum. Mol. Genet. 14 (2005) 693–701.

[79] C.Z. Bachrati, I.D. Hickson, RecQ helicases: guardian angels of the DNA replication fork, Chromosoma 117 (2008) 219–233.
[80] R.A. Burrell, et al., Replication stress links structural and numerical cancer chromosomal instability, Nature 494 (2013) 492–496.
[81] G. Lossaint, et al., FANCD2 binds MCM proteins and controls replisome function upon activation of s phase checkpoint signaling, Mol. Cell 51 (2013) 678–690.
[82] J.E. Yeo, E.H. Lee, E. Hendrickson, A. Sobeck, CtIP mediates replication fork recovery in a FANCD2-regulated manner, Hum. Mol. Genet. (2014).
[83] I. Chaudhury, A. Sareen, M. Raghunandan, A. Sobeck, FANCD2 regulates BLM complex functions independently of FANCI to promote replication fork recovery, Nucleic Acids Res. 41 (2013) 6444–6459.
[84] B.M. Sirbu, F.B. Couch, D. Cortez, Monitoring the spatiotemporal dynamics of proteins at replication forks and in assembled chromatin using isolation of proteins on nascent DNA, Nat. Protoc. 7 (2012) 594–605.
[85] N. Crosetto, et al., Nucleotide-resolution DNA double-strand break mapping by next-generation sequencing, Nat. Methods 10 (2013) 361–365.
[86] B. Chen, et al., Dynamic imaging of genomic loci in living human cells by an optimized CRISPR/Cas system, Cell 155 (2013) 1479–1491.

1.3. Nucleotide excision repair deficiencies and associated Diseases

Our knowledge in DNA repair and its complexity has expanded in the last decades, due to the technological progress that has been made in molecular biology. Using a combination of different approaches especially the power of next generation sequencing, revealed a direct implication of proteins mediating DNA repair in various human genetic disorders (Garinis, van der Horst et al., 2008, Jackson & Bartek, 2009, Mazouzi et al., 2014, Zeman & Cimprich, 2014). Defects in the genome stability machinery can display various phenotypic characteristics including cancer predisposition, premature ageing, immunodeficiency, developmental defects, growth retardation and neurological disorders, which are dependent on the DNA repair pathway that is affected. For instance, not all the aspects of cancer predisposition and/or degenerative ageing are enhanced to the same extent in all syndromes, supporting the idea that each DNA repair pathway deals with a specific subset of DNA lesions. Therefore, there is no pathway that can cover all the types of DNA alterations and cause the same severity of all the phenotypic characteristics associated with the pathology (Garinis et al., 2008). Studies in mouse models have shown that deficiencies in DNA repair pathways that protect against mutagenesis are usually prone to specific types of cancer and show minor ageing phenotypes as described in the case of xeroderma pigmentosum (XP) patients. Whereas, pathways that deal with the toxicity of DNA damage tend to display reduced cancer predisposition but appearance of premature ageing as observed in Cockayne syndrome (CS) patients. In rare cases, the both cancer predisposition and premature ageing can manifest in the same patient that carries a mutation in gene responsible for preventing mutagenesis and cell death as seen in patients with XP and CS (XPCS) (Garinis et al., 2008). Nucleotide excision repair (NER), one of the most investigated pathways, its deficiency displays several clinical manifestations due to the diversity of DNA alterations that are repaired by NER and also the presence of two sub-pathways (GG-NER and TCR-NER).

Defects in GG-NER cause Xeroderma pigmentosum (XP), a rare autosomal recessive pathology characterized by hypersensitivity to UV irradiation and greater than 1000-fold increased risk of cutaneous basal cell, squamous cell carcinoma or melanoma and various other internal tumors (DiGiovanna & Kraemer, 2012). Additionally, 20-30% of XP patients suffer from neurological abnormalities (Kraemer, Patronas et al., 2007).

Eight genes were found to cause XP including: XPA, XPB(ERCC3), XPC, XPD (ERCC2), XPE (DDB2), XPF (ERCC4), XPG (ERCC5) and XPV (POLH). The severity of the pathology depends on the defective protein. Patients with mutated XPG are known to be the most severely affected and show very low levels of residual repair (Cleaver, 2005).

TCR-NER deficiencies cause distinct pathology known as Cockayne syndrome (CS). CS patients show hypersensitivity to UV irradiation similar to XP patients but without any signs of cancer predisposition and increase risk in developing skin cancer (Marteijn et al., 2014, O'Driscoll, 2012). CS patients display several additional phenotypes such as growth arrest, microcephaly, mental retardation and many other characteristics associated with severe neurodevelopmental abnormalities and premature aging (Laugel, 2013). The average life expectancy of CS patients is about 12 years. There are only two genes found so far to be mutated in CS: CSA/ERCC8 or CSB/ERCC6. The progeroid phenotype observed in this disease could be explained by the accumulation of stalled transcription complexes that induce premature cell death in slowly proliferating or non-proliferating cells such as neurons, leading to premature ageing (Marteijn et al., 2014). Trichothiodystrophy (TTD) is another disorder which recapitulates the hallmarks of CS along with other phenotypes like brittle hair and nails and scaling of the skin (ichthyosis). However only half of TTD patients display photosensitivity. Mutations in TFIIH complex including XPB, XPD and TTD were found to cause Trichothiodystrophy syndrome. However, the type of the mutation defines whether the patients have XP or TTD (de Boer & Hoeijmakers, 2000, Dubaele, Proietti De Santis et al., 2003, Hashimoto & Egly, 2009).

1.4. Synthetic viability

Progress with genomic technologies has allowed us in the last few decades to expand our knowledge on the molecular basis of human pathology. Despite the great advances that have been made in revealing genetic mutations of various diseases associated with DNA repair pathways, the development of effective therapies has remained a challenge. For more than 6000 Mendelian disorders that have been characterized, only a few drugs have been developed (Dietz, 2010), and most of these therapies are preventives rather than being curative. Recently, however, several studies have highlighted a promising avenue and novel therapeutic approach for correcting defects

in human Mendelian disorders, including those affecting DNA repair, using synthetic viability concept (genetic suppression or rescue) (Chen, Shi et al., 2016, Friend & Schadt, 2014, van Leeuwen, Pons et al., 2016). This occurs when deficiencies caused by loss or mutation of one gene can be rescued by depletion or inhibition of another gene. This type of genetic interaction has been found across several model organisms and also in cases of human genetic disorders. In the budding yeast, it has been found that synthetic viability interactions are functionally enriched compared to other types of interactions. Moreover, most of these interactions connect genes that are functionally belong to the same biological process (van Leeuwen et al., 2016).

Furthermore, Chen et al analyzed the sequence and the genotype data from 589,306 healthy individuals over the age of 18, searching for genetic mutations that are known to be highly penetrant, causing Mendelian childhood disorders. Interestingly, they identified 13 totally healthy adults caring mutations that are believed to cause 8 severe Mendelian childhood disorders. However, these individuals did not show any clinical manifestation related to the respective disease (Chen et al., 2016). Appropriate decoding of the genomes of these individuals may permit identifying genetic suppression mechanisms of multiple pathologies that could help in developing effective novel therapies (Chen et al., 2016, Friend & Schadt, 2014).

Additionally, several other synthetic viability interactions have been reported in human genetic studies. For instance, mutations in the dystrophin gene (DMD) causes a very severe Mendelian disorder called Duchenne muscular dystrophy (Hoffman, Brown et al., 1987). The phenotypes of this disease can be alleviated by mutation of the promoter of Jagged1, triggering its overexpression, thus creating a novel binding site of myogenin, a transcription factor implicated in muscle differentiation and repair (Vieira, Elvers et al., 2015, Wright, Sassoon et al., 1989). Several gene mutations have been found to have a protective effect against certain diseases, including the homozygous mutation of the co-receptor CCR5 that is found to exhibit a high degree of resistance to sexual and parenteral HIV-1 infection (Philpott, Burger et al., 1999). Loss-of-function mutations in the zinc transporter SLC30A8 showed a protective effect of obese individuals to type 2 diabetes mellitus (Flannick, Thorleifsson et al., 2014, Yakala, 2014). Recently, the synthetic viability interactions have also emerged in DNA repair as a potential approach to correct DNA repair associated diseases. DNA repair pathways work in tight regulation and cooperation, where a defect in one pathway can deviate the balance of the system to another pathway that is able of repairing the same

type of lesions. This has been reported for non-homologous end-joining (NHEJ) deficient cells, where the loss of 53BP1 partially restores homologous recombination (HR) in BRCA1 mutant cells (Bouwman, Aly et al., 2010, Bunting, Callen et al., 2010). Similarly, deficiency in the Fanconi anaemia pathway can be restored by inhibition of non-homologous end-joining (NHEJ) (Adamo, Collis et al., 2010, Pace, Mosedale et al., 2010). Moreover, chemical inhibition of the lysine acetyltransferase NAT10 using small molecule can correct nuclear shape of lamin A/C–depleted cells, which may open novel opportunities for treating laminopathies including the accelerated-aging disease Hutchinson-Gilford progeria syndrome (Larrieu, Britton et al., 2014). Another example illustrating the genetic suppression in DNA repair is that the loss of PTIP or PARP1 (ARTD1) rescues the lethality of BRCA2 deficient cells, and confers resistance to a variety of DNA-damaging agents (Ding, Ray Chaudhuri et al., 2016, Ray Chaudhuri, Callen et al., 2016).

Synthetic viability interactions could represent compensatory systems, that allowed for genetic variation during evolution to select for certain phenotypes. Therefore, systematic and comprehensive analysis of these interactions may help understanding the causative effect of human pathologies and open possible avenues for developing curative therapies.

1.5. Aims of this thesis

Maintaining genomic integrity is a key biological process during DNA replication. This process can be challenged by different factors that block or slow replication fork progression which triggers replication stress. Although the role of ATM in response to double strand breaks is well investigated, its function in signaling DNA replication stress, via its cofactor ATMIN, is comparatively poorly understood. We therefore aimed in the first part of my thesis to (1) comprehensively map the dynamic cellular response to replication stress employing a combination of transcriptomics and phosphoproteomics approaches and (2) define in an unbiased and time-resolved manner the contribution of ATM and ATMIN to this response. Additionally, we planned to (3) characterize the relationship between ATM and ATMIN and (4) confirm whether ATMIN is indeed a specific co-factor for ATM or general factor involved in modulating the activity of other kinases in replication stress signaling. Finally, our ultimate goal was to (5) identify and investigate the molecular mechanism of novel players involved in replication stress response.

In the second part of my thesis, the main objective was to (6) search for synthetic viable interactions to alleviate a DNA repair deficiency using a high throughput drug screens. We focused on nucleotide excision repair (NER) because there are no curative therapies for patients associated with NER deficiency, and mutations within this pathway cause several pathologies with diverse clinical manifestations. Thus, we aimed to (7) use FDA-approved compounds to allow for potential drug repurposing and fast clinical applications. Additionally, we planned to (8) decipher the mode of action of the drug identified and (9) test its effect in other DNA repair pathways. Finally, (9) we aimed to examine whether the drug identified enhanced the repair of DNA damage and protected against genomic instability.

2. CHAPTER TWO: RESULTS

2.1. Prologue

A comprehensive analysis of the dynamic response to aphidicolin-mediated replication stress uncovers targets for ATM and ATMIN.

Mazouzi A, Stukalov A, Muller AC, Chen D, Wiedner M, Prochazkoya J, Chiang SC, Schuster M, Breitwieser FP, Pichlmair A, El-Khamisy S, Bock C, Kralovics R, Colinge J, Bennett K and Loizou JI. (2016). Cell Reports 15: 893-908.

Here, we combined the whole genome transcriptomics and global phosphoproteomics to comprehensively map the dynamic response to replication stress. Further, we determined the requirements for ATM- ATMIN pathway in modulating this process. Our data reveal that replication stress induces time-dependent and widespread changes to the transcriptome and phosphoproteome. Through our systematic analyses, we uncovered new proteins and phosphorylation events downstream of replication stress. We also reveal that H2AX is phosphorylated in ATMIN-dependent manner following replication stress. Additionally, we identified CRMP2 as a novel DNA damage response phosphoprotein, which is induced by replication stress and regulated by ATMIN. Abnormal activation of CRMP2 via phosphorylation is specifically associated with Alzheimer's disease, providing an insight into diseases that emerge from replication stress.

The author of this thesis designed and performed most of the experiments, including the quantitative mass spectrometry (MS)-based phosphoproteomics which assisted by Muller AC and the transcriptomics using RNA sequencing. I also performed the bioinformatics analysis of the data with help from Stukalov A for the phosphoproteomics and Chen D for the transcriptomics. Moreover, I did most of the functional validation experiments with help from Wiedner M. I prepared the figures and wrote the manuscript with the last author Loizou JI.

Resource

Cell Reports

A Comprehensive Analysis of the Dynamic Response to Aphidicolin-Mediated Replication Stress Uncovers Targets for ATM and ATMIN

Graphical Abstract

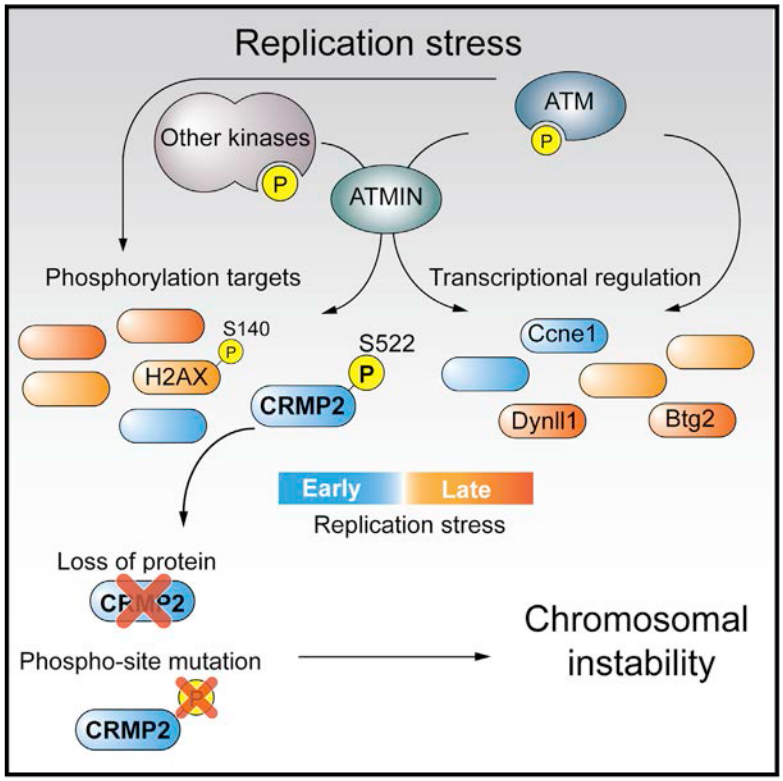

Authors

Abdelghani Mazouzi, Alexey Stukalov, André C. Müller, ..., Jacques Colinge, Keiryn L. Bennett, Joanna I. Loizou

Correspondence

jloizou@cemm.oeaw.ac.at

In Brief

The global cellular response to replication stress is poorly understood. To elucidate the contribution of ATM-ATMIN signaling to the replication stress response, Mazouzi et al. combine phosphoproteomics and transcriptomics. They identify known and novel events, including the phosphorylation of CRMP2, a protein implicated in Alzheimer's disease but not in the DNA damage response.

Highlights

- Replication stress triggers widespread changes in phosphorylation and expression
- ATM-ATMIN regulate phosphorylation events and expression upon replication stress
- ATMIN modulates the phosphorylation of H2AX and CRMP2 following replication stress
- Replication-stress-induced phosphorylation of CRMP2 regulates genome stability

Accession Numbers

GSE72275

Mazouzi et al., 2016, Cell Reports *15*, 893–908
April 26, 2016
http://dx.doi.org/10.1016/j.celrep.2016.03.077

CellPress

Cell Reports
Resource

A Comprehensive Analysis of the Dynamic Response to Aphidicolin-Mediated Replication Stress Uncovers Targets for ATM and ATMIN

Abdelghani Mazouzi,[1] Alexey Stukalov,[1,2] André C. Müller,[1] Doris Chen,[1] Marc Wiedner,[1] Jana Prochazkova,[1] Shih-Chieh Chiang,[3] Michael Schuster,[1] Florian P. Breitwieser,[1,4] Andreas Pichlmair,[2] Sherif F. El-Khamisy,[3] Christoph Bock,[1] Robert Kralovics,[1] Jacques Colinge,[1,5] Keiryn L. Bennett,[1] and Joanna I. Loizou[1,*]

[1]CeMM Research Center for Molecular Medicine of the Austrian Academy of Sciences, Lazarettgasse 14, AKH BT 25.3, 1090 Vienna, Austria
[2]Max Planck Institute of Biochemistry, Am Klopferspitz 18, 82152 Martinsried, Germany
[3]Krebs Institute, Department of Molecular Biology and Biotechnology, University of Sheffield, Sheffield S10 2TN, UK
[4]Present address: McKusick-Nathans Institute of Genetic Medicine, Johns Hopkins University School of Medicine, Monument Street, Baltimore, MD 21205, USA
[5]Present address: Institut de Recherche en Cancérologie de Montpellier, Campus Val d'Aurelle, 34298 Montpellier Cedex 5, France
*Correspondence: jloizou@cemm.oeaw.ac.at
http://dx.doi.org/10.1016/j.celrep.2016.03.077

SUMMARY

The cellular response to replication stress requires the DNA-damage-responsive kinase ATM and its cofactor ATMIN; however, the roles of this signaling pathway following replication stress are unclear. To identify the functions of ATM and ATMIN in response to replication stress, we utilized both transcriptomics and quantitative mass-spectrometry-based phosphoproteomics. We found that replication stress induced by aphidicolin triggered widespread changes in both gene expression and protein phosphorylation patterns. These changes gave rise to distinct early and late replication stress responses. Furthermore, our analysis revealed previously unknown targets of ATM and ATMIN downstream of replication stress. We demonstrate ATMIN-dependent phosphorylation of H2AX and of CRMP2, a protein previously implicated in Alzheimer's disease but not in the DNA damage response. Overall, our dataset provides a comprehensive resource for discovering the cellular responses to replication stress and, potentially, associated pathologies.

INTRODUCTION

During DNA replication, genome integrity is challenged by factors that impede replication fork progression, hence resulting in replication stress (Mazouzi et al., 2014; Zeman and Cimprich, 2014). In turn, this can lead to replication fork collapse and consequently to the formation of DNA double-strand breaks (DSBs) (Fernandez-Capetillo and Nussenzweig, 2013; Toledo et al., 2013). Replication stress can be induced stochastically during cell-cycle progression or pathologically by the disregulation of oncogene expression, thus promoting oncogene induced transformation (Bartek et al., 2012; Halazonetis et al., 2008). Replication fork instability can also be triggered by exogenous agents such as aphidicolin (APH), which inhibits the replicative DNA polymerases (Glover et al., 1984) and leads to instability of particular genomic regions known as common fragile sites (CFSs). Such regions are particularly difficult to replicate and are susceptible to replication-stress-induced DSBs (Durkin and Glover, 2007). As such, these regions are hotspots for genomic aberrations (Wang et al., 1997).

To counteract DNA damage during DNA replication, cells have evolved a network of DNA damage surveillance pathways that maintain genome integrity. The DNA damage response is orchestrated by the PIKK kinases (phosphatidylinositol-3-kinase related kinases) Ataxia Telangiectasia Mutated protein (ATM); Ataxia Telangiectasia and Rad3 related protein (ATR); and DNA-dependent protein kinase, catalytic subunit (DNA-PKcs) that target a plethora of substrates for phosphorylation at serine or threonine residues followed by glutamine (the "SQ/TQ" motif) (Matsuoka et al., 2007). ATM and DNA-PKcs have most widely been studied in response to DNA DSBs, yet ATM has been reported to respond to diverse stimuli (Derheimer and Kastan, 2010; Kaidi and Jackson, 2013; Lavin and Kozlov, 2007). ATR is activated by its physical recruitment to single-stranded DNA (ssDNA), which can occur at persistent DSBs, but is found more extensively at stalled replication forks (López-Contreras and Fernandez-Capetillo, 2010). ATR and its downstream effectors can then delay cell-cycle progression and also stabilize stalled forks (Friedel et al., 2009). In addition to ATR, ATM is also required during the cellular response to replication stress (Harrigan et al., 2011; Lukas et al., 2011; Petermann and Helleday, 2010; Ward et al., 2005), yet its role has been largely underappreciated.

ATM is activated by two major cofactors—NBS1, which is part of the MRN complex (for MRE11-RAD50-NBS1), and ATMIN (ATM interactor; also known as ASCIZ for ATM substrate Chk2-interacting Zn^{2+}-finger protein)—in a stimulus-dependent manner (Kanu and Behrens, 2008). ATM is also activated after oxidative damage in a cofactor-independent manner (Guo et al., 2010). In response to DNA DSBs, the MRN complex leads

to ATM activation (Difilippantonio et al., 2005; Falck et al., 2005; Lee and Paull, 2007; Uziel et al., 2003), while ATMIN is required for ATM activation upon replication stress (Kanu and Behrens, 2007; Kanu et al., 2015; Loizou et al., 2011; Schmidt et al., 2014).

Following replication stress, ATM has been shown to be required for recruiting DNA repair proteins, including 53BP1, to nuclear bodies at loci that are particularly susceptible to erosion, hence protecting these regions from degradation (Harrigan et al., 2011; Lukas et al., 2011). Furthermore, this event has been shown to occur in an ATMIN-dependent manner (Kanu et al., 2015; Schmidt et al., 2014). Within such genomic regions, OPT (for OCT-1, PTF, transcription) domains form in an ATM-dependent manner that represent regions of low transcriptional activity (Harrigan et al., 2011). Since these regions lack the phosphorylated, elongating forms of RNA polymerase II (Pol II), they denote regions of DNA damage that lead to transcription inhibition, which assists in the maintenance of genomic integrity (Harrigan et al., 2011).

Considering that both ATM and ATMIN are required for regulating the cellular response to replication stress, and yet their contribution to this fundamental cellular process is understudied, we devised an experimental system that would allow us to gain a comprehensive view of the events induced by replication stress. Furthermore, our system allowed us to delineate the contribution of ATM and ATMIN to this response in a global, unbiased, and time-resolved approach. We combined transcriptomics and quantitative mass spectrometry (MS)-based phosphoproteomics, in cells exposed to APH-induced replication stress, in a time-resolved manner. To map events dependent on the ATM signaling pathway, we utilized cells that have been genetically engineered to lack either ATM or ATMIN. Our study reveals that APH-induced replication stress leads to altered gene expression and that ATM and ATMIN contribute significantly to this effect. In parallel, we map widespread phosphorylation events on multiple proteins, in a time-dependent manner. Although some of the identified proteins and phosphorylation sites have already been implicated in the DNA damage response, a significant number has not. To validate our comprehensive data resource, we show that the phosphorylation of H2AX at serine 140 (also referred to as serine 139 in the mature protein; known as γH2AX in the phosphorylated form) occurs in an ATMIN-dependent manner upon exposure to replication stress. Furthermore, we identify CRMP2 as a replication-stress-induced phosphoprotein that requires ATMIN for its phosphorylation at S522. Phosphorylation at this site on CRMP2 is required for cell survival in response to replication stress. In summary, we have established the comprehensive and timed orchestration of gene expression and protein phosphorylation in known and novel sites (as well as proteins) that are involved in the cellular response to replication stress, induced by APH.

RESULTS

Charting the Global Cellular Response to Replication Stress

The cellular response to replication stress involves altering the expression of genes and the posttranslational modifications of proteins, including phosphorylation. To globally chart the cellular response to APH-induced replication stress over time, we took the following two approaches: using global phosphoproteomics, we quantified the changes in protein phosphorylation events by mass spectrometry, and using RNA sequencing (RNA-seq) we quantified the changes in the transcriptome. Furthermore, to delineate the contribution of the ATM-ATMIN signaling pathway, we performed these analyses in cells lacking either of these two proteins.

To determine the kinetics of DNA strand breaks induced by APH, we used the alkaline comet assay, which measures both DNA single- and double-strand breaks, and the neutral comet assay, which quantifies specifically DNA double-strand breaks. Mouse embryonic fibroblasts (MEFs) were treated with APH (1 μM) over a period of 24 hr. In response to APH treatment, DNA damage accumulated gradually over time (Figures 1A and 1B). This correlated with the increased localization of γH2AX and 53BP1 (two DNA damage markers) to damage sites (Figures 1C, S1A, and S1B). In its phosphorylated form, H2AX is crucial for the recruitment of DNA damage repair proteins in response to DSBs. Furthermore, H2AX has been previously shown to be phosphorylated in response to replication stress (Flach et al., 2014; Burhans and Weinberger, 2007). In addition, we noted that the early cellular stress response to APH (4 hr) did not affect cell-cycle progression, whereas prolonged stress for 24 hr caused a block in cell-cycle progression at S phase (Figures 1D and S1C).

Protein phosphorylation mediated by the ATM and ATR kinases is known to be important in signaling DNA replication stress. We measured ATM activation by examining the phosphorylation of known downstream targets, including KAP1 at S824 (mouse ortholog S823) and SMC1 at S957, and the autophosphorylation of ATM itself at S1981 (mouse ortholog S1987). Similarly, to monitor ATR activation we assessed the phosphorylation of CHEK1 at S345. We also monitored H2AX phosphorylation at S140 (γH2AX), which can be mediated by both ATM and ATR. Phosphorylation of ATR substrates is apparent within the first hour after APH treatment, whereas the phosphorylation of ATM substrates appeared between 2 hr and 12 hr (Figure 1E).

To identify the cellular response to replication stress (and to define the roles of ATM and ATMIN within this response), we performed transcriptomics and quantitative global phosphoproteomics at 4 hr and 24 hr post APH treatment (using *Atm*- and *Atmin*-deficient MEFs; Figure S1D). This approach allowed for global evaluation of the early and late events of replication stress signaling (Figure 1F).

Mapping Replication-Stress-Induced Transcriptional Events Dependent on ATM or ATMIN

To chart the transcriptional changes in response to replication stress, we performed RNA-seq of *Atm*- or *Atmin*-deficient MEFs ($Atm^{-/-}$ and $Atmin^{\Delta/\Delta}$) and their corresponding controls ($Atm^{+/+}$ and $Atmin^{+/+}$) at 4 hr and 24 hr post APH treatment. We defined APH-responsive genes as those shared between the two wild-type (WT) cell lines, when comparing APH treated to DMSO treated cells (Figure S2A), which led to the identification of 266 genes and 1,346 genes with significantly altered

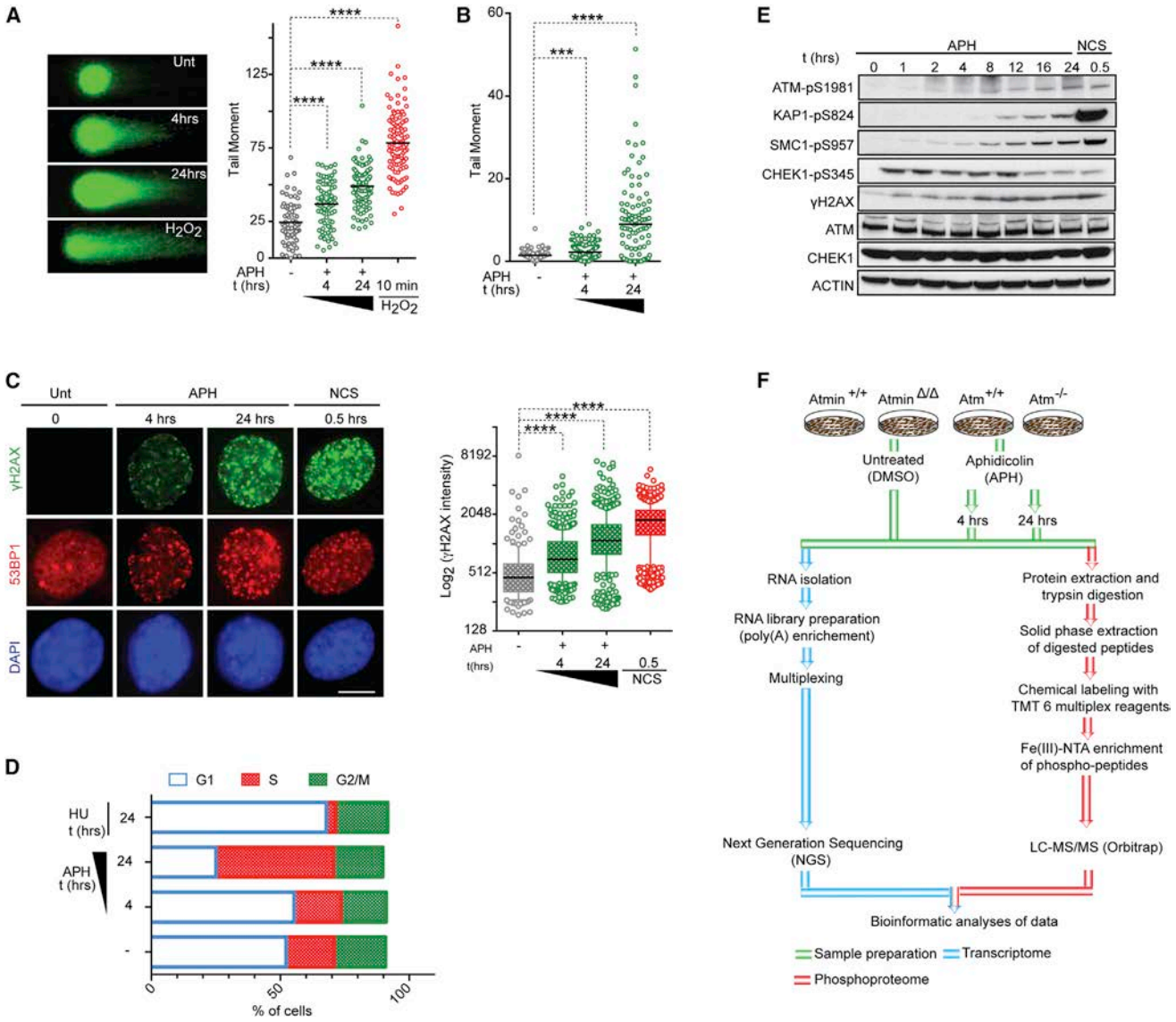

Figure 1. Mapping Early and Late APH-Induced Phosphorylation Events

(A) Left: DNA double- and single-strand breaks were detected, using the alkaline comet assay, in mouse embryonic fibroblasts (MEFs) treated with 1 μM aphidicolin (APH) for the indicated times or 100 μM H_2O_2 for 10 min. Right: box and whisker plot for the quantification of the tail moment of >100 cells.

(B) Box and whisker plot for the quantification of the tail moment using the neutral comet assay to measure specifically DNA double-strand breaks in MEFs treated with 1 μM APH for the indicated times.

(C) MEFs were treated with 1 μM APH or neocarzinostatin (NCS; a radiomimetic compound used as a positive control, at 50 ng/mL) for the indicated times and immunostained with anti-53BP1 and γH2AX antibodies, and nuclear DNA was counterstained with DAPI. Scale bar, 10 μm. Right: box and whisker plot for the quantification of γH2AX intensities displayed as a.u. of > 1,000 cells. ****$p < 0.0001$, ***$p < 0.001$ (p value was calculated by the Mann-Whitney U test).

(D) Analysis of cell-cycle progression of MEFs treated with 1 μM APH or 1 mM hydroxyurea (HU), for indicated times.

(E) Asynchronous MEFs were treated with APH (1 μM) or NCS for the indicated times. Whole-cell extracts were immunoblotted with the indicated antibodies.

(F) Schematic representation of the experimental setup used to identify roles for ATM and ATMIN in the cellular response to APH-induced replication stress. Transcriptomics and global phosphoproteomics were performed in *Atm*- and *Atmin*-deficient MEFs in the presence or absence of APH-induced replication stress at the indicated times.

expression using a multiple hypothesis adjusted p value of <0.01 (herein referred to as "adjusted p value") at 4 hr and 24 hr, respectively (Figures 2A and S2A). Eighty differential genes were shared between the two time points (Figure 2A). To determine the cellular processes predicted to be affected by replication stress, we performed gene ontology (GO) enrichment analysis on the genes significantly altered in expression upon exposure of WT MEFs to APH. Enriched biological processes

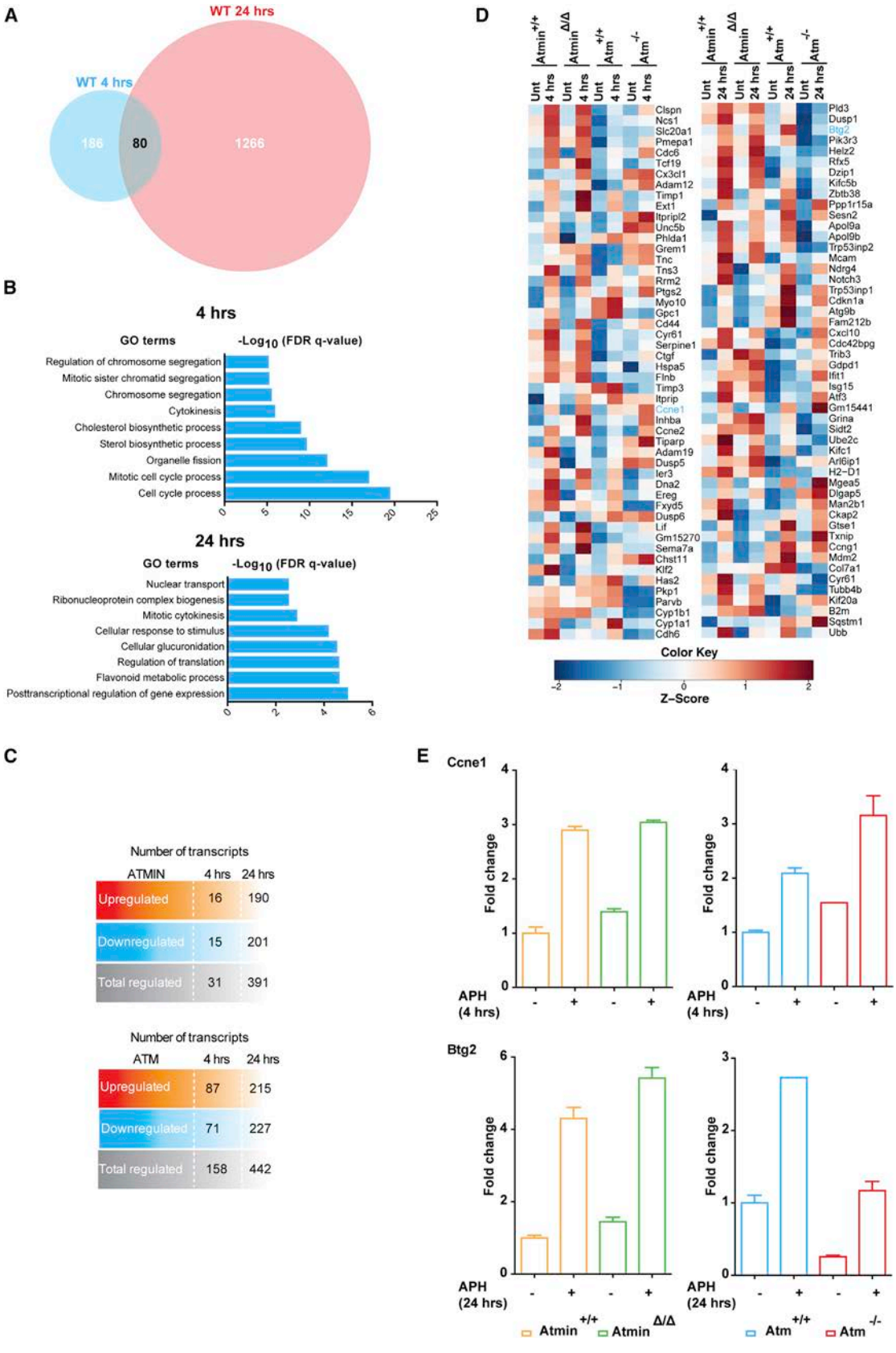

(legend on next page)

at 4 hr and 24 hr post APH treatment included those related to cell-cycle regulation and response to stimuli (Figures 2B and S2B).

Next, we identified APH responsive genes that require ATMIN or ATM as those genes that are APH responsive in WT cells but not in ATMIN- or ATM-deficient cells (Figure S2A). By applying an adjusted p value cutoff of <0.01, we found that ATM influenced the expression of around 59.4% and 32.8% of APH-responsive genes at 4 hr and 24 hr post treatment, respectively, compared to ATMIN, which modulated the expression of 11.7% at 4 hr and 29% at 24 hr post APH treatment genes (Figures 2C, S2A, and S2C; Table S1). These data highlight the importance of both ATM and ATMIN in regulating gene expression following replication stress induced by APH, but also reveal their requirement in regulating gene expression in the absence of exogenous stress (Figure S2D). The 50 most significantly downregulated genes in *Atmin*-deficient or *Atm*-deficient cells are displayed in Figure S2E. The effect of ATMIN or ATM loss on the expression of the 50 most significantly upregulated APH responsive genes in WT cells is shown in Figure 2D. Among these, the expression of several genes required for cell-cycle regulation was altered in an ATMIN- and/or ATM-dependent manner, including Cyclin E1 (*Ccne1*) and B Cell Translocation Gene 2 (*Btg2*) (Figure 2D). BTG2 plays an important role in the regulation of the cell division cycle via downregulation of *Ccne1* biosynthesis, along with CDK4 activity (Corrente et al., 2002). qRT-PCR was used to independently confirm these data (Figure 2E). In summary, this dataset has allowed for the identification of APH responsive genes and moreover has revealed the extent to which ATM and ATMIN are required to alter the regulation of these genes.

Time-Resolved Phosphorylation Dynamics Mediated by ATM and ATMIN in Response to Replication Stress

Next, we investigated the impact of replication stress on protein phosphorylation and the requirement of ATM and ATMIN in this process. By analyzing WT cells as well as *Atm*- and *Atmin*-deficient cells in the presence or absence of APH (4 hr and 24 hr APH exposure), we identified a total of 13,801 unique phosphorylation sites within 4,094 proteins, with a false discovery rate (FDR) of <0.1% for peptide and <1% for proteins (Figure 3A). The distribution of the individual phosphorylated residues (serine [S] = 80.6%, threonine [T] = 16.7%, tyrosine [Y] = 2.7%) and the number of phosphoryl groups per peptide were comparable to published data (Bensimon et al., 2010; Bodenmiller et al., 2007; Olsen et al., 2006) (Figures 3A and S3A). Of the identified phosphorylation sites, 27.3% have not been reported previously in the PhosphoSitePlus database (Figure 3B).

We defined significant time-resolved APH-induced alterations in phosphopeptides in WT MEFs using both an adjusted p value cutoff of 0.05 (herein referred to as the "confident" sites; blue dashed line) as well as a more stringent unadjusted p value cutoff of 0.001 (herein referred to as the "less stringent" sites; black dashed line) (Figures 3C, 3D, and S3B). Our motivation in selecting these two cutoffs was to acquire a broader perspective of the phosphorylation landscape. We illustrate the phosphorylation of proteins known to be required for DNA replication, the DNA damage response, and cell-cycle progression as green dots in Figures 3C and 3D. For example, following early replication stress, we observed phosphorylation of H2AX (at S137 and S140), CDK2/3 (at T14 and Y15), TP53 (S307; p53), MCM3 (T719), and RIF1 (S1565). Following late replication stress, we identified additional phosphorylation sites on H2AX (S121, S122, S137, and S140). We also identified phosphorylation sites on BRCA1 (S686, S706, S717), MCM6 (S704 and S762), MDC1 (S157, S176, and S943), SMC3 (S1065 and S1067), RFC1 (S281), TP53 (S307 and S309), and TRIM28 (S473; KAP1), among many others (Figures 3C and 3D; Tables S2 and S3). Of note, phosphorylation of MDC1 at S943 and of RFC1 at S281 had not previously been identified. To identify which pathways are represented by changes in phosphorylation events following APH exposure, we used GO enrichment analyses. This revealed the pathways of nucleic acid metabolism and chromatin assembly and/or disassembly to be among the most significantly represented at 4 hr post APH treatment (Figure 3E). At 24 hr post APH, the pathways of cell cycle, DNA repair, DNA damage response, and nucleosome assembly were most significantly enriched (Figure 3E).

To gain insights into the protein sequences that were preferentially phosphorylated upon APH treatment, we generated a motif representation of the overrepresented phosphosites (Figures 3F and S3C). The ATM superfamily of kinases is known to target SQ/TQ substrate motifs for phosphorylation. As expected, we identified the SQ motif in the group of sites that increased in phosphorylation, comprising ~50% of the detected replication-stress-responsive phosphorylation sites at 4 hr and a relatively small fraction (~10%) at 24 hr. Other overrepresented motifs were SP, SD, TP, and TE (Figures 3F and S3C), which is in line with phosphorylation events reported in response to the radiomimetic drug neocarzinostatin (NCS), which generates DNA double-strand breaks, as well as other lesions (Bensimon et al., 2010).

Figure 2. Dynamic Analyses of Transcriptional Responses to APH-Induced Replication Stress

(A) Venn diagram illustrating the overlap of genes that are differentially expressed (adjusted p value < 0.01) in both wild-type MEF cell lines treated with APH for 4 hr or 24 hr compared to untreated cells.

(B) Gene ontology (GO) enrichment analysis of the significantly differentially expressed genes in wild-type MEFs upon APH treatment (1 μM APH compared to DMSO), at the indicated times. The x axis represents $-\log_{10}$ values of the multiple-test corrected p values.

(C) Numbers of APH-responsive transcripts that are ATM or ATMIN dependent at 4 hr or 24 hr post treatment (adjusted p value < 0.01). See Figure S2A for details.

(D) Heatmaps illustrating the 50 most significantly upregulated APH responsive genes in both wild-type MEF cell lines treated for 4 hr or 24 hr compared to DMSO. The effects of ATMIN and ATM deficiencies on the expression of these genes are displayed as well. Genes marked in blue are validated experimentally in (E). *Z* score normalized values are shown.

(E) mRNA expression analysis of indicated genes by qRT-PCR. Expression of mEF1α was used as a reference. Error bars indicate SEM (n = 2). GO, gene ontology; Unt, untreated.

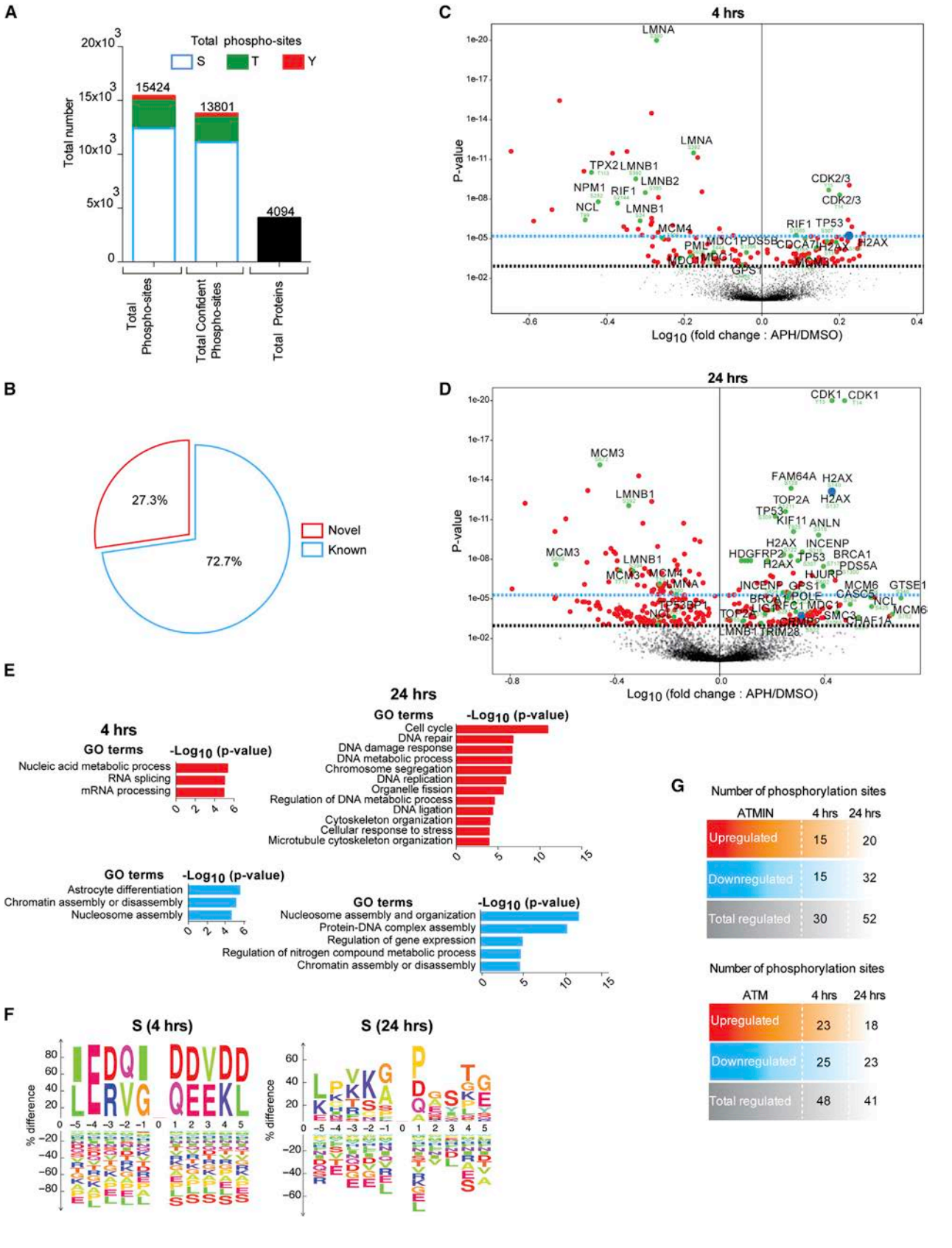

(legend on next page)

Using the same analytical approach utilized previously for gene expression (Figure S2A), we identified 73.8% of phosphorylation sites to be modulated by ATM following early replication stress (4 hr [Figures 3G and S3D], by applying a p value cutoff of 0.001; data correlating the biological replicates at early and late time points are shown in Figure S3E). These data highlight an important role for ATM in the early response to replication stress induced by APH. Around 52.6% of the APH-induced phosphorylation events were found to be regulated by ATM at the late time point of 24 hr. At early replication stress (4 hr) ATMIN modulated 46.2% of the APH-responsive phosphorylation sites compared to 66.7% for 24 hr post treatment. Approximately 30% of the APH-dependent phosphorylation sites that are ATM dependent are also ATMIN dependent, hence demonstrating the importance of ATMIN as an ATM cofactor (Figure S3D). Yet, the phosphorylation sites that are not shared between ATMIN and ATM raise the possibility that ATMIN potentially regulates these phosphorylation events on multiple substrates independently of ATM (Figures 3G and S3D).

Next, we systematically investigate the dynamic relationship between putative kinase-substrate and phosphatase-substrate networks that may correspond to the phosphosites regulated by replication stress using the NetworKIN software (Horn et al., 2014). In addition to ATM and PRKDC (DNA-PKcs) (Figure S4, blue squares), multiple other kinases were predicted to respond to replication stress based on the observed phosphosite changes (gray squares) including CDKs and ABL1, among many others. These results suggest that replication-stress-induced phosphorylation mediated via the use of APH is considerably wider than PIKK-mediated phosphorylation events.

ATMIN Mediates the Phosphorylation of Multiple Substrates in a Stress- Dependent Manner

An additional analytical approach was taken to display ATM- or ATMIN-dependent phosphorylation substrates. First, ATMIN- or ATM-deficient cell lines were compared to their corresponding WT cells (in the presence or absence of APH) (Figure S3F). Next, the significant ATM- or ATMIN-dependent phosphorylation sites were selected if they were APH responsive in WT cells and unchanged in unperturbed cells (Figures 4A and S5, blue and red dots). This led to the identification of several ATMIN-dependent phosphorylation sites on proteins known to be involved in the DNA damage response, as noted by the altered phosphorylation of several DNA replication and repair factors (Figure 4A, green hollow circles). At 4 hr post APH treatment the following ATMIN-dependent phosphoproteins, among others, were diminished in phosphorylation: RIF1 (at S2144), PML (at S609), and MCM4 (at T109) (Table S3). At 24 hr post APH, the following ATMIN-dependent phosphoproteins were reduced in phosphorylation: POLE (at T2020), PML (at S490), and MCM6 (at S704) (Table S3). We identified H2AX (also known as H2AFX) to be phosphorylated upon APH treatment in an ATMIN-dependent manner (at S140) at 4 hr post APH treatment and at two phosphorylation sites (S122 and S140) at 24 hr post APH exposure.

We constructed a putative ATMIN-dependent kinase/phosphatase-substrate network using NetworKIN for all the significantly induced phosphorylation sites by comparing WT cells to ATMIN-deficient cells following APH treatment, over time (Figure 4B; ATMIN-dependent substrates are illustrated as red octagons with black borders). The resulting network revealed substantial involvement of multiple kinases dependent on ATMIN for the cellular response to replication stress, including CDK5 and GSK3B (Figure 4B).

ATMIN is an essential Zn^{+2} finger protein that functions as a transcription factor during development, where it regulates expression of Dynll1 (Figure S2E) (Jurado et al., 2012). To exclude the possibility that ATMIN regulates the identified phosphoproteins via transcription, similarly we investigated the expression levels of all the significantly induced phosphproteins by comparing WT cells to ATMIN-deficient cells (4 hr and 24 hr post APH treatment). Given the good reproducibility of the biological replicates (Figure S6A), we were able to exclude ATMIN-dependent genes (Figure 4A) that displayed altered expression upon loss of ATMIN (Figure S6B), hence leading to the identification of ATMIN-dependent phosphorylation substrates that are independent of transcription (Figure 4C, bold).

H2AX Phosphorylation in Response to APH Requires ATMIN

We chose to validate the phosphorylation of H2AX at S140 (γH2AX) that we observed to be both affected by APH treatment and ATMIN dependent (Figures 3C, 3D, and 4A, dark blue dots; Figure 5A). Manual inspection of the respective MS spectrum

Figure 3. Identification of Proteome-wide Phosphorylation Changes Dependent on ATM and ATMIN, in Response to APH-Induced Replication Stress

(A) Total number of phosphorylation sites and proteins, which were confidently identified. The proportion of phosphorylated serine (S), threonine (T), and tyrosine (Y) residues is also indicated.

(B) Percentage of novel and known phosphorylation sites identified based on the PhosphoSitePlus database.

(C and D) Analysis of phosphorylation events occurring in wild-type MEFs treated with 1 μM APH for 4 hr (C) or 24 hr (D), compared to DMSO treated cells. Volcano plots display the decimal logarithm of the fold change plotted against the p value. Black dashed lines indicate the significance cutoff for the identification of "confident" sites, and blue dashed lines indicates the significance cutoff for the identification of "less stringent" sites (as defined in the manuscript). Green dots indicate phosphorylation sites on DNA damage response proteins. Red dots indicate phosphorylation sites on other proteins that have not previously been implicated in the DNA damage response. Blue dots indicate the phosphorylation of H2AX at S140 that is validated experimental in following sections.

(E) Gene ontology (GO) enrichment analysis of the significantly increased (red) or decreased (blue) phosphorylation events in wild-type MEFs upon APH treatment (1 μM APH compared to DMSO), at the indicated times. The x axis represents the $-\log_{10}$ of the p value.

(F) Ice-Logo plots indicating the frequency of five amino acids flanking each side of phosphorylated serine residues (0 position) that are significantly increased in phosphorylation in wild-type MEFs (APH compared to DMSO) at the indicated times.

(G) Number of ATMIN- and ATM-dependent phosphorylation sites induced upon APH treatment at 4 hr or 24 hr.

See Figure S3D for details.

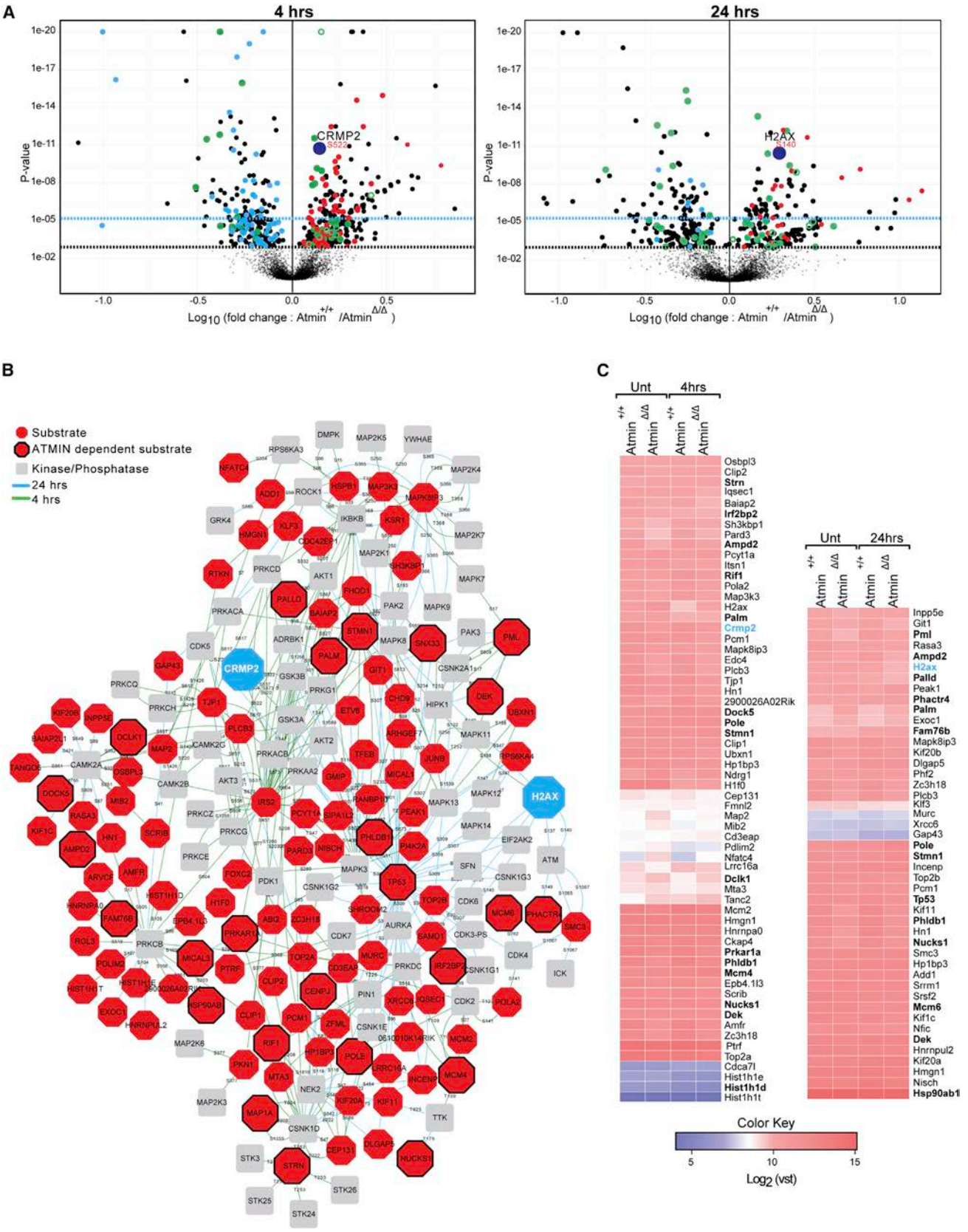

(legend on next page)

confirmed the correct identification and phosphosite assignment of S140 on H2AX (Figure 5B). Immunoblotting provided further support for a reduction in the APH-induced phosphorylation of H2AX in cells lacking ATMIN, at both early and late time points after treatment (Figure 5C). Moreover, immunofluorescence indicated that although γH2AX accumulated in control MEFs upon APH treatment, this was reduced in MEFs lacking ATMIN (Figures 5D and 5E). Taken together, these data confirm the results of the MS-based approach that identified ATMIN-dependent γH2AX accumulation.

Next, we investigated the effect of ATMIN on the clearance of γH2AX. We found that γH2AX decreased over a 6-hr repair period upon removal of APH from WT cells. In contrast, the phosphorylation of H2AX remained substantially low, but unchanged, in ATMIN-null cells 6 hr after APH removal (Figure 5F). Thus, ATMIN appears to promote the accumulation of γH2AX during the DNA damage response.

CRMP2 Is a Replication-Dependent Phosphoprotein Requiring ATMIN

Next, we chose to validate the ATMIN- and APH-dependent phosphorylation of the Collapsin response mediator protein-2 (CRMP2), a protein not previously implicated in the DNA damage response. CRMP2 (also known as DPYSL2) is a largely cytosolic multifunctional adaptor protein that has been shown to mediate the addition of tubulin dimers to the growing microtubule (Fukata et al., 2002). Additionally, CRMP2 has high sequence homology to the dihydropyrimidinase enzymes (DPYS) responsible for uracil and thymine catabolism; however, CRMP2 itself has no known enzymatic activity. CRMP2 has also been studied extensively in the context of the CNS and is associated with several neuropathological or psychiatric conditions including Alzheimer's disease (AD) and schizophrenia (Hensley et al., 2011). CRMP2 appears to be involved in many essential neurophysiological functions as well as in different cellular processes in other tissues including vesicle transport, migration, and mitosis (Hensley et al., 2011). Interestingly, nuclear CRMP-2 phosphorylated at T514 has been linked to poor prognosis in non-small-cell lung cancer (NSCLC) and was found to interact with the mitotic spindle in a phosphorylation-dependent manner in NSCLC cells (Oliemuller et al., 2013). Given these observations, we decided to investigate the role of CRMP2 phosphorylation induced by replication stress. First, we treated ATMIN-proficient and -deficient MEFs with APH for 4 hr or 24 hr. We noted a time-dependent increase in the phosphorylation of CRMP2 at S522 in WT cells, but not cells lacking ATMIN (Figure 6A), supporting the MS data (Figures 3D and 4A, dark blue dot). Importantly, the total protein levels of CRMP2 remained unchanged in response to replication stress and/or loss of ATMIN. We confirmed these findings by immunofluorescence, where we noted a time- and ATMIN-dependent increase in phosphorylation of CRMP2-S522 upon APH treatment of MEF cells (Figures 6B and 6C). The specificity of the phospho-S522 CRMP2 antibody is illustrated in Figure S7A.

To understand the cellular function of CRMP2 and the APH-induced phosphorylation of S522, we generated CRMP2-depleted cells using three independent short hairpin RNAs (shRNAs) (Figure 6D). Cell-cycle analysis of human A549 cells treated with APH for different durations showed that the distribution of G1, S, and G2/M populations in cells expressing CRMP2-specific shRNAs was comparable to control cells (Figure S7B). However, loss of CRMP2 impaired cell-cycle progression recovery following APH-induced stress. Surprisingly, upon release from APH-induced stress, cells depleted for CRMP2 showed a blockage in G1 and delayed progression through S phase (Figure S7C), suggesting that CRMP2 is involved in the resumption of normal cell-cycle kinetics following replication stress.

Efficient depletion of CRMP2 also triggered an increase in phosphorylation of TP53 at S15 upon APH treatment, indicative of increased apoptosis and/or cell-cycle arrest (Kruse and Gu, 2009; Shaw, 1996) (Figure 6D). To determine whether CRMP2-depleted cells display increased levels of DNA damage in response to APH, triggering increased S15-TP53, we evaluated H2AX phosphorylation. Depletion of CRMP2 led to diminished levels of γH2AX both by immunoblotting (Figure 6E) and immunofluorescence (Figures 6F, 6G, S7D, and S7E). Under these conditions phosphorylation of the ATM target, KAP1, was modestly effected (Figure 6E). Furthermore, the two shRNAs that gave the most pronounced knockdown of CRMP2 (shCRMP2-1 and shCRMP2-2) vastly reduced survival and proliferation as measured by a clonogenic assay (Figure S7F). A hallmark of H2AX-deficient cells is an accumulation of chromosomal

Figure 4. ATMIN Is an Important Regulator of APH-Induced Phosphorylation

(A) Analysis of APH-induced phosphorylation sites in wild-type (*Atmin*$^{+/+}$) cells compared to ATMIN-deficient cells (*Atmin*$^{\Delta/\Delta}$) in a time-dependent manner. Volcano plot shows the decimal logarithm of the fold change and the p value. Black dashed lines indicate the significance cutoff for the identification of "confident" sites, and blue dashed lines indicate the significance cutoff for the identification of "less stringent" sites, as previously defined. Green dots represent phosphorylation sites that occur on known DNA damage response proteins. ATMIN-dependent phosphorylation sites that are induced by APH are represented by red dots, and sites that are reduced upon APH treatment in an ATMIN-dependent manner are represented by blue dots. Green hollow circles represent ATMIN-dependent phosphorylation sites that occur in on known DNA damage response proteins. Black dots represent all remaining APH-induced phosphorylation sites obtained by comparing wild-type (*Atmin*$^{+/+}$) cells to ATMIN-deficient cells (*Atmin*$^{\Delta/\Delta}$). The two dark blue dots highlight two ATMIN- and APH-dependent substrates (CRMP2-S522 and H2AX-S140) validated experimentally in following sections.

(B) NetworKIN predictions of the kinase-substrate and phosphatase-substrate networks for APH-induced phosphorylation sites that are reduced in ATMIN-deficient cells (*Atmin*$^{\Delta/\Delta}$) compared to wild-type (*Atmin*$^{+/+}$) cells. Gray squares denote kinases or phosphatases and red octagons denote their substrates. Red octagons with black borders represent ATMIN-dependent substrates. The edges indicate phosphorylation events occurring at 4 hr (green edges) and 24 hr (blue edges) post APH. The edges are annotated with the corresponding phosphorylation sites. The blue octagons denote two ATMIN- and APH-dependent substrates (CRMP2-S522 and H2AX-S140) validated experimentally in the following sections.

(C) mRNA expression levels of phosphoproteins that are ATMIN dependent and are not differentially expressed are illustrated with bold gene names. Expression values were obtained from the mean of two biological replicates. Genes in blue are validated experimentally in the following sections. Vst, variance-stabilizing transformation.

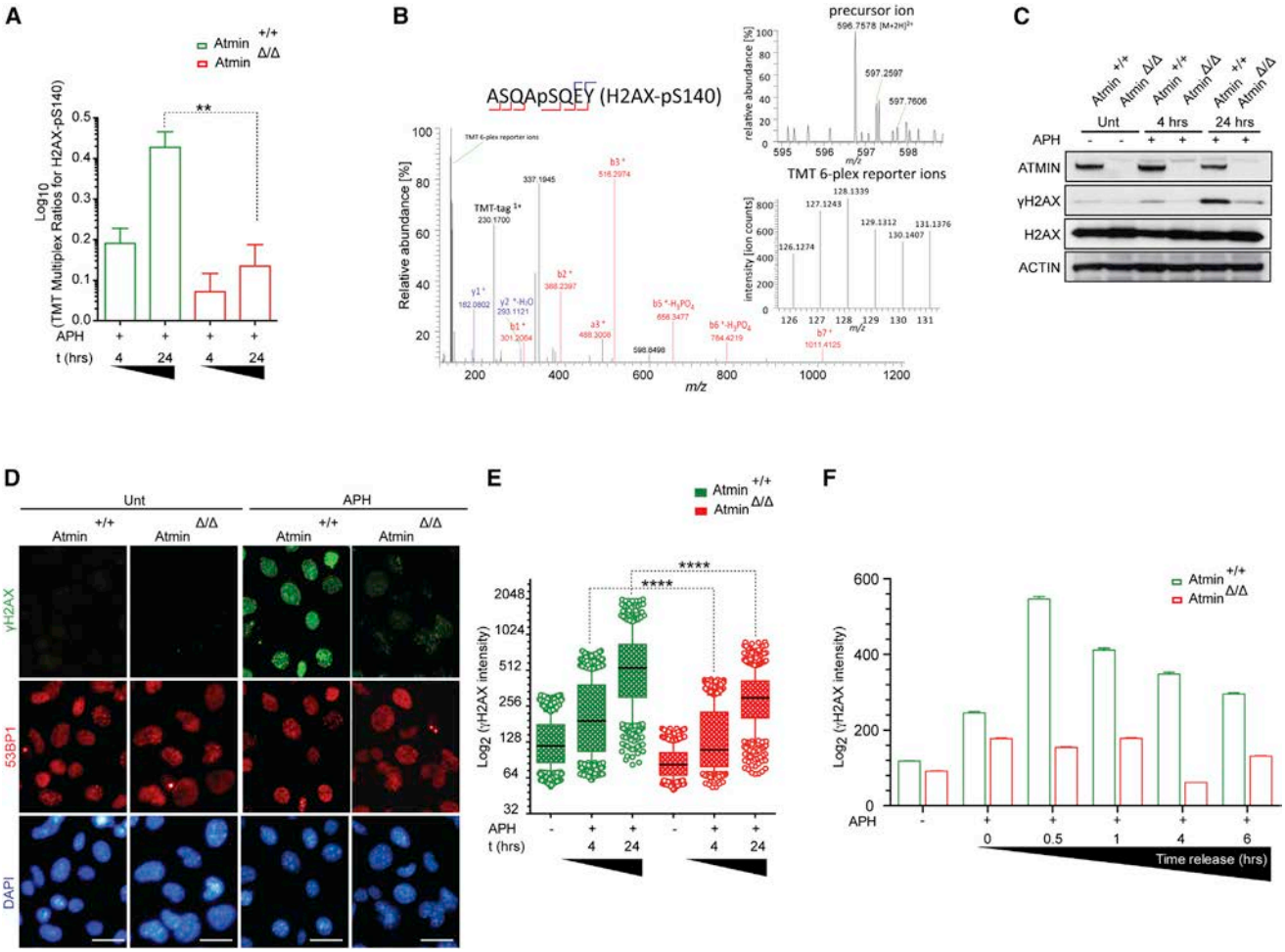

Figure 5. H2AX Requires ATMIN for Phosphorylation upon APH-Induced Replication Stress

(A) TMT Multiplex Ratios of H2AX phosphorylated at Ser-140 in ATMIN wild-type (*Atmin*$^{+/+}$) in comparison to ATMIN-deficient (*Atmin*$^{\Delta/\Delta}$) MEFs treated with APH. Data are normalized to *Atmin*$^{+/+}$ MEFs treated with DMSO at the indicated time points.

(B) TMT mass spectrometry spectra for H2AX (S140) phosphopeptide.

(C) *Atmin*$^{+/+}$ and *Atmin*$^{\Delta/\Delta}$ MEFs were treated with 1 μM APH for 4 hr or 24 hr and phosphorylation of H2AX at S-140 (known as γH2AX) was analyzed by immunoblotting.

(D) *Atmin*$^{+/+}$ and *Atmin*$^{\Delta/\Delta}$ MEFs were treated with 1 μM APH for 24 hr and immunostained with γH2AX and 53BP1 antibodies. Nuclear DNA was counterstained with DAPI. Scale bar, 10 μm.

(E) The quantification of γH2AX intensities per nucleus of *Atmin*$^{+/+}$ and *Atmin*$^{\Delta/\Delta}$ MEFs in the presence or absence of 1 μM APH (for the indicated times) of more than 1,000 cells. Black lines within each column represent median intensities. ****$p < 0.0001$ (p value was calculated by the Mann-Whitney U test).

(F) *Atmin*$^{+/+}$ and *Atmin*$^{\Delta/\Delta}$ MEFs were treated with 1 μM APH for 24 hr and then released into compound-free medium for the indicated time points. Cells were immunostained for γH2AX and displayed are γH2AX intensities per nucleus quantified for more than 1,000 cells. Error bars indicate SEM.

aberrations (Celeste et al., 2002). Indeed, CRMP2-depleted cells displayed increased micronuclei upon exposure to APH compared to control cells (Figure 6H). Taken together, these data indicate a requirement of CRMP2 to clear DNA damage upon exposure to replication stress, by preventing micronuclei formation. This could potentially be mediated via CRMP2-dependent phosphorylation of H2AX.

To investigate the role of phosphorylation of CRMP2 at S522, we reconstituted shCRMP2-3 cells (this shRNA does not affect proliferation, as opposed to shCRMP2-1 and -2) with either WT CRMP2 or CRMP2 carrying a serine to alanine mutation at position 522. We had observed that CRMP2 depletion increased the sensitivity of A549 cells to hydroxyurea (HU). HU is an alternative agent that induces replication stress by blocking the synthesis of deoxynucleotides, thus inhibiting DNA synthesis and inducing cell death more potently than APH (Figures 7A and 7B). We found that this sensitivity could be rescued by reconstitution with WT, but not with the S522A phospho mutant CRMP2 (Figures 7A–7C). Additionally, although reconstitution with the WT CRMP2 could rescue the increased sub-G1 population of apoptotic cells upon APH treatment, the S522A phospho mutant could not (Figure 7D). These data indicate that the ATMIN-mediated phosphorylation of CRMP2 is required to suppress apoptosis in response to replication stress.

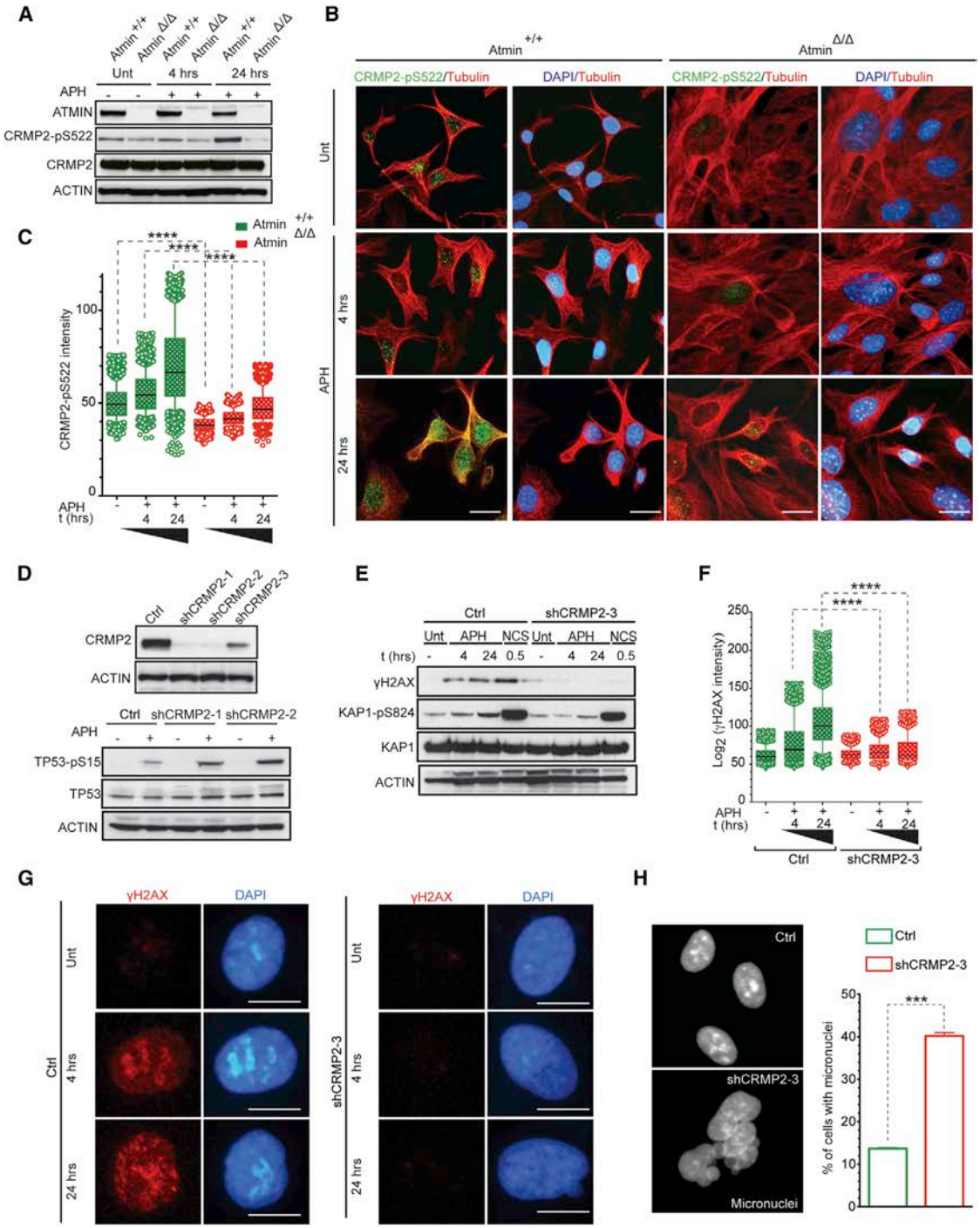

Figure 6. CRMP2 Is a Replication- and ATMIN-Dependent Phosphoprotein

(A) *Atmin*$^{+/+}$ and *Atmin*$^{\Delta/\Delta}$ MEFs were treated with 1 μM APH for the indicated times, and whole-cell extracts were analyzed for CRMP2 phosphorylation at Ser-522, by immunoblotting.

(B) MEFs were treated as in (A) and then immunostained for CRMP2-pS522 and Tubulin. DNA was counterstained with DAPI. Scale bar, 10 μm.

(C) Quantification of CRMP2-pS522 intensities per nucleus for more than 1,000 cells as in (B). Black lines inside columns represents median intensities. ****$p < 0.0001$ (p value was calculated by the Mann-Whitney U test).

(D) Top: depletion of CRMP2 in A549 cells, mediated by three independent shRNAs, is confirmed by immunoblotting using an anti-CRMP2 antibody. Bottom: CRMP2-depleted A549 cells (expressing shCRMP2-1 and shCRMP2-2 as well as a Control sequence; Ctrl) were treated with 1 μM APH for 24 hr and analyzed by immunoblotting for phosphorylated TP53 (at S15).

(legend continued on next page)

DISCUSSION

The approach we have taken to systematically map the cellular response to replication stress, for maintaining genomic integrity, relies on the combination of transcriptomics and phosphoproteomics. Here we present a global time course of the cellular response to APH-induced replication stress. Moreover, we show that the kinase ATM and its cofactor ATMIN regulate many of these changes in response to replication stress induced by APH. Although several proteome-wide studies have identified phosphorylation events regulated by DNA double-strand breaks (Beli et al., 2012; Bensimon et al., 2010; Choi et al., 2012; Matsuoka et al., 2007), to our knowledge none have investigated the cellular response to replication stress. Here, we used high-throughput MS-based proteomics and RNA sequencing to map early and late changes in the phosphoproteome and the transcriptome induced by replication stress. Furthermore, we have revealed the dynamics of the ATM-ATMIN signaling pathway in this process. The unbiased, systems-level approach presented here shows that ATMIN and ATM are required for the phosphorylation of many shared sites, establishing the importance of ATMIN as a cofactor supporting ATM kinase activity in response to replication stress (see Figure 7E). We also reveal an underappreciated role for ATM in the early response to replication stress.

ATMIN physically interacts with ATM using a short carboxy-terminal motif, in a manner analogous to how NBS1 associates with ATM (Kanu and Behrens, 2007; Zhang et al., 2012). Our data provide evidence that ATMIN modulates the phosphorylation of many sites independently of ATM. Interestingly, the putative kinase-substrate network derived from our data suggests a substantial involvement of multiple other kinases in the cellular response to replication stress. Furthermore, our data propose that ATMIN could function as a cofactor for several kinases in regulating the phosphorylation events induced by replication stress. The data derived by analyzing the requirement for ATMIN in transcription exclude the possibility that ATMIN regulates the levels of protein phosphorylation indirectly through altering gene expression. This is an important distinction since, in addition to its role as an ATM cofactor, ATMIN has been reported to also function as a transcription factor (Jurado et al., 2012). Although ATM is known to respond to a wide range of cellular stresses, most studies have focused on its role following the induction of DNA double-strand breaks. Here we highlight the importance of ATM in the context of signaling after replication stress and in regulating phosphorylation of multiple substrates, both at early and late time points. Indeed, a large-scale analysis of proteins specifically localized at stalled forks after replication stress revealed ATM recruitment to nascent chromatin at early stages of DNA replication (Alabert et al., 2014).

Our proteome-wide approach of identifying replication-stress-induced phosphorylation sites, mediated via the use of APH, revealed a requirement for ATMIN in the regulation of H2AX phosphorylation, a posttranslational modification that occurs on chromatin to amplify the DNA damage signal. Notably, in the absence of γH2AX, many DNA damage response proteins, including the mediator proteins MDC1 and 53BP1, fail to localize effectively at DNA damage sites (Celeste et al., 2002, 2003; Paull et al., 2000). It has been shown that ATMIN is required for 53BP1 localization following replication stress (Kanu et al., 2015; Schmidt et al., 2014). This suggests that ATMIN might modulate the phosphorylation of H2AX, which consequently affects the downstream localization of 53BP1 to sites of damage hence promoting errors during replication, resulting in increased micronulei and anaphase bridges (Schmidt et al., 2014).

In this study, we also identify CRMP2 as a replication-stress-dependent phosphoprotein that requires ATMIN for its phosphorylation at S522. CRMP2 is part of the aminohydrolase family of enzymes, a large metal-dependent hydrolase superfamily, yet CRMP2 lacks hydrolase activity. CRMP2 has been shown to bind microtubules and is necessary for signaling by class 3 semaphorins and subsequent remodeling of the cytoskeleton. It is known that CRMP2 interacts with the mitotic spindle and that this association is affected by its phosphorylation. The kinase CDK5 phosphorylates CRMP2 at S522. This primes CRMP2 for subsequent phosphorylation by the kinase GSK3β at residues T509 and T514 during pro-metaphase (Oliemuller et al., 2013). We observed phosphorylation of the priming residue of CRMP2 at 24 hr post APH-induced replication stress. Under such treatment conditions, cells are blocked in S phase, suggesting that CRMP2 phosphorylation at S522 has an additional role besides its function during mitosis. Since mutation of this site renders cells sensitive to replication-stress-induced DNA damage, we propose that CRMP2 plays a role in the DNA damage response. These data also suggest that ATMIN may regulate CDK5 in response to replication stress, thereby promoting the phosphorylation of CRMP2 at S522.

CRMP2 is specifically hyperphosphorylated (at S522) in the brains of AD patients within peptide-rich plaques and neurofibrillary tangles (NFTs) (Hensley et al., 2011). Our finding that ATMIN regulates CRMP2 phosphorylation suggests a link between ATMIN function and the neuropathology of AD. Furthermore, since we find that CRMP2 is phosphorylated in response to APH-induced replication stress, this suggests that the hyperphosphorylation observed in AD might be the result of replication stress originating from the abortive cell cycle in neuronal cells (known as cell-cycle re-entry) (Yang et al., 2001).

In summary, we have charted the cellular response to replication stress (induced by APH), and we highlight the importance of

(E) CRMP2-depleted A549 (shCRMP2-3) and control A549 cells (Ctrl) were treated with 1 μM APH for the indicated times or NCS (a radiomimetic compound used as a positive control, at 50 ng/mL) for 30 min and analyzed by immunoblotting with indicated antibodies.
(F) γH2AX intensities (a.u.) per nucleus of (G). Results are displayed as box and whisker plots. The black lines within each column represent median intensities. More than 1,000 cells were counted for each condition. ****$p < 0.0001$ (p value was calculated by the Mann-Whitney U test).
(G) A549 cells depleted for CRMP2 (by expressing shCRMP2-3 or the control; Ctrl) were treated with 1 μM APH for the indicated times and analyzed by immunostaining for γH2AX. DNA was counterstained with DAPI. Scale bar, 10 μm.
(H) A549 cells depleted for CRMP2 (expressing shCRMP2-3 or Ctrl) were treated with 1 μM APH for 24 hr followed by incubation in compound-free media for 8 hr and stained with DAPI. Defects in cell division, marked by micronuclei formation, were imaged and quantified. At least 200 cells were analyzed per condition. Results from two independent experiments (mean ± SEM, t test ***$p < 0.001$) are shown.

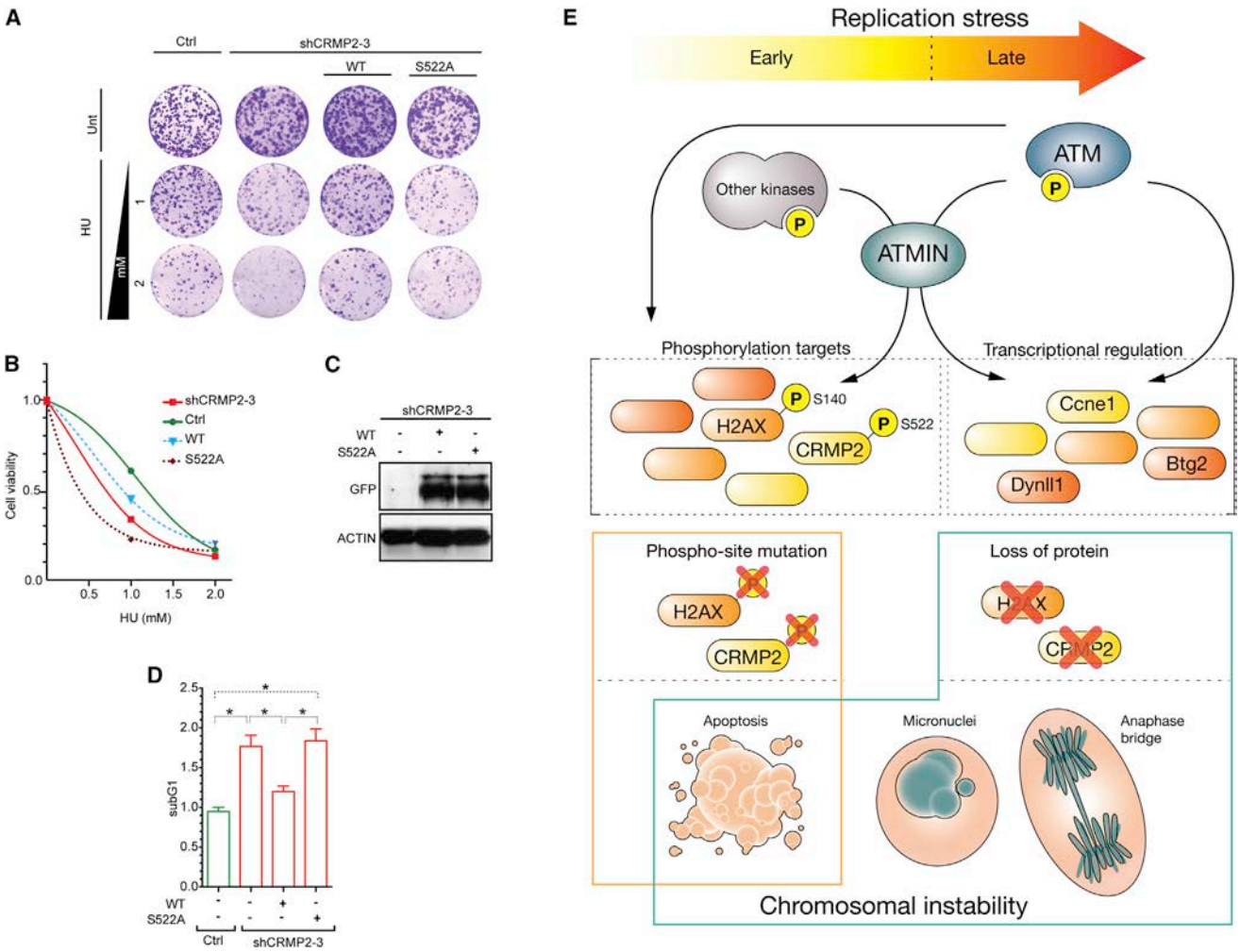

Figure 7. CRMP2 Phosphorylation at S522 Is Required for Cellular Responses to Replication Stress

(A) Clonogenic survival of A549 CRMP2-depleted cells (expressing shCRMP2-3, that targets the 3′UTR region of CRMP2) or control cells (Ctrl) were transfected with either wild-type CRMP2 (WT) or CRMP2 carrying a serine to alanine mutation at position 522 (S522A). Cells were treated with hyrdroxyurea to induce cell death via replication stress (HU; 1 mM, 2 mM) or left untreated for 24 hr, then the cells were incubated in compound-free media for 10 days.

(B) Macroscopic colonies were stained with crystal violet and quantified.

(C) The expression of the transfected constructs was confirmed by immunoblotting.

(D) Ctrl and CRMP2-depleted A549 cells (shCRMP2-3) were transfected with CRMP2 WT or S522A constructs. Cells were then treated with 1 μM APH for 24 hr, followed by incubation in compound-free media for 8 hr. Apoptotic subG1 populations were analyzed by propidium iodide staining. Results from two independent experiments (mean ± SEM, t test $^*p < 0.05$) are shown.

(E) Model illustrating the role of ATMIN and ATM in regulating phosphorylation and transcriptional events during replication stress (see main text for details).

ATM and ATMIN in regulating widespread phosphorylation events on multiple substrates, including DNA damage response factors, in a time-dependent manner. Through validating specific phosphorylation events, we identified previously unappreciated functions for ATMIN in modulating the phosphorylation of H2AX and CRMP2 (at S140 and S522, respectively). Moreover, we demonstrate that replication-stress-induced phosphorylation of CRMP2 at S522 is required for cell survival and chromosomal stability. Our findings suggest that many kinases in addition to ATM regulate the response to replication stress, perhaps employing ATMIN as a cofactor. The resource provided by our work will facilitate the discovery of new signaling pathways that function in the distinct response to DNA damage resulting from replication stress. Further, it will provide insight into pathologies that arise from replication stress.

EXPERIMENTAL PROCEDURES

Cell Culture, Plasmids, and Reagents

Atmin$^{+/+}$ and *Atmin*$^{\Delta/\Delta}$ MEFs (Kanu and Behrens, 2007) as well as *Atm*$^{+/+}$ and *Atm*$^{-/-}$ MEFs (Callén et al., 2009) were cultured in DMEM (Gibco), and A549 cells were cultured in RPMI-1640 (Gibco). All cells were grown in the presence of 10% fetal bovine serum (FBS) (Thermo Fisher Scientific) and 1% penicillin-streptomycin (Sigma-Aldrich) at 37°C with 5% CO_2 and 3% O_2. APH, NCS, and HU were purchased from Sigma. WT CRMP2 or CRMP2 S522A was

expressed from the pEGFP-C1 vector (Clontech Laboratories) and provided by Dr. Ana Rouzaut (Center for Applied Medical Research, University of Navarra, Pamplona, Spain) and Dr. Manuel Serrano (Spanish National Cancer Research Centre, Madrid, Spain). For shRNA mediated depletion of CRMP2, two shRNAs (shCRMP2-1 and shCRMP2-2) targeting the coding region of the gene (5′-CTGAGTGTGATCCGGGATATT-3′, 5′-AGCCAAAGTCTT CAACCTTTA-3′) and one shRNA (shCRMP2-3) targeting the 3′UTR region (5′-TTAAGAGCCTGTGATAGTTAC-3′) were used. The shRNA sequences were obtained from the TRCN database (http://www.broadinstitute.org/rnai/public/gene/search) and cloned into the lentiviral vector pLKO.1 (Addgene) using AgeI and EcoRI restriction sites. Insertion of shRNA sequences was verified by sequencing. Lentiviral particles were produced by calcium phosphate transfection of the shRNA containing pLKO.1 constructs along with packaging plasmids into HEK293T cells. Two days after transfection, virus-containing supernatant was harvested and filtered to remove HEK293T cells from the supernatant. A549 cells were infected with the virus-containing supernatant in the presence of polybrene (final concentration 8 μg/mL). Infected cells were selected using puromycin (2 μg/mL; Sigma-Aldrich) for 48 hr. For transfection of the CRMP2 expression constructs, the Effectene transfection reagent from QIAGEN was used.

Protein Extracts and Immunoblotting

Cells were lysed in RIPA lysis buffer supplemented with protease inhibitors (Sigma) and phosphatase inhibitors (Sigma-Aldrich, NEB). Lysates were sonicated, centrifuged, and heated with reducing sample buffer. Protein samples were separated by SDS–PAGE (3%–8% or 4%–12% gradient gels; Invitrogen) and subsequently transferred onto nitro-cellulose membranes. All primary antibodies were used at 1:1,000 dilution and secondary antibodies at 1:5,000. Antibodies used were as follows: ATM 2C1 (Santa Cruz), P-S1981-ATM (10H11.E12; NEB), ASCIZ (Millipore), P-S824-KAP1 (Bethyl Laboratories), KAP1 (Bethyl Laboratories), P-S15-TP53 (16G8; NEB), TP53 (Pab-421; CR-UK generated antibody), P-S957-SMC1 (5D11G5; Millipore), P-S345-CHEK1 (2341S; Cell Signaling Technology), CHEK1 (DCS-310; Santa Cruz), CRMP2 (ab129082; Abcam), P-S522-CRMP2 (CP2191; Biotrend), H2AX (7631P; Cell Signaling Technology), P-S140-H2AX (07-164; Millipore), GFP (3E1; CR-UK generated antibody), and β-actin (Sigma).

Immunofluorescence and Associated Microscopy

Cells were seeded onto coverslips (VWR) in 24-well plates or directly in 96-well plates. On the following day, cells were treated as indicated, washed twice with ice-cold PBS, fixed with ice-cold methanol for 20 min at −20°C, and then permeabilized with 0.5% Triton X-100 in PBS for 20 min at room temperature and blocked with 10% FCS/0.1% Triton X-100 in PBS for 1 hr with three washes (PBS) between individual steps. Primary (53BP1 [H300; Santa Cruz], P-S140-H2AX [05-636-I; Millipore], P-S522-CRMP2 [CP2191; Biotrend]) and secondary (Alexa Fluor 546 goat anti-rabbit and Alexa Fluor 488 goat anti-mouse; Invitrogen) antibodies were diluted in blocking solution (1:600) and incubated on cells for 1 hr at room temperature. Finally, cells were stained with DAPI (Sigma-Aldrich) for 20 min at room temperature in the dark. Cell images were taken on a deconvolution microscope (Leica) for slides or Operetta High Content Imaging microscope (PerkinElmer) for the 96-well plates.

Colony Formation Assay

A549 cells (at a density of 1,000 cells/well) were seeded into 6-well plates and treated as indicated for approximately 2 weeks until clear colonies formed. Then, the medium was removed and cells were washed with PBS and fixed using 3.7% PFA (paraformaldehyde). After the removal of PFA, a solution of 0.1% crystal violet in 5% ethanol was added and cells were stained overnight. The next day, staining solution was removed, wells were washed extensively, and images were taken. For quantification, Crystal Violet was extracted from cells with pure ethanol and absorbance was measured using a spectrophotometer at 595 nm.

qRT-PCR

Cells were harvested and RNA was isolated using phenol-chlorophorm extraction. RNA was treated with 1 μl DNase (Sigma) and then reverse transcribed with the SuperScript III Reverse Transcriptase protocol (Invitrogen) to obtain cDNA. An amount of 1 μg of cDNA template was used for the qRT-PCR using SYBR Green qPCR Mastermix (QIAGEN). Analysis was performed out in duplicates using expression of mEF1α for normalization of data. The PCR was performed on a 7900HT Fast Real-Time PCR System (Applied Biosystems). The following primers were used:

Ccne1: 5′-GTTCCGTTCGCCATGGTTAT-3′; 5′-CCCGGAAGTGCTTGAG CTT-3′,
Btg2: 5′-CGGTGGCTGCCTCCTATG-3′; 5′-TCCTGCCCAGCATCATC TG-3′,
mEF1α: 5′-GCAAAAACGACCCACCAATG-3′ 5′- GGCCTGGATGGTTCAG GATA-3′.

Comet Assays

The neutral comet assay was performed as described (El-Khamisy et al., 2005). For the alkali comet assay, cells at a density of 3×10^4 were treated with 1 μM APH for 4 or 24 hr or with 100 μM H_2O_2 for 10 min, as a positive control. Cells were washed in pre-chilled PBS and then mixed in 100 μl 1.2% low melting agarose (Sigma-Aldrich, type VII) maintained at 42°C. The cell suspension was then immediately layered onto pre-chilled frosted glass slides pre-coated with 0.6% agarose and maintained in the dark at 4°C for all following steps. Slides were immersed in pre-chilled lysis buffer (2.5 M NaCl, 10 mM Tris-HCl, 100 mM EDTA [pH 8.0], 1% Triton X-100, 1% DMSO [pH 10]; DMSO and Triton X added shortly before use) overnight. Slides were washed with pre-chilled distilled water (2 × 10 min) and next placed for 45 min in pre-chilled alkaline electrophoresis buffer (55 mM NaOH, 1 mM EDTA, 1% DMSO). Electrophoresis was conducted at 30 V for 25 min, followed by neutralization in 400 mM Tris-HCl [pH 7.0] for 1 hr. Finally, DNA was stained with SYBR Gold (1:10,000 dilution in H_2O; Life Technologies) for 10 min. The comet tail moment was measured for at least 100 cells per sample using the CASP image-analysis program (Końca et al., 2003).

Cell Cycle Analysis

Cells were treated with either DMSO or 1 μM APH at different time points as indicated, or treated with 1 μM APH for 24 hr and then released for different time points. Cell-cycle stages were analyzed using propidium iodide staining. Briefly, cells were harvested, resuspended in PBS, and fixed overnight with cold 70% ethanol. After centrifugation, ethanol was removed and cells were resuspended in PBS containing 1 μg/mL RNase A and 1 μg/mL propidium iodide. Finally, cells were analyzed on a FACScalibur flow cytometer. Following cell acquisition, analysis was performed using FlowJo software (Tree Star).

Statistical Analysis

Data are expressed as ± SEM unless otherwise stated. Statistical analysis of the RNA sequencing and the phosphoproteomics data can be found in the Supplemental Experimental Procedures section. All reported p values are two-tailed unless stated otherwise.

Other Methods

See the Supplemental Experimental Procedures.

ACCESSION NUMBERS

The accession number for the RNA-seq data reported in this paper is GEO: GSE72275. Processed data are available in Table S1.

SUPPLEMENTAL INFORMATION

Supplemental Information includes Supplemental Experimental Procedures, seven figures, and four tables and can be found with this article online at http://dx.doi.org/10.1016/j.celrep.2016.03.077.

AUTHOR CONTRIBUTIONS

Conceptualization, A.M. and J.I.L.; Methodology, A.M., A.S., A.C.M., D.C., M.W., J.P., and S.-C.C.; Data Curation, A.M., A.S., D.C., M.S., and F.P.B.;

Writing, A.M. and J.I.L.; Visualization, A.M., A.S., D.C., and J.I.L.; Supervision, A.P., S.F.E.-K., C.B., R.K., J.C., K.L.B., and J.I.L.; Project Administration, J.L.; Funding Acquisition, A.M., S.F.E.-K., and J.I.L.

ACKNOWLEDGMENTS

We thank Dr. A. Nussenzweig (Centre for Cancer Research, NIH) for providing the *Atm* control and knockout MEFs. CRMP2 constructs (pEGFP-C1-CRMP2 and pEGFP-C1-CRMP2-S522A) were kindly provided by Dr. Ana Rouzaut (Center for Applied Medical Research, University of Navarra) and Dr. Manuel Serrano (Spanish National Cancer Centre). We thank the Biomedical Sequencing Facility at CeMM for technical advice and for performing the next generation sequencing experiments. We also thank Drs S.P. Jackson, G. Superti-Furga, J. Lukas, K. Caldecott, and C. Schliehe for critical reading of the manuscript. Dr. B. Vilagos helped in preparing the graphical model. A.M. and J.P. were supported by a project grant from the FWF (project number P 24766-B20) to J.I.L. Additionally, A.M. was funded by a DOC fellowship from the Austrian Academy of Sciences (24102). The J.I.L. lab is supported by a Marie-Curie Career Integration Grant (project no. 321602-NonCanATM). S.-C.C. is funded by a Wellcome Trust investigator award (103844) to S.F.E.-K. CeMM is funded by the Austrian Academy of Sciences.

Received: August 24, 2015
Revised: January 21, 2016
Accepted: March 21, 2016
Published: April 14, 2016

REFERENCES

Alabert, C., Bukowski-Wills, J.C., Lee, S.B., Kustatscher, G., Nakamura, K., de Lima Alves, F., Menard, P., Mejlvang, J., Rappsilber, J., and Groth, A. (2014). Nascent chromatin capture proteomics determines chromatin dynamics during DNA replication and identifies unknown fork components. Nat. Cell Biol. *16*, 281–293.

Bartek, J., Mistrik, M., and Bartkova, J. (2012). Thresholds of replication stress signaling in cancer development and treatment. Nat. Struct. Mol. Biol. *19*, 5–7.

Beli, P., Lukashchuk, N., Wagner, S.A., Weinert, B.T., Olsen, J.V., Baskcomb, L., Mann, M., Jackson, S.P., and Choudhary, C. (2012). Proteomic investigations reveal a role for RNA processing factor THRAP3 in the DNA damage response. Mol. Cell *46*, 212–225.

Bensimon, A., Schmidt, A., Ziv, Y., Elkon, R., Wang, S.Y., Chen, D.J., Aebersold, R., and Shiloh, Y. (2010). ATM-dependent and -independent dynamics of the nuclear phosphoproteome after DNA damage. Sci. Signal. *3*, rs3.

Bodenmiller, B., Mueller, L.N., Mueller, M., Domon, B., and Aebersold, R. (2007). Reproducible isolation of distinct, overlapping segments of the phosphoproteome. Nat. Methods *4*, 231–237.

Burhans, W.C., and Weinberger, M. (2007). DNA replication stress, genome instability and aging. Nucleic Acids Res. *35*, 7545–7556.

Callén, E., Jankovic, M., Wong, N., Zha, S., Chen, H.T., Difilippantonio, S., Di Virgilio, M., Heidkamp, G., Alt, F.W., Nussenzweig, A., and Nussenzweig, M. (2009). Essential role for DNA-PKcs in DNA double-strand break repair and apoptosis in ATM-deficient lymphocytes. Mol. Cell *34*, 285–297.

Celeste, A., Petersen, S., Romanienko, P.J., Fernandez-Capetillo, O., Chen, H.T., Sedelnikova, O.A., Reina-San-Martin, B., Coppola, V., Meffre, E., Difilippantonio, M.J., et al. (2002). Genomic instability in mice lacking histone H2AX. Science *296*, 922–927.

Celeste, A., Fernandez-Capetillo, O., Kruhlak, M.J., Pilch, D.R., Staudt, D.W., Lee, A., Bonner, R.F., Bonner, W.M., and Nussenzweig, A. (2003). Histone H2AX phosphorylation is dispensable for the initial recognition of DNA breaks. Nat. Cell Biol. *5*, 675–679.

Choi, S., Srivas, R., Fu, K.Y., Hood, B.L., Dost, B., Gibson, G.A., Watkins, S.C., Van Houten, B., Bandeira, N., Conrads, T.P., et al. (2012). Quantitative proteomics reveal ATM kinase-dependent exchange in DNA damage response complexes. J. Proteome Res. *11*, 4983–4991.

Corrente, G., Guardavaccaro, D., and Tirone, F. (2002). PC3 potentiates NGF-induced differentiation and protects neurons from apoptosis. Neuroreport *13*, 417–422.

Derheimer, F.A., and Kastan, M.B. (2010). Multiple roles of ATM in monitoring and maintaining DNA integrity. FEBS Lett. *584*, 3675–3681.

Difilippantonio, S., Celeste, A., Fernandez-Capetillo, O., Chen, H.T., Reina San Martin, B., Van Laethem, F., Yang, Y.P., Petukhova, G.V., Eckhaus, M., Feigenbaum, L., et al. (2005). Role of Nbs1 in the activation of the Atm kinase revealed in humanized mouse models. Nat. Cell Biol. *7*, 675–685.

Durkin, S.G., and Glover, T.W. (2007). Chromosome fragile sites. Annu. Rev. Genet. *41*, 169–192.

El-Khamisy, S.F., Saifi, G.M., Weinfeld, M., Johansson, F., Helleday, T., Lupski, J.R., and Caldecott, K.W. (2005). Defective DNA single-strand break repair in spinocerebellar ataxia with axonal neuropathy-1. Nature *434*, 108–113.

Falck, J., Coates, J., and Jackson, S.P. (2005). Conserved modes of recruitment of ATM, ATR and DNA-PKcs to sites of DNA damage. Nature *434*, 605–611.

Fernandez-Capetillo, O., and Nussenzweig, A. (2013). Naked replication forks break apRPArt. Cell *155*, 979–980.

Flach, J., Bakker, S.T., Mohrin, M., Conroy, P.C., Pietras, E.M., Reynaud, D., Alvarez, S., Diolaiti, M.E., Ugarte, F., Forsberg, E.C., et al. (2014). Replication stress is a potent driver of functional decline in ageing haematopoietic stem cells. Nature *512*, 198–202.

Friedel, A.M., Pike, B.L., and Gasser, S.M. (2009). ATR/Mec1: coordinating fork stability and repair. Curr. Opin. Cell Biol. *21*, 237–244.

Fukata, Y., Itoh, T.J., Kimura, T., Ménager, C., Nishimura, T., Shiromizu, T., Watanabe, H., Inagaki, N., Iwamatsu, A., Hotani, H., and Kaibuchi, K. (2002). CRMP-2 binds to tubulin heterodimers to promote microtubule assembly. Nat. Cell Biol. *4*, 583–591.

Glover, T.W., Berger, C., Coyle, J., and Echo, B. (1984). DNA polymerase alpha inhibition by aphidicolin induces gaps and breaks at common fragile sites in human chromosomes. Hum. Genet. *67*, 136–142.

Guo, Z., Kozlov, S., Lavin, M.F., Person, M.D., and Paull, T.T. (2010). ATM activation by oxidative stress. Science *330*, 517–521.

Halazonetis, T.D., Gorgoulis, V.G., and Bartek, J. (2008). An oncogene-induced DNA damage model for cancer development. Science *319*, 1352–1355.

Harrigan, J.A., Belotserkovskaya, R., Coates, J., Dimitrova, D.S., Polo, S.E., Bradshaw, C.R., Fraser, P., and Jackson, S.P. (2011). Replication stress induces 53BP1-containing OPT domains in G1 cells. J. Cell Biol. *193*, 97–108.

Hensley, K., Venkova, K., Christov, A., Gunning, W., and Park, J. (2011). Collapsin response mediator protein-2: an emerging pathologic feature and therapeutic target for neurodisease indications. Mol. Neurobiol. *43*, 180–191.

Horn, H., Schoof, E.M., Kim, J., Robin, X., Miller, M.L., Diella, F., Palma, A., Cesareni, G., Jensen, L.J., and Linding, R. (2014). KinomeXplorer: an integrated platform for kinome biology studies. Nat. Methods *11*, 603–604.

Jurado, S., Gleeson, K., O'Donnell, K., Izon, D.J., Walkley, C.R., Strasser, A., Tarlinton, D.M., and Heierhorst, J. (2012). The Zinc-finger protein ASCIZ regulates B cell development via DYNLL1 and Bim. J. Exp. Med. *209*, 1629–1639.

Kaidi, A., and Jackson, S.P. (2013). KAT5 tyrosine phosphorylation couples chromatin sensing to ATM signalling. Nature *498*, 70–74.

Kanu, N., and Behrens, A. (2007). ATMIN defines an NBS1-independent pathway of ATM signalling. EMBO J. *26*, 2933–2941.

Kanu, N., and Behrens, A. (2008). ATMINistrating ATM signalling: regulation of ATM by ATMIN. Cell Cycle *7*, 3483–3486.

Kanu, N., Zhang, T., Burrell, R.A., Chakraborty, A., Cronshaw, J., Costa, C.D., Grönroos, E., Pemberton, H.N., Anderton, E., Gonzalez, L., et al. (2015). RAD18, WRNIP1 and ATMIN promote ATM signalling in response to replication stress. Oncogene, Published online November 9, 2015.

Końca, K., Lankoff, A., Banasik, A., Lisowska, H., Kuszewski, T., Góźdź, S., Koza, Z., and Wojcik, A. (2003). A cross-platform public domain PC image-analysis program for the comet assay. Mutat. Res. *534*, 15–20.

Kruse, J.P., and Gu, W. (2009). Modes of p53 regulation. Cell *137*, 609–622.

Lavin, M.F., and Kozlov, S. (2007). ATM activation and DNA damage response. Cell Cycle *6*, 931–942.

Lee, J.H., and Paull, T.T. (2007). Activation and regulation of ATM kinase activity in response to DNA double-strand breaks. Oncogene *26*, 7741–7748.

Loizou, J.I., Sancho, R., Kanu, N., Bolland, D.J., Yang, F., Rada, C., Corcoran, A.E., and Behrens, A. (2011). ATMIN is required for maintenance of genomic stability and suppression of B cell lymphoma. Cancer Cell *19*, 587–600.

López-Contreras, A.J., and Fernandez-Capetillo, O. (2010). The ATR barrier to replication-born DNA damage. DNA Repair (Amst.) *9*, 1249–1255.

Lukas, C., Savic, V., Bekker-Jensen, S., Doil, C., Neumann, B., Pedersen, R.S., Grøfte, M., Chan, K.L., Hickson, I.D., Bartek, J., and Lukas, J. (2011). 53BP1 nuclear bodies form around DNA lesions generated by mitotic transmission of chromosomes under replication stress. Nat. Cell Biol. *13*, 243–253.

Matsuoka, S., Ballif, B.A., Smogorzewska, A., McDonald, E.R., 3rd, Hurov, K.E., Luo, J., Bakalarski, C.E., Zhao, Z., Solimini, N., Lerenthal, Y., et al. (2007). ATM and ATR substrate analysis reveals extensive protein networks responsive to DNA damage. Science *316*, 1160–1166.

Mazouzi, A., Velimezi, G., and Loizou, J.I. (2014). DNA replication stress: causes, resolution and disease. Exp. Cell Res. *329*, 85–93.

Oliemuller, E., Peláez, R., Garasa, S., Pajares, M.J., Agorreta, J., Pío, R., Montuenga, L.M., Teijeira, A., Llanos, S., and Rouzaut, A. (2013). Phosphorylated tubulin adaptor protein CRMP-2 as prognostic marker and candidate therapeutic target for NSCLC. Int. J. Cancer *132*, 1986–1995.

Olsen, J.V., Blagoev, B., Gnad, F., Macek, B., Kumar, C., Mortensen, P., and Mann, M. (2006). Global, in vivo, and site-specific phosphorylation dynamics in signaling networks. Cell *127*, 635–648.

Paull, T.T., Rogakou, E.P., Yamazaki, V., Kirchgessner, C.U., Gellert, M., and Bonner, W.M. (2000). A critical role for histone H2AX in recruitment of repair factors to nuclear foci after DNA damage. Curr. Biol. *10*, 886–895.

Petermann, E., and Helleday, T. (2010). Pathways of mammalian replication fork restart. Nat. Rev. Mol. Cell Biol. *11*, 683–687.

Schmidt, L., Wiedner, M., Velimezi, G., Prochazkova, J., Owusu, M., Bauer, S., and Loizou, J.I. (2014). ATMIN is required for the ATM-mediated signaling and recruitment of 53BP1 to DNA damage sites upon replication stress. DNA Repair (Amst.) *24*, 122–130.

Shaw, P.H. (1996). The role of p53 in cell cycle regulation. Pathol. Res. Pract. *192*, 669–675.

Toledo, L.I., Altmeyer, M., Rask, M.B., Lukas, C., Larsen, D.H., Povlsen, L.K., Bekker-Jensen, S., Mailand, N., Bartek, J., and Lukas, J. (2013). ATR prohibits replication catastrophe by preventing global exhaustion of RPA. Cell *155*, 1088–1103.

Uziel, T., Lerenthal, Y., Moyal, L., Andegeko, Y., Mittelman, L., and Shiloh, Y. (2003). Requirement of the MRN complex for ATM activation by DNA damage. EMBO J. *22*, 5612–5621.

Wang, L., Paradee, W., Mullins, C., Shridhar, R., Rosati, R., Wilke, C.M., Glover, T.W., and Smith, D.I. (1997). Aphidicolin-induced FRA3B breakpoints cluster in two distinct regions. Genomics *41*, 485–488.

Ward, I.M., Difilippantonio, S., Minn, K., Mueller, M.D., Molina, J.R., Yu, X., Frisk, C.S., Ried, T., Nussenzweig, A., and Chen, J. (2005). 53BP1 cooperates with p53 and functions as a haploinsufficient tumor suppressor in mice. Mol. Cell. Biol. *25*, 10079–10086.

Yang, Y., Geldmacher, D.S., and Herrup, K. (2001). DNA replication precedes neuronal cell death in Alzheimer's disease. J. Neurosci. *21*, 2661–2668.

Zeman, M.K., and Cimprich, K.A. (2014). Causes and consequences of replication stress. Nat. Cell Biol. *16*, 2–9.

Zhang, T., Penicud, K., Bruhn, C., Loizou, J.I., Kanu, N., Wang, Z.Q., and Behrens, A. (2012). Competition between NBS1 and ATMIN controls ATM signaling pathway choice. Cell Rep. *2*, 1498–1504.

Cell Reports, Volume *15*

Supplemental Information

A Comprehensive Analysis of the Dynamic Response to Aphidicolin-Mediated Replication Stress Uncovers Targets for ATM and ATMIN

Abdelghani Mazouzi, Alexey Stukalov, André C. Müller, Doris Chen, Marc Wiedner, Jana Prochazkova, Shih-Chieh Chiang, Michael Schuster, Florian P. Breitwieser, Andreas Pichlmair, Sherif F. El-Khamisy, Christoph Bock, Robert Kralovics, Jacques Colinge, Keiryn L. Bennett, and Joanna I. Loizou

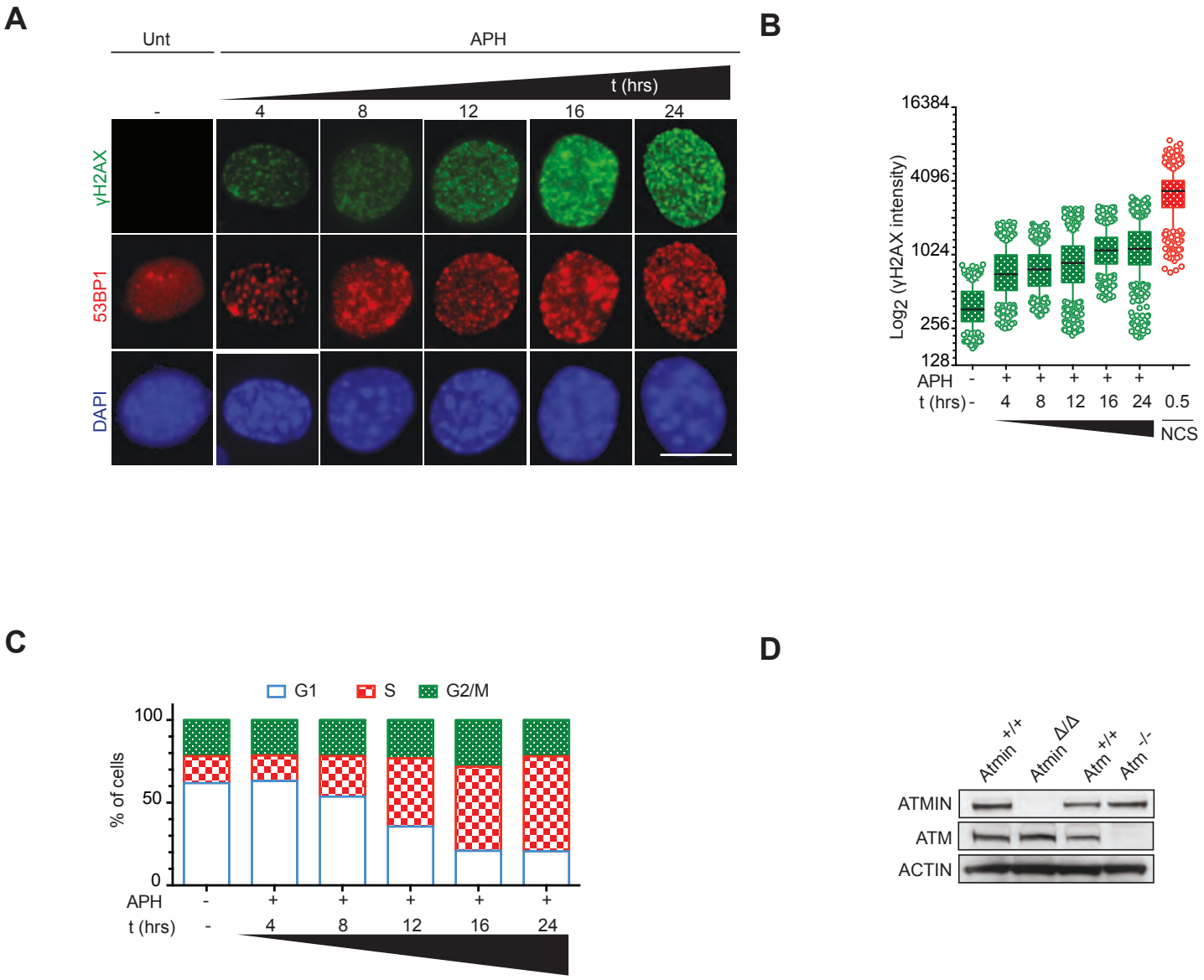

Figure S1. Cellular Responses to APH-induced Replication Stress, Related to Figure 1.

(A) Asynchronous wild-type MEFs were treated with APH (1 μM) for the indicated times, immunostained with anti-53BP1 and γH2AX antibodies and nuclear DNA was counterstained with DAPI. Scale bar, 10 μm.

(B) Box and whisker plot for the quantification of the γH2AX intensities displayed as arbitrary units, quantified for >1000 cells.

(C) Analysis of cell cycle progression using propidium iodide staining of cells treated as in A.

(D) Immunoblot of ATM and ATMIN for Atmin$^{+/+}$, Atmin$^{\Delta/\Delta}$, Atm$^{+/+}$ and Atm$^{-/-}$ MEFs. Actin was used as a loading control.

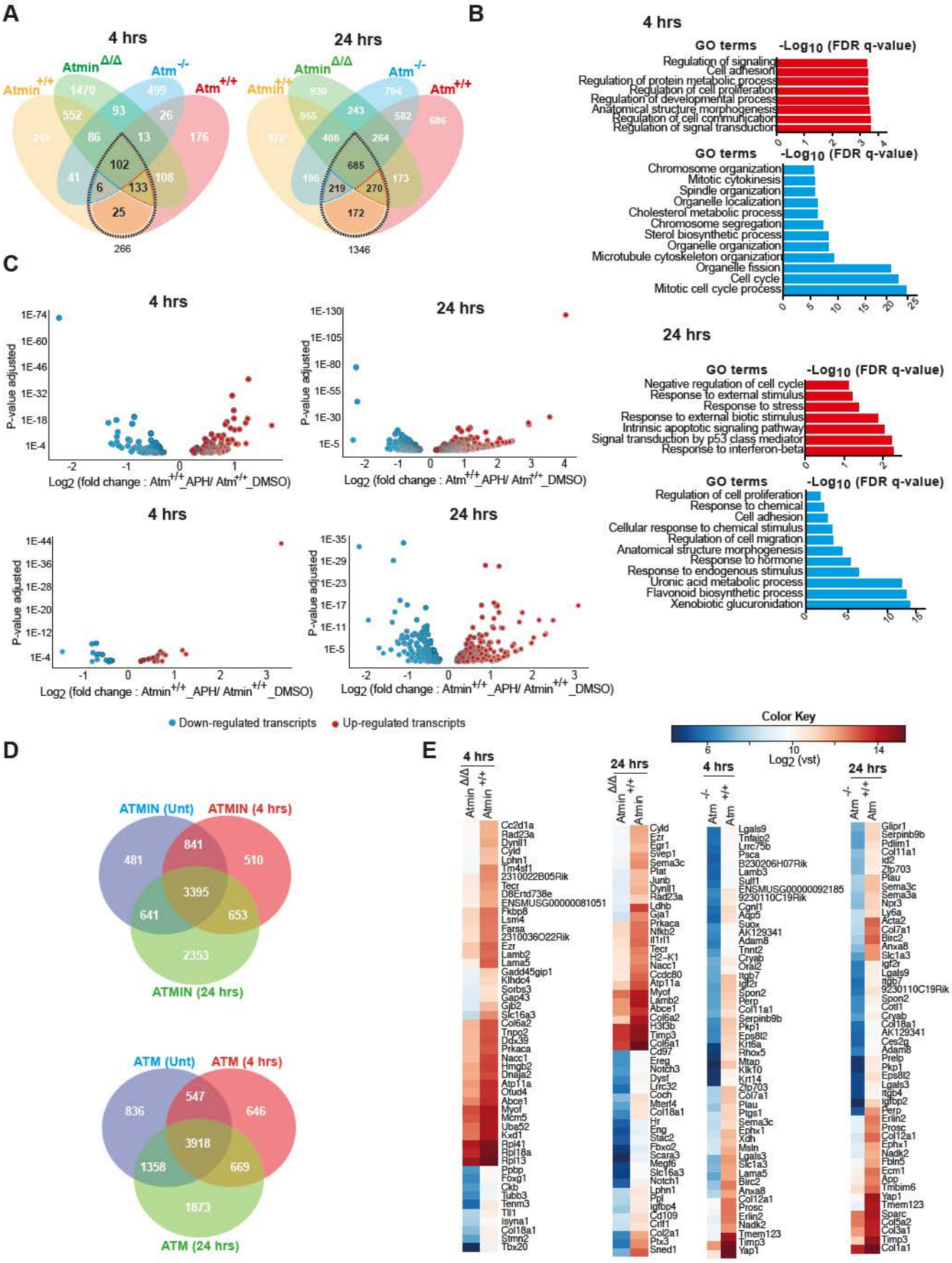

Figure S2. Transcriptional Regulation of the Cellular Response to APH-induced Replication Stress, Related to Figure 2.
(A) Venn diagrams showing the number of genes differentially expressed (adjusted p-value <0.01) in an ATMIN- and/or ATM-dependent manner upon APH treatment, for 4 hrs or 24 hrs (Atmin$^{+/+}$: Atmin$^{+/+}$ cells treated with APH/untreated Atmin$^{+/+}$; Atmin$^{\Delta/\Delta}$: Atmin$^{\Delta/\Delta}$ cells treated with APH/untreated Atmin$^{\Delta/\Delta}$; Atm$^{+/+}$: Atm$^{+/+}$ cells treated with APH/untreated Atm$^{+/+}$; Atm$^{-/-}$: Atm$^{-/-}$ cells treated with APH/untreated Atm$^{-/-}$).
(B) Gene ontology (GO) enrichment analysis for genes altered in expression in wild-type cells (increased in red and decreased in blue) following APH treatment for 4 hrs and 24 hrs.
(C) Magnitude of transcript alterations that are ATMIN and ATM dependent following 4 hrs and 24 hrs APH treatment (numbers of transcripts that are increased or decreased in expression are indicated in Figure 2C).
(D) Venn diagrams comparing ATMIN or ATM dependent transcripts (ATMIN: Atmin$^{\Delta/\Delta}$/Atmin$^{+/+}$ and ATM: Atm$^{-/-}$/Atm$^{+/+}$) for each given condition (untreated, 4 hrs and 24 hrs APH) to define ATMIN or ATM specific genes.
(E) Heatmaps depict the 50 most significantly down-regulated genes following 1 μM APH for the indicated times and genotype. The mean of two biological replicates is shown; vst, variance-stabilizing transformation; Unt, untreated.

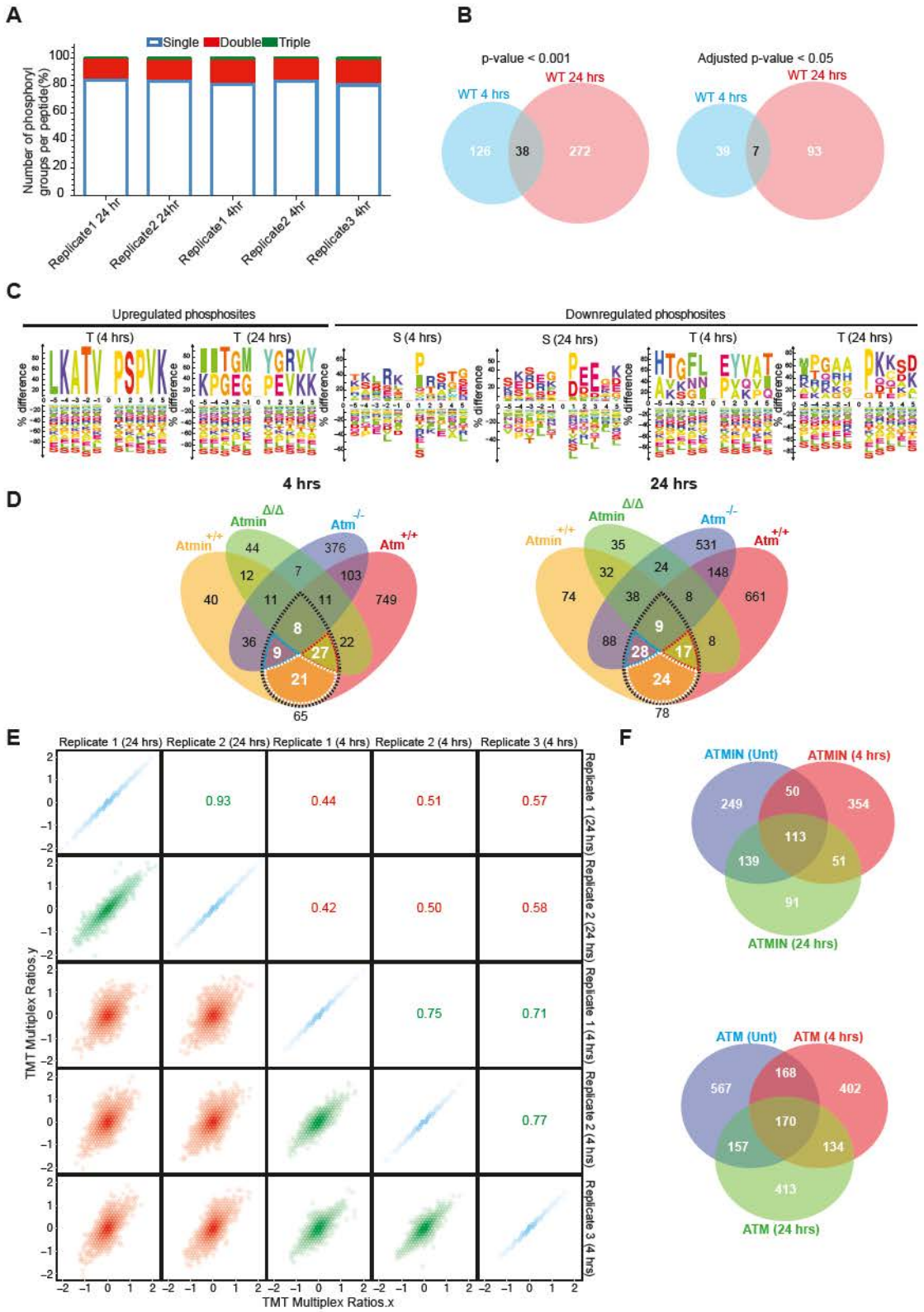

Figure S3. Samples for Proteome-wide Phosphoproteomics and Correlations Between Replicates, Related to Figure 3 and 4.

(A) The distribution of the number of phosphoryl groups per phosphopeptide. More than 80% of identified phosphopeptides identified have a single phosphorylation.

(B) Venn diagrams showing the overlap of the altered phosphorylation sites in wild-type cells ($Atmin^{+/+}$ APH treated/$Atmin^{+/+}$ DMSO treated) for 4 hrs compared to 24 hrs by applying either an unadjusted p-value of 0.001 or an adjusted p-value cutoff of 0.05.

(C) Ice-Logo plots indicating the frequency of five amino acids flanking each side of phosphorylated serine or threonine residues (positioned at '0') that are significantly up or down-regulated in phosphorylation in wild-type MEFs (APH compared to DMSO) at the indicated times.

(D) Venn diagrams showing the overlap of sites that are significantly phosphorylated (unadjusted p-value<0.001) in an ATM and ATMIN dependent manner upon APH treatment at 4 hrs or 24 hrs ($Atmin^{+/+}$: $Atmin^{+/+}$ cells treated with APH/$Atmin^{+/+}$untreated; $Atmin^{\Delta/\Delta}$: $Atmin^{\Delta/\Delta}$ cells treated with APH/$Atmin^{\Delta/\Delta}$ untreated; $Atm^{+/+}$: $Atm^{+/+}$ cells treated with APH/$Atm^{+/+}$untreated; $Atm^{-/-}$: $Atm^{-/-}$ cells treated with APH/$Atm^{-/-}$untreated).

(E) Pearson's correlation coefficient to determine the experimental reproducibility of three and two biological replicates for the phosphoproteome analyses, performed at 4 hrs and 24 hrs, respectively.

(F) Venn diagrams showing the comparison of the deregulated phosphorylation sites of each knockout to it corresponding wild-type (ATM: Atm-/-/Atm+/+ and ATMIN: AtminΔ/Δ/Atmin+/+) for each given condition (untreated, 4 hrs and 24 hrs) to define ATMIN or ATM specific phospho-sites.

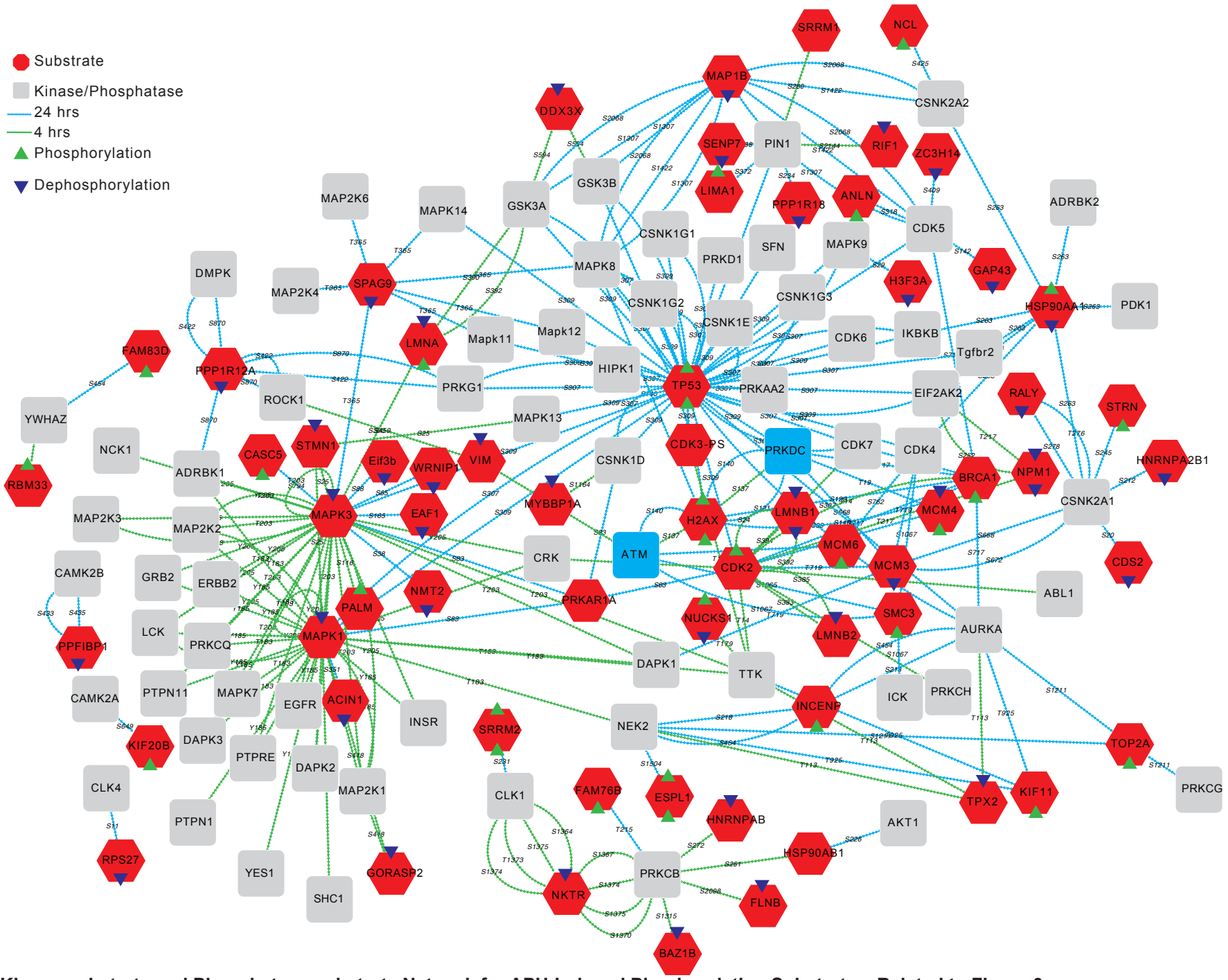

Figure S4. Kinase-substrate and Phosphatase-substrate Network for APH-Induced Phophorylation Substrates, Related to Figure 3.
NetworKIN predictions of kinase-substrate and phosphatase-substrate network for phosphorylation sites significantly induced following APH treatment in wild-type cells. Gray squares represent kinases and phosphatases that are connected to their substrates, indicated by red octagons. The edges represent phosphorylation events at 4 hrs (green edges) and 24 hrs (blue edges) post APH treatment, labeled with the phosphorylation sites. Green and dark blue triangles represent increased and decreased phosphorylation respectivelly; triangles located at the top of the red octagons correspond to 4 hrs and triangles located at the bottom represent 24 hrs APH treatment.

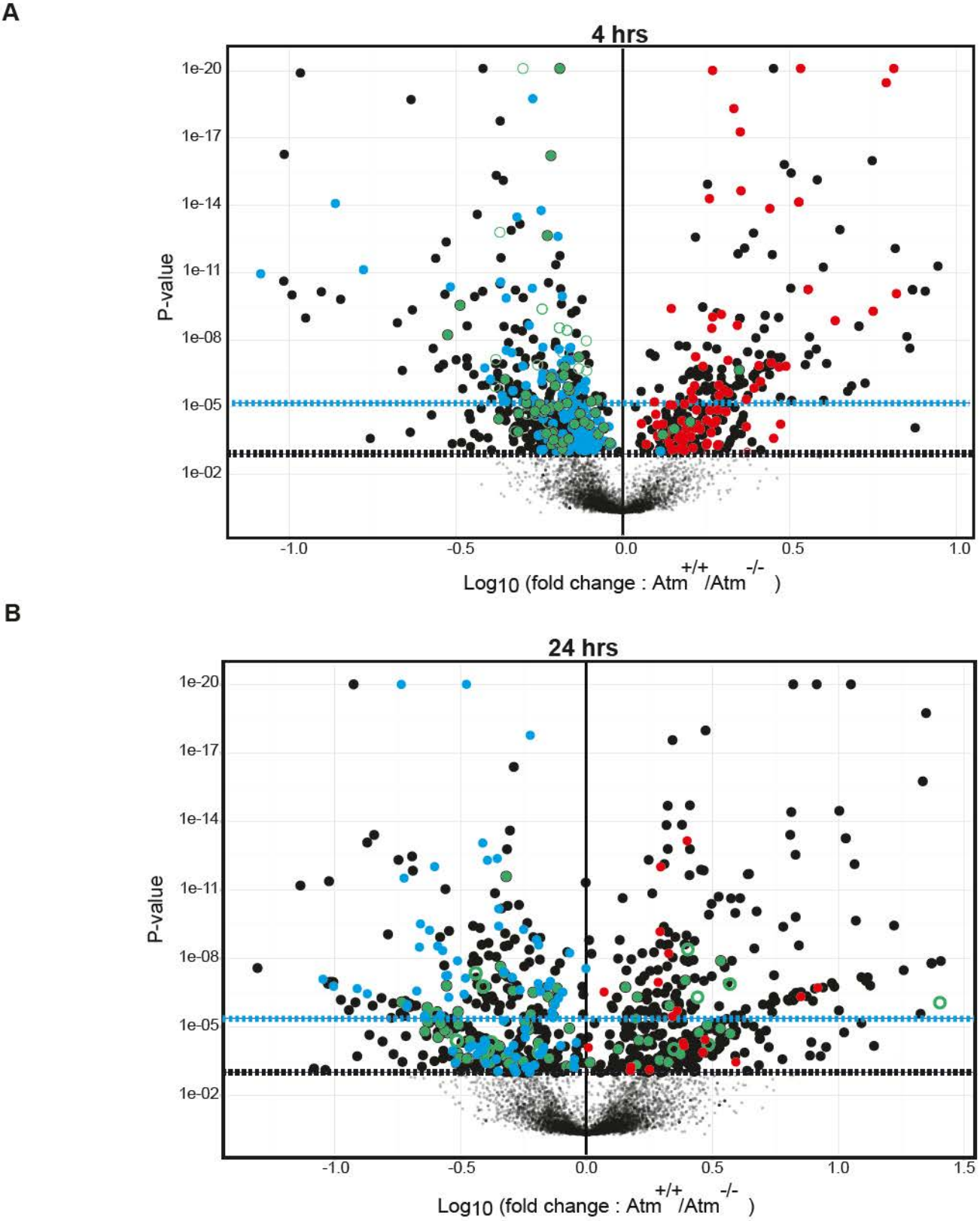

Figure S5. Phosphorylation Events Regulated by ATM, Related to Figure 4.
(A) Analysis of APH-induced phosphorylation sites in wild-type ($Atm^{+/+}$) cells treated with 1 μM APH compared to ATM knock-out ($Atm^{-/-}$) cells , at 4 hrs post APH. Volcano plot shows the decimal logarithm of the fold change and the p-value. Black dashed line indicates the significance cutoff for the identification of 'confident' sites and blue dashed line indicates the significance cutoff for the identification of 'less stringent' sites, as defined previously. Green dots represent phosphorylation sites that occur on known DNA damage response proteins. ATM dependent phosphorylation sites that are induced by APH are represented by red dots and sites that are reduced upon APH treatment in an ATM-dependent manner are represented by blue dots. Green hollow circle represent ATM-dependent phosphorylation sites that occur in on known DNA damage response proteins.
(B) Analysis performed as in (A) but at 24 hrs post APH.

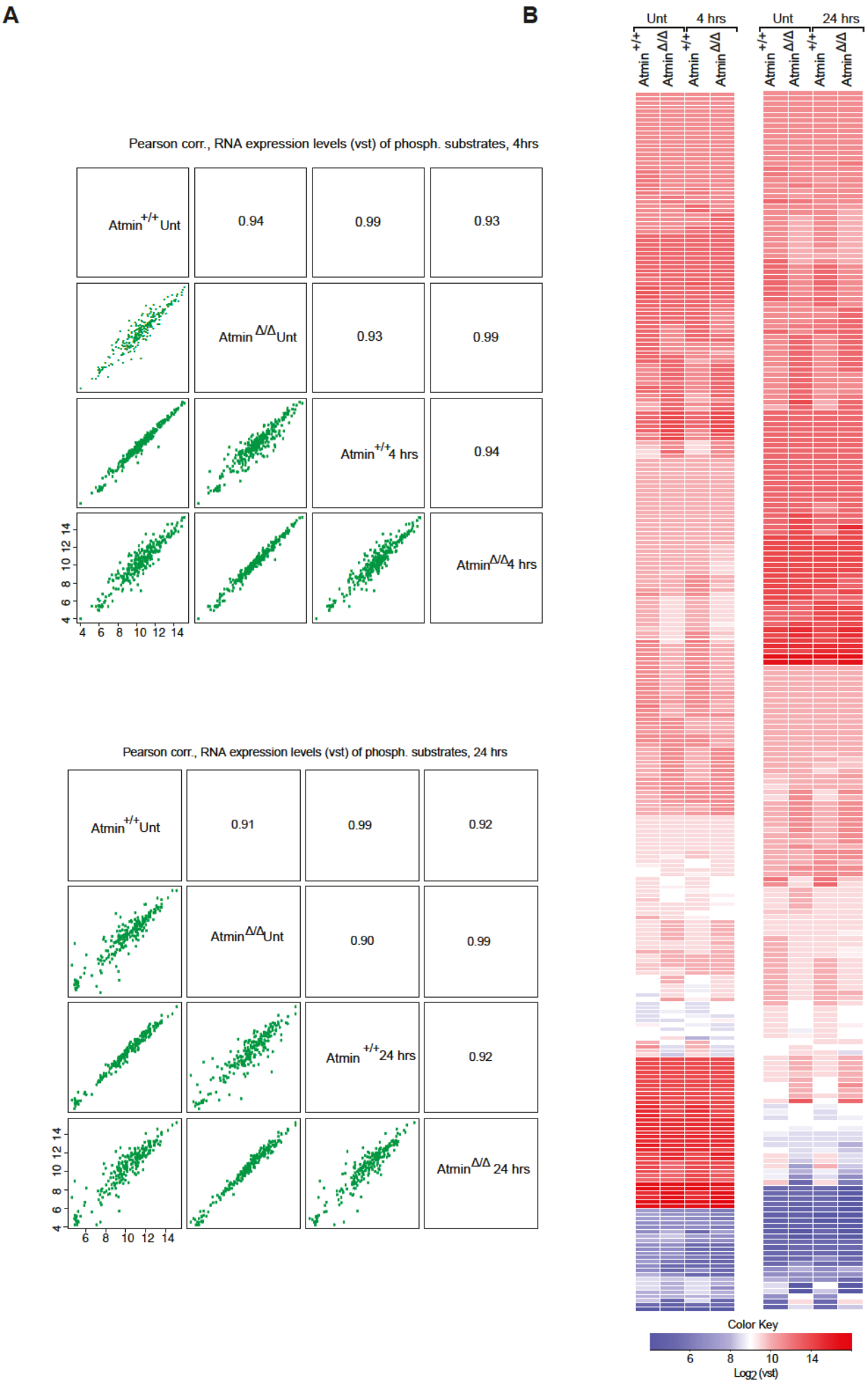

Figure S6. ATMIN Regulates Phosphorylation Events, Independent of Transcription, Related to Figure 5.

(A) Pearson's correlation coefficient of mRNA expression between two biological replicates of phosphoproteins that require ATMIN for phosphorylation with or without APH treatment for 4 hrs and 24 hrs.

(B) Heatmaps displaying gene expression values of proteins requiring ATMIN for phosphorylation following 1 μM APH (compared to DMSO) for the indicated times.

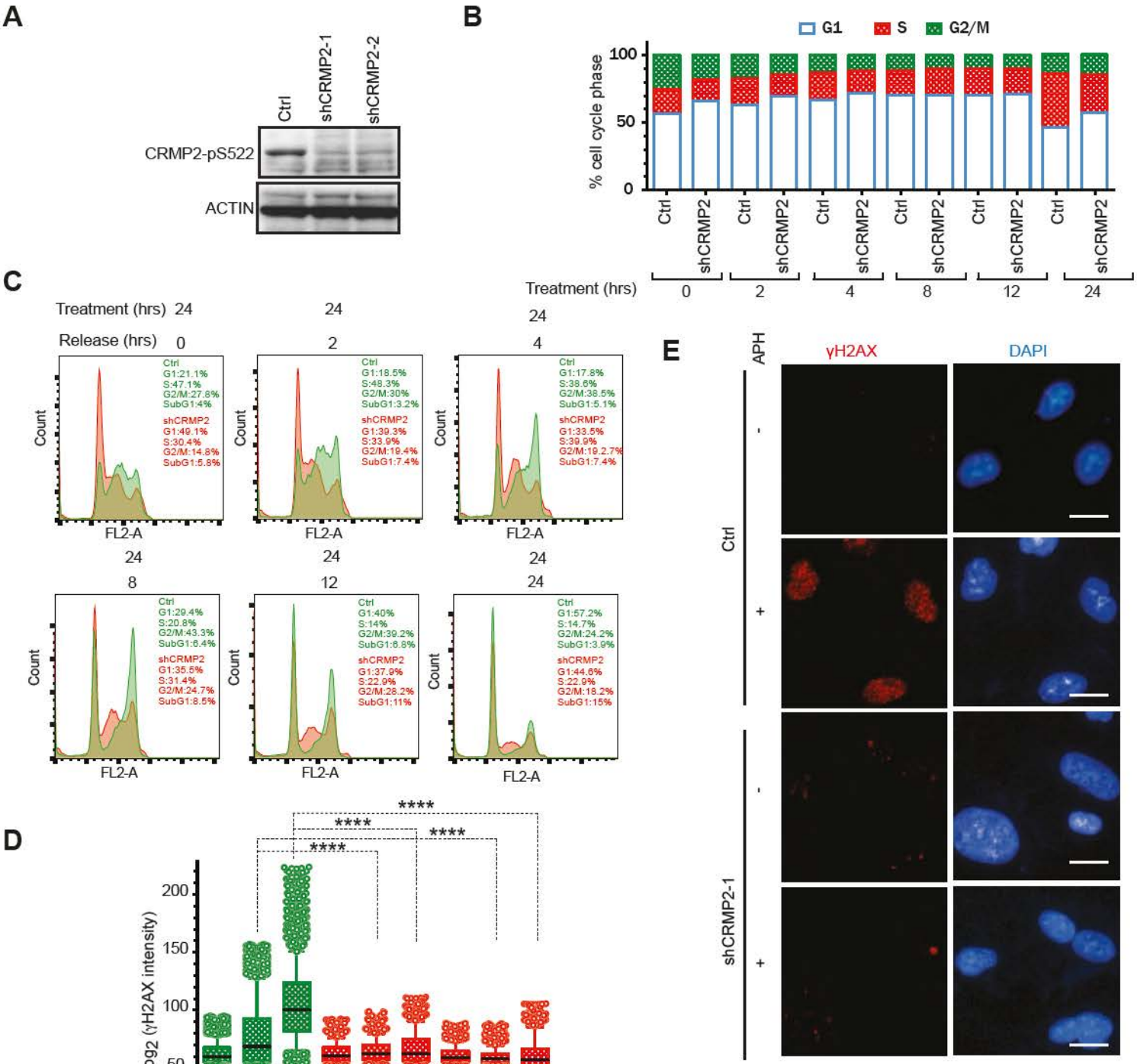

Figure S7. CRMP2 Functions in Response to Replication Stress, Related to Figure 6 and 7.

(A) A549 cells depleted for CRMP2 (shCRMP2-1 and shCRMP2-2) or control cells (Ctrl) were immunoblotted with a phospho-serine 522 CRMP2 antibody. Actin was used as a loading control.

(B) A549 cells depleted for CRMP2 (shCRMP2-2) or Control cells (Ctrl) were either treated with DMSO or 1 μM APH for the indicated times. Cell cycle profiles were determined using propidium iodide staining followed by FACS.

(C) Cells indicated in B were treated with 1 μM APH for 24 hrs then released into compound-free media for the indicated time points. Cell cycle profiles were analyzed by propidium iodide staining followed by FACS.

(D) Quantification of γH2AX intensities displayed as arbitrary units per nucleus of Ctrl or CRMP2 depleted (shCRMP2-1 and shCRMP2-2) A549 cells following treatment with 1 μM APH for the indicated times. Results are displayed as box and whisker plots and the black line within each column represents the median of the intensities. More than 1000 cells were counted for each condition. **** $P < 0.0001$ (p-value was calculated using the Mann–Whitney U-test).

(E) Representative images of the quantification in D. Scale bar, 10 μm.

(F) Clonogenic assay for A549 cells Ctrl or depleted for CRMP2 (shCRMP2-1 and shCRMP2-2). Cells were incubated for 10 days, which were fixed and stained with crystal violet.

SUPPLEMENTAL INFORMATION

Supplemental Table Legends

Table S1, Related to Figure 2. List of all genes that are significantly up or down-regulated for all given pair-wise comparisons. *Atmin_pos*: $Atmin^{+/+}$ cells treated with APH/$Atmin^{+/+}$untreated; *Atmin_neg*: $Atmin^{\Delta/\Delta}$ cells treated with APH/$Atmin^{\Delta/\Delta}$ untreated; *Atm_pos*: $Atm^{+/+}$ cells treated with APH/$Atm^{+/+}$ untreated; *Atm_neg*: $Atm^{-/-}$ cells treated with APH/$Atm^{-/-}$ untreated. The comparisons of different conditions, genes names, $\log_2$ fold-changes and adjusted *p*-value are indicated as well as expression values.

Table S2, Related to Figure 3. **Output of the Isobar analysis which contains all quantified phosphorylation sites.** Data from ATM- or ATMIN-deficient MEFs ($Atm^{-/-}$ and $Atmin^{\Delta/\Delta}$) and their corresponding controls ($Atm^{+/+}$ and $Atmin^{+/+}$) in separated replicates after 4 hrs (3 biological replicates) and 24 hrs (2 biological replicates) of APH treatment are indicated.

Table S3, Related to Figure 3 and 4. **List of all quantified phosphorylation sites that are significantly increased or decreased in phosphorylation.** Conditions are: 4 hrs and 24 hrs APH treatment (*Atmin_pos*: $Atmin^{+/+}$ cells treated with APH/$Atmin^{+/+}$untreated; *Atmin_neg*: $Atmin^{\Delta/\Delta}$ cells treated with APH/$Atmin^{\Delta/\Delta}$ untreated; *Atm_pos*: $Atm^{+/+}$ cells treated with APH/$Atm^{+/+}$ untreated; *Atm_neg*: $Atm^{-/-}$ cells treated with APH/$Atm^{-/-}$ untreated). The comparisons of different conditions, the name of proteins, the position of the phospho-sites and unadjusted and adjusted *p*-values are indicated for each comparison. All biological replicates are combined.

Supplemental Experimental Procedures

RNA Sequencing and Analysis

MEF cells were treated with DMSO or APH (1 μM) in duplicate for 4 hrs or 24 hrs. After treatment, RNA was extracted and sequencing libraries for HiSeq2000 were generated using the Truseq 2.0 kit (poly-A enrichment, Illumina). RNA libraries were sequenced with 50 bp single-end reads on a HiSeq 2000 (Illumina) machine, obtaining on average 15.5M reads per replicate. For each sample, two biological replicates were generated. Alignments to genome version mm10 and the corresponding Ensgene annotation were performed with Bowtie2 (v2.4.0)(Langmead and Salzberg, 2012) and Tophat 2 v2.0.13 (Kim et al., 2013), using a seed length of 15nt, less than 4% error rate and discarding reads with more than 100 alignment positions. Read counts per gene were generated by RPKM_count.py v2.6.1; RseQC (Wang et al., 2012), which served as input for the R Bioconductor package DESeq2 v1.6.3 (Love et al., 2014) with which normalization and differential expression was performed. Default settings were used except for a "local" dispersion fit and a multiple hypothesis adjusted *p*-value (herein refer to as 'adjusted *p*-value') cutoff of 0.01. For DESeq2 analysis, only genes covered by at least 1 read in at least 3 samples were taken into account. For data visualisation (heatmaps and Pearson correlation scatter plots), count values were first normalized by library size over all samples and subjected to variance-stabilizing transformation (as recommended by the DESeq2 authors), resulting in $\log_2$-transformed data and independence of the gene expression variances on their mean. If indicated, values displayed in heatmaps were furthermore scaled by their z-scores (per row). For heatmaps, in case of missing gene symbols, the corresponding Ensembl gene IDs were indicated; in rare cases of duplicate gene symbols, these were labelled with consecutive numbers (e.g. Akap2.1, Akap2.2). For selection of the top up- or down-regulated genes, the DESeq2 result tables were first ranked by the multiple-test corrected p-values ("padj") and subsequently split according to the sign of the $\log_2$-fold changes. For determination of not differentially expressed genes in all 4 conditions illustrated in Figure 4D, a coefficient of variation cutoff of <0.2 was selected. GO enrichment analysis was performed with the help of the GOrilla web server (http://cbl-gorilla.cs.technion.ac.il/). If not otherwise specified, plots were generated with custom R scripts.

Phosphoproteomics and Analysis

1. Sample preparation and tryptic digestion

MEF cells were treated with DMSO or APH (1 μM) in duplicate for 4 hrs and in triplicate for 24 hrs. Whole cell extracts (WCE) were prepared by lysing 1× PBS-washed cells in 2 mL 8 M urea lysis buffer containing HALT phosphatase inhibitor cocktail (1:100, Thermo Fisher Scientific Inc., USA) and 1 mM EDTA. Cell extraction and DNA shearing was assisted by sonication (S2×; Covaris Inc) and cell debris pelleted by centrifugation at 20,000 × g for 5 min at 4°C. The supernatant was removed and protein concentration determined using the 660 nm protein assay (Pierce; Thermo Fisher Scientific, Waltham, MA, USA). A total of 100 μg protein per condition was reduced with dithiothreitol (DTT, 10 mM), alkylated with iodoacetamide (55 mM), and digested with modified porcine trypsin (1:100; Promega Corp., Madison, WI,

USA) at 37°C for approximately 24 hrs. Completeness of digestion was assessed on a 1D-SDS-polyacrylamide gel visualised by silver staining. Quenched peptide digests were extracted by solid-phase extraction using Sep-Pak classic C18 cartridges (Waters Corporation, Milford, MA, USA). The peptides were eluted with 90% acetonitrile containing 100 mM of triethylammonium bicarbonate (TEAB) buffer pH 8.4 and the solvent was removed in a vacuum centrifuge at 45°C.

2. TMT6plex-labelling of tryptic peptides

100 µg of peptide-digest per cell line was resuspended in a final 500 mM TEAB buffer and labeled with TMT 6-plex™ reagents according to the manufacturer (Pierce; Thermo Fisher Scientific Inc). After 2 hrs incubation at room temperature samples were quenched and corresponding TMT-labelled samples pooled as described in Table S4.

3. Phosphopeptide-Enrichment using a Modified IMAC-Procedure

After evaporation of the solvent samples were reconstituted in 400 µL 80% acetonitrile containing 0.1% trifluoroacetic acid and used for phosphopeptide enrichment applying a modified method of immobilized metal affinity chromatography (IMAC) published by (Ficarro et al., 2009). Briefly, two times 100 µL of Ni-NTA superflow slurry (QIAGEN Inc., Valencia, USA) were washed with LCMS-grade water and Ni^{2+} stripped off the beads by incubation with 100 mM of EDTA, pH 8 solution for 1 hr at room temperature. Stripped NTA resin was recharged with Fe^{3+}-ions by incubation with a fresh solution of $Fe(III)Cl_3$ and 150 µL of charged resin used for the enrichment of a total of 600 µg TMT-labelled peptide. The unbound fraction was transferred to a fresh glass vial and approximately half (~200µg) used for offline fractionation for the analysis of the whole cell proteome. After washing the slurry with 0.1% TFA, phosphopeptides were eluted with a freshly prepared ammonia solution containing 3mM EDTA, pH 8 and all used for offline fractionation for the analysis of the phophoproteome.

4. 2d-RPRP-liquid chromatography and mass spectrometry

4. A. Offline Fractionation via RP-HPLC at high pH

Tryptic peptides were re-buffered in 20 mM ammonium formiate buffer shortly before separation by reversed phase liquid chromatography at pH 10. The unbound fraction of the phosphopeptide enrichment was separated into 50 fractions on a Phenomenex column (150 × 2.0 mm Gemini-NX 3 µm C18 110Å, Phenomenex, Torrance, CA, USA) using an Agilent 1200 series HPLC system fitted with a binary pump delivering solvent at 100 µL/min. The bound fraction containing the phosphopeptides was separated into 10 fractions on a Dionex column (500 µm × 50 mm PepSwift RP, monolithic, Dionex Corporation, Sunnyvale, CA, USA) using an Agilent 1200 series nanopump delivering solvent at 4 µL/min. Peptides were separated by applying a gradient of 90% aceonitrile containing 20 mM ammonium formiate, pH 10 as described by (Gilar et al., 2005). Collected fractions were acidified, solvent evaporated in a speed vac at 45°C until 2-4 µL were left and samples reconstituted in 5% formic acid. Prepared samples were kept at -80°C until the analysis.

4. B. Online Liquid Chromatography and Mass Spectrometry

Mass spectrometry was performed on a hybrid LTQ-Orbitrap Velos mass spectrometer (ThermoFisher Scientific, Waltham, MA) using the Xcalibur version 2.1.0.1140 coupled to an Agilent 1200 HPLC nanoflow system (dual pump system with one precolumn and one analytical column) via a nanoelectrospray ion source using liquid junction (Proxeon, Odense, Denmark). Solvents for LCMS separation of the digested samples were as follows: solvent A consisted of 0.4% formic acid in water and solvent B consisted of 0.4% formic acid in 70% methanol and 20% isopropanol. From a thermostatted microautosampler, 8 µL of the tryptic peptide mixture were automatically loaded onto a trap column (Zorbax 300SB-C18 5µm, 5×0.3 mm, Agilent Biotechnologies, Palo Alto, CA) with a binary pump at a flow rate of 20 µL/min. 0.1% TFA was used for loading and washing the pre-column. After washing, the peptides were eluted by back-flushing onto a 25 cm fused silica analytical column with an inner diameter of 50 µm packed with C18 reversed phase material (ReproSil-Pur 120 C18-AQ, 3 µm, Dr. Maisch GmbH, Ammerbuch-Entringen, Germany) operated at 35°C. For the first three fractions, peptides were separated and eluted from the analytical column by applying a 30 minute gradient ranging from 3 to 30% solvent B, followed by a 25 minute gradient from 30 to 70% solvent B. All other fractions were separated using a longer 160 minute gradient ranging from 3 to 35% solvent B, followed by a 11 minute gradient from 35 to 50% solvent B. In both cases, columns were regenerated by increasing the percent solvent B to 100%, holding it for 10 minutes before equilibrating back to 3% prior to the next injection. Peptide separation was performed at a constant flow rate of 100 nL/min. The analysis of the phosphopeptides was performed in a data-dependent acquisition (DDA) mode using a top 10 hybrid method, where each collision-induced dissociation (CID) MS^2 event was followed by a higher-energy collision-induced dissociation (HCD) MS^2 event on the same precursor ion. Lock mass correction of the siloxane 445.12003 was employed (Olsen et al., 2005). Dynamic exclusion for selected ions was 30 seconds with an exclusion mass width of 10 ppm.

Preview mode for FTMS scans were disabled while charge state screening with monoisotopic precursor selection was enabled with singly and unrecognized charge states being rejected for MS^2 -fragmentation. Maximum ion accumulation times allowed for MS^2-events were 50 ms for CID and 250 ms for HCD, respectively. For full MS scans a maximum 500 ms were allowed. Automatic gain control was used to prevent overfilling of the ion traps and was set to $10e^5$ ions for a full FTMS scan while allowing $10e^3$ ions (CID) and $10e^4$ ions (HCD) in MS^2 mode in the LTQ and FT, respectively. Resolution of spectral acquisition in the Orbitrap was set to 30,000 for full FTMS scans and 7,500 for HCD-based MS^2 scans. Settings for MS^2 fragmentation events were: (A) a triggering threshold of 10,000 counts, (B) a precursor isolation width of m/z of 2.0 and (C) a normalized collision energy of 35% and 40% for CID and HCD, respectively. For FT scans the first mass was fixed at m/z of 100. For the analysis of the phosphopeptide-depleted proteome, a 100 minute top 10 method using higher-energy collision-induced dissociation (HCD) only was applied. Similar settings were used with the following changes: I) a triggering threshold of 5,000 counts and II) a precursor isolation width of m/z of 1.2.

5. Mass Spectrometry Data Acquisition

Peak lists were extracted from the RAW MS files using ProteoWizard (release 3.0.3201, http://proteowizard.sourceforge.net/). The resulting MGF files were searched against the mouse SwissProt sequence database version 2014.03 {40,055 sequences including isoforms obtained from varsplic.pl (Kersey et al., 2000) and appended known contaminants}. Initially, the data was analysed using Mascot search engine (v2.3.02, MatrixScience, London, UK) with relatively broad precursor and fragment mass tolerances (±10 p.p.m. and ±0.6 Da, respectively) and a high peptide score threshold. Resultant high-confidence identifications were used to recalibrate mass lists using a linear regression. The second protein identification pass utilised two search engines: Mascot and Phenyx (v2.5.14, GeneBio, Geneva, Switzerland). The precursor ion mass tolerances were reduced to ±4 p.p.m and the fragment ion mass tolerances were reduced ±0.3 and ±0.025 Da for CID and HCD spectra, respectively. Further analysis was processed by the internal data processing pipeline (Isobar) as described previously (Breitwieser et al., 2011). These settings corresponded to a false discovery rate (FDR) of <0.1 % for peptide and <1% for proteins, when compared to the revered sequence database.

6. Bioinformatic Analysis of the Proteomic Data

To minimise data set redundancy, when a phosphopeptide was assigned to several isoforms of the protein, only the isoform with the minimal index was retained. The phosphorylated peptides were mapped onto known mouse phosphorylation sites annotated in the PhosphoSitePlus database version 111515 (Hornbeck et al., 2015) (www.phosphosite.org). In case of ambiguous phosphosite localization, PhosphoRS version 2.0 (Taus et al., 2011) was used to assess the probability of phosphorylation at a specific residue. Novel phosphorylation sites were discarded if the localisation probability was <1.0. For known phosphorylation sites, the acceptance threshold was 0.95. Isobar R package version 1.16 (Breitwieser et al., 2011) (bioinformatics.cemm.oeaw.ac.at/isobar) was used to calculate the protein and phosphorylated peptide ratios between conditions and to assess the significance of the ratios. Specifically, the 'calcCumulativeProbXGreaterThanY()' function of the Isobar package was applied to each phosphorylation site to calculate the two-sided *p*-value for the hypothesis that phosphopeptide-specific ratios observed in all biological replicates are different from the background noise. Bonferroni-Holm correction was applied to each pair of conditions using the standard p.adjust() R method. A multiple hypothesis adjusted *p*-value (herein refer to as 'adjusted *p*-value') of 0.05 was used to identify the confident phosphosites. An unadjusted *p*-value cutoff 0.001 was used to identify potential phsphosites.

NetworKIN (Horn et al., 2014) (www.networkin.info, version 3.0) was used to construct putative kinase-substrate and phosphatase-substrate networks for significantly-regulated sites. As NetworKIN only supports human or yeast phosphorylation sites, the significantly-regulated mouse phosphorylation sites were mapped onto orthologous human sequences by pair-wise sequence alignment (using the orthologous mapping provided by Ensembl BioMart). The enzyme-substrate connection was preserved in the final network if either the NetworKIN score was >2.0 or it was the highest scoring connection for a given phosphorylation site. The predicted human kinases and phosphatases were mapped back to the mouse orthologues. Substrate motif logos of significantly-regulated phosphorylation sites were generated using dagLogo Bioconductor package (http://bioconductor.org/packages/release/bioc/html/dagLogo.html, version 1.6). The background model was constructed from the sequences flanking all the identified phosphorylations of the corresponding amino acid (S or T).

Table S4. Table summarizing the pooling of the TMT-labelled samples and which samples were run together for mass spectrometery.

Exp N °	Sample	TMT 6-plex channels	Replicates N°
1	*Atm*$^{+/+}$_4h_APH	126	Rep1
	Atm$^{-/-}$_4h_APH	127	
	Atmin$^{+/+}$_4h_APH	128	
	Atmin$^{\Delta/\Delta}$_4h_APH	129	
	Atmin$^{+/+}$_Unt	130	
	Atmin$^{\Delta/\Delta}$_Unt	131	
2	*Atm*$^{+/+}$_4h_APH	126	Rep2
	Atm$^{-/-}$_4h_APH	127	
	Atmin$^{+/+}$_4h_APH	128	
	Atmin$^{\Delta/\Delta}$_4h_APH	129	
	Atmin$^{+/+}$_Unt	130	
	Atmin$^{\Delta/\Delta}$_Unt	131	
3	*Atm*$^{+/+}$_4h_APH	126	Rep3
	Atm$^{-/-}$_4h_APH	127	
	Atmin$^{+/+}$_4h_APH	128	
	Atmin$^{\Delta/\Delta}$_4h_APH	129	
	Atmin$^{+/+}$_Unt	130	
	Atmin$^{\Delta/\Delta}$_Unt	131	
4	*Atmin*$^{+/+}$_Unt	126	Rep1
	Atmin$^{\Delta/\Delta}$_Unt	127	
	Atmin$^{+/+}$_24h_APH	128	
	Atmin$^{\Delta/\Delta}$_24h_APH	129	
	Atm$^{+/+}$_24h_APH	130	
	Atm$^{-/-}$_24h_APH	131	
5	*Atmin*$^{+/+}$_Unt	126	Rep2
	Atmin$^{\Delta/\Delta}$_Unt	127	
	Atmin$^{+/+}$_24h_APH	128	
	Atmin$^{\Delta/\Delta}$_24h_APH	129	
	Atm$^{+/+}$_24h_APH	130	
	Atm$^{-/-}$_24h_APH	131	
6	*Atm*$^{+/+}$_Unt	126	Rep 1
	Atm$^{+/+}$_Unt	127	Rep2
	Atm$^{+/+}$_24h_APH	128	Rep 1
	Atm$^{+/+}$_4h_APH	129	Rep 1
	Atm$^{+/+}$_4h_APH	130	Rep 2
	Atm$^{-/-}$_Unt	131	Rep 1
7	*Atm*$^{+/+}$_Unt	126	Rep3
	Atm$^{-/-}$_Unt	127	Rep2
	Atm$^{-/-}$_Unt	128	Rep 3
	Atm$^{+/+}$_4h_APH	129	Rep3
	Atm$^{+/+}$_24h_APH	130	Rep2
	Atm$^{+/+}$_24h_APH	131	Rep 3

References

Breitwieser, F.P., Muller, A., Dayon, L., Kocher, T., Hainard, A., Pichler, P., Schmidt-Erfurth, U., Superti-Furga, G., Sanchez, J.C., Mechtler, K.*, et al.* (2011). General statistical modeling of data from protein relative expression isobaric tags. Journal of proteome research *10*, 2758-2766.

Ficarro, S.B., Adelmant, G., Tomar, M.N., Zhang, Y., Cheng, V.J., and Marto, J.A. (2009). Magnetic bead processor for rapid evaluation and optimization of parameters for phosphopeptide enrichment. Analytical chemistry *81*, 4566-4575.

Gilar, M., Olivova, P., Daly, A.E., and Gebler, J.C. (2005). Two-dimensional separation of peptides using RP-RP-HPLC system with different pH in first and second separation dimensions. Journal of separation science *28*, 1694-1703.

Horn, H., Schoof, E.M., Kim, J., Robin, X., Miller, M.L., Diella, F., Palma, A., Cesareni, G., Jensen, L.J., and Linding, R. (2014). KinomeXplorer: an integrated platform for kinome biology studies. Nature methods *11*, 603-604.

Hornbeck, P.V., Zhang, B., Murray, B., Kornhauser, J.M., Latham, V., and Skrzypek, E. (2015). PhosphoSitePlus, 2014: mutations, PTMs and recalibrations. Nucleic acids research *43*, D512-520.

Kersey, P., Hermjakob, H., and Apweiler, R. (2000). VARSPLIC: alternatively-spliced protein sequences derived from SWISS-PROT and TrEMBL. Bioinformatics *16*, 1048-1049.

Kim, D., Pertea, G., Trapnell, C., Pimentel, H., Kelley, R., and Salzberg, S.L. (2013). TopHat2: accurate alignment of transcriptomes in the presence of insertions, deletions and gene fusions. Genome biology *14*, R36.

Langmead, B., and Salzberg, S.L. (2012). Fast gapped-read alignment with Bowtie 2. Nature methods *9*, 357-359.

Love, M.I., Huber, W., and Anders, S. (2014). Moderated estimation of fold change and dispersion for RNA-seq data with DESeq2. Genome biology *15*, 550.

Olsen, J.V., de Godoy, L.M., Li, G., Macek, B., Mortensen, P., Pesch, R., Makarov, A., Lange, O., Horning, S., and Mann, M. (2005). Parts per million mass accuracy on an Orbitrap mass spectrometer via lock mass injection into a C-trap. Molecular & cellular proteomics : MCP *4*, 2010-2021.

Taus, T., Kocher, T., Pichler, P., Paschke, C., Schmidt, A., Henrich, C., and Mechtler, K. (2011). Universal and confident phosphorylation site localization using phosphoRS. Journal of proteome research *10*, 5354-5362.

Wang, L., Wang, S., and Li, W. (2012). RSeQC: quality control of RNA-seq experiments. Bioinformatics *28*, 2184-2185.

2.2. Interlude

UV sensitivity and genomic instability due to defective nucleotide excision repair is alleviated by MUTYH loss.

Mazouzi A, Moser SC, Wiedner M, Lardeau CH, Ringler A, Weil B, Neesen J, Kubicek S and Loizou JI. Molecular Cell. submitted.

In the present study we identify a compound synthetic viable interaction via a chemical screen for agents that enhance survival of nucleotide excision repair defective cells. We found that the anti-diabetic drug acetohexamide enhances the ability of nucleotide excision repair-defective cells to remove UV-induced lesions, in an error-free manner. We identify that this occurs due to the regulation of MUTYH, a DNA glycosylase that has not been previously implicated in the clearance of UV-induced lesions. This synthetic viable interaction could lead to the development of new therapeutic approaches for patients, particularly with inherited diseases caused by defective nucleotide excision repair pathway.

The author of this thesis designed the project, performed most of the experiments, analyzed and interpreted the data, prepared the figures and wrote the manuscript. Moser SC helped in doing: colony formation assay, survival dose response assays, immunofluorescence and dot blot for cyclobutane-pyrimidine dimers (CPDs). Wiedner M generated the DNA repair knockout cell lines. Lardeau CH, Ringler A and Kubicek S assisted with the drug screen and data analysis. Weil B and Neesen J performed the chromosomal abnormalities measurements. Loizou JI designed, supervised the project and prepared the manuscript.

UV sensitivity and genomic instability due to defective nucleotide excision repair is alleviated by MUTYH loss

Abdelghani Mazouzi[1], Sarah C. Moser[1], Marc Wiedner[1], Charles-Hugues Lardeau[1,2], Anna Ringler[1], Beatrix Weil[3], Jürgen Neesen[3], Stefan Kubicek[1,2] and Joanna I. Loizou[1,4]

[1]CeMM Research Center for Molecular Medicine of the Austrian Academy of Sciences, Lazarettgasse 14, AKH BT 25.3 1090 Vienna, Austria

[2]Christian Doppler Laboratory for Chemical Epigenetics and Antiinfectives, CeMM Research Center for Molecular Medicine of the Austrian Academy of Sciences, Vienna, Austria

[3]Institute of Medical Genetics, Medical University of Vienna, Währinger Strasse 10, 1090 Vienna, Austria

[4]Corresponding author

Running title: MUTYH loss corrects nucleotide excision repair deficiency

Key words: Nucleotide excision repair, UV, XPA, MUTYH, Acetohexamide

To whom correspondence should be addressed: Joanna I Loizou, CeMM Research Center for Molecular Medicine of the Austrian Academy of Sciences, Lazarettgasse 14, AKH BT 25.3, 1090 Vienna, Austria

Tel: +43-1/40160-70 058

Fax: +43-1/40160-970 000

Email: jloizou@cemm.oeaw.ac.at

ABSTRACT

Defects in nucleotide excision repair (NER) lead to an inability to repair DNA lesions induced by UV, leading to increased mutation rates and genomic instability. Patients carrying mutations within genes that function in this pathway display a range of pathologies, including an increased susceptibility to cancer, premature ageing, and neurological defects. There are currently no curative therapies available. Here, we exploited haploid human cells and CRISPR-Cas9 technology to perform a high-throughput chemical screen for agents that could alleviate the cellular sensitivity of NER-deficient cells to UV-induced DNA damage. This led to the identification of the clinically approved anti-diabetic drug acetohexamide, which functioned to clear UV-induced DNA damage without the accumulation of chromosomal instability, hence promoting cellular survival. Acetohexamide exerted this protective function by regulating the stability of the DNA glycosylase, MUTYH. Together, we have identified a novel synthetic viable interaction between acetohexamide and UV-induced cell death that could be used to develop new therapeutic approaches for a variety of diseases.

Cells of all living organisms have evolved a compendium of DNA repair pathways to deal with a range of different types of DNA damage in order to maintain genomic integrity and protect from cell death and disease. Nucleotide excision repair (NER) is one of the most versatile and flexible DNA repair pathways, due to its capacity to deal with a wide range of structurally distinct DNA lesions. This pathway repairs ultraviolet (UV) radiation-induced lesions that are commonly in the form of cyclobutane-pyrimidine dimers (CPDs) but also 6-4 pyrimidine-pyrimidone photoproducts (6-4PPs), and also removes other bulky adducts (Marteijn et al., 2014). CPDs form rapidly upon UV exposure, and if unrepaired lead to cytosine to thymine transition mutations, which are associated with melanoma (Lo & Fisher, 2014). NER is comprised of two major sub-pathways: transcription-coupled repair (TC-NER), which functions on transcribed strands of active genes and engages RNA polymerase II in the recognition of the DNA damage; and global genome repair (GG-NER), which repairs lesions in other regions of the genome including repressed non-coding regions and non-transcribed strands of active genes (Fousteri & Mullenders, 2008).

The importance of NER, as a DNA damage repair pathway, is also highlighted by the fact that mutations within this pathway give rise to several diseases with diverse clinical manifestations, including Xeroderma pigmentosum (XP), Cockayne syndrome (CS),

UV-sensitive syndrome (UVSS) and Trichothiodystrophy (TTD). All patients display enhanced sensitivity to sunlight. Specifically, XP patients are more than 1,000 times more prone to developing cutaneous basal cell carcinoma, squamous cell carcinoma or melanoma. In addition, 20% of these patients suffer from neurological symptoms typical of neurodegeneracy. There are no curative therapies for NER deficient patients. Recently, several studies have highlighted a new potential therapeutic approach for correcting defects associated with human diseases, including those associated with defective DNA repair, based on the concept of synthetic viability (Chen et al., 2016, Larrieu et al., 2014, Motter, Gulbahce et al., 2008), whereby defects caused by loss or mutation of one gene can be alleviated by the loss of another gene (or inhibition of its gene product). These genetic and chemical interactions have been found across several model organisms as well as in human cells (van Leeuwen et al., 2016, Vieira et al., 2015). Within the context of NER, dietary restriction has been shown to reduce DNA damage and extend lifespan in mice carrying mutations in various DNA repair genes (Vermeij, Dolle et al., 2016).

Since synthetic viable interactions represent a promising approach for correcting defects associated with human disorders defective in DNA repair (Adamo et al., 2010, Bouwman et al., 2010, Bunting et al., 2010, Chen et al., 2016, Ding et al., 2016, Larrieu et al., 2014, Pace et al., 2010), we sought to identify compounds that may alleviate the UV sensitivity of nucleotide excision repair (NER) deficient cells, which could lead directly to the identification of new treatments. The ability to do this has only recently been made possible by the development of human haploid cell technology combined with CRISPR-Cas9 for gene editing, where generating knockouts is simplified by the fact that there is only one allele to modify (Blomen, Majek et al., 2015, Wang, Birsoy et al., 2015). This has enabled high-throughput loss-of-function screens to be performed across isogenic cell lines that were not previously possible in diploid human cells (Forment, Herzog et al., 2017, Winter, Radic et al., 2014).

We used the CeMM Library of Unique Drugs (CLOUD; to be described elsewhere), which contains around 300 compounds representing all structurally distinct Food and Drug Administration (FDA) approved compounds to allow for potential drug repurposing. First, we generated an NER-deficient cell line by making a frameshift mutation in XPA, one of the central components of NER that functions in both TC-NER and GG-NER (Camenisch et al., 2006), utilizing clustered, regularly interspaced short palindromic repeats (CRISPR)-Cas9 in the human near haploid cell line HAP1

(denoted ΔXPA) **(Figure S1A)**. As expected, and similar to an XPA-patient derived fibroblastoid cell line (denoted $XPA^{\Delta/\Delta}$), ΔXPA cells displayed enhanced sensitivity to UV irradiation **(Figure S1B-C)**. Next, we exposed ΔXPA and wildtype cells to the CLOUD (with each drug used at five times maximal plasma concentration) for 24 hours, followed by UV exposure (at a dose of 2,000 J/M^2; selected to kill ΔXPA cells but not wildtype cells) **(Figures 1A and S1D)**. The compounds were scored based on their efficiency to improve cellular survival of ΔXPA cells, compared to wildtype cells **(Figure 1B)**. A correlation greater than 0.9 was obtained between the biological replicates with sufficient separation between ΔXPA and wildtype cells **(Figure S2A-B)**.

We identified ten compounds that showed more than a 40% correction of survival of ΔXPA cells compared to wildtype cells **(Figure S2C)**. Eight of the ten compounds were excluded for further analysis due to their ability to block UV-induced DNA damage and hence indirectly increasing cellular survival. One of the two remaining compounds was acetohexamide **(Figure 1C)**, an anti-diabetic drug that belongs to the first generation of sulfonylurea drugs (Joseph, Anguizola et al., 2010). Acetohexamide alleviated the UV sensitivity of ΔXPA cells almost to the level of wildtype cells both in a short-term dose response assay **(Figure 1D)** and in a long-term colony formation assay **(Figure 1E)**. Moreover, this increase in survival was also observed for ΔXPC and ΔCSB cells **(Figure 1F)**, key factors involved in GG-NER and TC-NER respectively, suggesting that acetohexamide alleviates UV-induced cell death via a general mechanism. The minimal incubation time of acetohexamide required to give a protective effect, prior to UV exposure was determined to be 6 hours **(Figure S3A)**. To determine whether acetohexamide could also correct cellular survival following other sources of DNA crosslinking damage, we exposed wildtype and ΔXPA cells to illudin S, a genotoxin that induces bulky adducts that are repaired by NER **(Figure 2A and Figure S3B)**. We observed that indeed, acetohexamide could increase cellular survival following illudin S treatment. We also confirmed that acetohexamide could alleviate UV-induced cell death of the $XPA^{\Delta/\Delta}$ patient-derived cells **(Figure 2B)**, indicating that the mode of rescue is not cell type specific. Furthermore, this protective effect is independent from replication fork collapse and double strand breaks (DSBs) formation caused by replication stress **(Figure S3C-D)**. Next, we determined whether incubation with acetohexamide leads to a clearance of UV-induced lesions by measuring the levels of

CPDs, the most predominant lesions induced by UV and representing approximately 75% of UV lesions. As expected wildtype cells that are NER proficient were able to clear CPDs 24 hours post UV irradiation, whereas, NER deficient XPA$^{\Delta/\Delta}$ cells continued to show elevated levels of CPDs at 24 hours post UV irradiation. However, strikingly acetohexamide led to the clearance of CPDs in XPA$^{\Delta/\Delta}$ cells, suggesting that acetohexamide enhances the ability of NER deficient cells to clear CPDs lesions. Importantly, acetohexamide did not affect the initial amount of CPDs. The same observation was also made for HAP1 cell lines **(Figures 2C-D and S3E-F)**.

To gain insight into the mode of action of acetohexamide, we assessed cell cycle profiles upon exposure to the compound. There was no difference between wildtype or ΔXPA cells upon acetohexamide treatment, ruling out an effect on cell cycle phases **(Figure S4A)**. To exclude the possibility that acetohexamide has a general anti-apoptotic effect, we treated wildtype cells with a variety of different DNA damaging agents including the DNA crosslinking agent mitomycin C (MMC), hydroxyurea (HU), which depletes cellular pools of ribonucleosides thereby inducing replication stress, the DNA double-strand break inducing agent neocarzinostatin (NCS), and the alkylating agent methyl methanesulfonate (MMS). Acetohexamide only increased cellular survival following exposure to NCS, but not MMC, HU and MMS. Thus acetohexamide does not act as an anti-apoptotic agent following DNA damage **(Figure S4B-E).** Furthermore, the potent antioxidant N-acetylcysteine (NAC) showed a very minor effect in alleviating UV-induced sensitivity compared to acetohexamide **(Figure S4F)**, suggesting that acetohexamide is not exerting its effect simply by quenching reactive oxygen species.

Sulfonylureas, including acetohexamide, target ATP sensitive potassium channels and play a prominent role in regulating insulin secretion. Sulfonylureas are reported to block the inward rectifier of Kir6.2 subunits through their binding to SUR1 (for sulfonylurea receptor 1), leading to membrane depolarization, Ca^{2+} influx, and subsequent insulin release (Burke, Mutharasan et al., 2008, Proks, Reimann et al., 2002). However, expression profiling via RNA sequencing analysis did not detect any SUR1 transcript in HAP1 cells **(Figure S5A)**. Moreover, SUR1 was not expressed in ΔXPA cells following UV irradiation or acetohexamide treatment **(Figure S5B)**. Based on this data, we disregarded SUR1 as the target of acetohexamide within this context. Next, we tested three additional sulfonylureas that stimulate insulin release via ATP-dependent

K^+ channels including gliclazide (GLC), glimepiride (GLM) and glibenclamide. Only glimepiride showed a protective effect of ΔXPA cells against UV **(Figure S6A-D)**. Two additional derivatives of sulfonylurea showed a potent effect within the range of μM amounts **(Figure S6E)**.

Since acetohexamide enhanced the clearance of CPDs in NER deficient cells, we speculated that its mode-of-action could be *via* one the known DNA excision repair pathways. This rationale is supported by a recent study in yeast, which proposed that genetic suppression interactions are found to connect functionally related genes, including those that belong to the same pathway or biological process such as DNA repair pathways (van Leeuwen et al., 2016). Therefore, we generated a panel of 20 DNA repair-deficient cell lines using CRISPR-Cas9, representing all seven DNA repair pathways. Subsequently, we treated these cell lines (as well as two wildtype controls) with acetohexamide and exposed them to UV irradiation. We defined the 'percentage of rescue' as the difference in survival of a given cell line treated with acetohexamide compared to untreated, following UV irradiation **(Figure 3A)**. Acetohexamide had a comparable protective effect against UV-induced damage on all the knockout cell lines tested (and also to wildtype cells) but had no effect on cells lacking MUTYH **(Figure 3A)**. This suggests that acetohexamide and MUTYH have a related function. It also provides further evidence that acetohexamide has a general effect on protecting cells against UV-induced DNA damage. We additionally performed a whole genome based CRISPR screen in XPA deficient cells, searching for genes in which their depletion alleviates the XPA sensitivity to UV irradiation. First, the cells where infected with a library of more than 120 000 gRNAs targeting 19 000 human genes, subsequently challenged with UV irradiation that killed 90% of the cells. The genomic DNA of the remaining resistant cells was then extracted and subjected to next generation sequencing **(Figure S5C)**. The data was analyzed as described by Li et al (Li, Xu et al., 2014). Interestingly, the gRNAs targeting MUTYH in XPA deficient cells showed two-fold enrichment in survival to UV irradiation compared to gRNAs controls **(Figure S5D)**.

MUTYH is a DNA glycosylase that catalyzes the excision of the adenine mis-paired with 8-oxo-guanine in the base excision repair (BER) pathway. Thus, MUTYH is an unusual glycosylase since it removes an undamaged base situated opposite a DNA lesion, instead of removing the damaged base (Markkanen, Dorn et al., 2013). We

found that loss of MUTYH conferred resistance to UV irradiation compared to wildtype cells, similar to the effect of acetohexamide treatment and furthermore pre-incubation with acetohexamide did not have a noticeable effect on survival **(Figure 3B)**, further suggesting that acetohexamide and loss of MUTYH have functionally related effects. To test a role for MUTYH in NER more directly, we analyzed whether MUTYH deletion could alleviate the sensitivity of ΔXPA cells by generating a double knockout (ΔXPA-MUTYH) using CRISPR-Cas9 **(Figure 3C)**. We observed enhanced cellular survival of ΔXPA-MUTYH cells following UV exposure compared to ΔXPA cells **(Figure 3D)**. To confirm this finding we labeled ΔXPA cells with mCherry and ΔXPA-MUTYH with GFP. Next we mixed these cell lines in equal amounts and then irradiated the mixed population with UV at different doses. After 10 days in culture the cells were analyzed by flow cytometry. While the ΔXPA-mCherry cells were no longer detected, the ΔXPA-MUTYH-GFP cells were, indicating that loss of MUTYH confers cellular resistance to UV **(Figure S7A)**.

Thus far, our results have shown that both acetohexamide and loss of MUTYH protect both wildtype and NER-deficient cells from UV-induced cell death. To determine whether acetohexamide works via MUTYH we first analysed its effect on MUTYH protein levels. We found that acetohexamide treatment of wildtype cells led to a decrease in MUTYH protein levels in a proteasome dependent manner **(Figure 4A-B)**. This suggests that acetohexamide is indeed exhibiting its functions by promoting the degradation of MUTYH. In further support of this, acetohexamide treatment of the double knockout ΔXPA-MUTYH did not lead to a further increase in survival upon UV treatment **(Figure 4C)**. Importantly, ΔXPA-MUTYH cells cleared CPDs more efficiently compared to ΔXPA cells 24 hours post UV irradiation **(Figure 4D and S7B)**, suggesting that the observed toxicity in ΔXPA cells, following UV activity is MUTYH dependent. This supports our model where MUTYH generates complex lesions containing DNA single-strand breaks next to CPDs, which can be dealt with in wildtype cells but not XPA deficient cells. Hence, removing MUTYH alleviates this toxicity. Thus, in addition to acetohexamide, this makes MUTYH a candidate drug target for developing novel therapies for NER-deficient patients.

Next, we determined whether the alleviation of UV sensitivity in ΔXPA-MUTYH cells has an effect on chromosomal instability. Hence we measured chromosomal abnormalities in ΔXPA cells compared to ΔXPA-MUTYH cells, following UV exposure.

ΔXPA-MUTYH cells displayed a significant reduction in chromosomal abnormalities after UV irradiation compared to ΔXPA cells **(Figure 4E)**. Taken together, we conclude that MUTYH loss has protective effects on genomic stability in ΔXPA cells following UV irradiation.

Collectively, our data show that acetohexamide, an anti-diabetic drug, can alleviate the sensitivity of NER deficient cells and enhance the repair of UV lesions through degradation of MUTYH. However, how acetohexamide targets MUTYH for degradation through the proteasome remains still unclear. It has been shown that MUTYH is ubiquitinated by the E3 ligase Mule, thereby reducing its protein levels and subsequent recruitment to chromatin (Dorn, Ferrari et al., 2014). Hence we hypothesized that loss of Mule would sensitize cells to UV irradiation due to an accumulation of MUTYH protein. Indeed, Mule deficient cells (ΔMule) also showed enhanced sensitivity to UV irradiation **(Figure 4F)**. Thus, we propose a model whereby acetohexamide functions by inhibiting a deubiquitin ligase, that in turn leads to MUTYH ubiquitination by Mule and subsequent degradation **(Figure 4G)**. Interestingly, the whole-genome CRISPR screen showed that several deubiquitin ligases such as USP3 and OTUD5 have a protective effect for XPA deficient cells against UV irradiation **(Figure S7C)**.

The presented data indicate that acetohexamide, or one of its derivatives may be used to alleviate symptoms associated with a deficiency in NER hence opening a new therapeutic approach for the treatment of NER associated diseases. This approach may be potentially beneficial for the range of syndromes characterised by UV sensitivity, including XP, CS, UVSS and TTD. Since this protective effect is also achieved by genetic loss of MUTYH, the development of specific inhibitors could potentially have a similar effect on cells deficient for NER.

Moreover, a murine model lacking the base excision repair enzyme OGG1 has been shown to develop severe striatal neurodegeneration. Deletion of MUTYH in this mouse model led to a resistance in neurodegeneration. These results indicate that MUTYH promotes neurodegeneration within certain DNA repair-deficient backgrounds and hence loss of MUTYH activity may indeed improve pathologies associated with neurodegeneration (Sheng, Oka et al., 2012).

However, caution should be taken since MUTYH has been implicated in playing a protective role against intestinal tract malignancies as well as lymphomas and adenomas (Russo, De Luca et al., 2009, Sakamoto, Tominaga et al., 2007). Moreover,

loss-of-function mutations have been reported to occur in familial adenomatous polyposis (FAP), which is an autosomal dominant disease characterized by the formation of adenomatous polyps in the colons and rectums (Al-Tassan, Chmiel et al., 2002), indicating that MUTYH plays important role in clearing oxidative structures in highly proliferative tissues, such as the intestinal tract. Therefore, developing small-molecule inhibitors for MUTYH that function specifically in the brain or the skin may provide therapeutic opportunities for alleviating NER deficiency diseases such as XP and CS.

EXPERIMENTAL PROCEDURES

Cell Culture, Plasmids and Reagents

HAP1 cells were cultured in Iscove's Modified Dulbecco's Medium (Gibco) medium. The XPA patient-derived fibroblast cell line was purchased from Coriell Biorepository (GM04429) and cultured in MEM (Gibco), as were BJ cells. All cells were grown in the presence of 10% fetal bovine serum (FBS) (Thermo Fisher Scientific) and 1% penicillin-streptomycin (Sigma-Aldrich) at 37°C with 5% CO_2 and 3% O_2. Illudin S, neocarzinostatin (NCS), hydroxyurea (HU) acetohexamide, N-acetylcysteine, MMC, gliclazide, glimepiride, glibenclamide. MMS, NCS, HU, L100889, PH003986, CDS021537 and PH000650 were purchased from Sigma-Aldrich.

Generation of CRISPR-Cas9 Edited Cell Lines

The DNA repair knockout cell lines were generated in collaboration with Horizon Genomics. Briefly, HAP1 cells were transfected with plasmids expressing Cas9 (pX165 from the Zhang lab), a gRNA, and a blasticidin resistance gene using Xfect (clontech). The cells then treated with 20 μg/ml blasticidin for 24 hours to eliminate untransfected cells. After allowing the cells to recover for 5 to 7 days from antibiotic selection, clonal cell lines were isolated by limiting dilution. Subsequently, the genomic DNA was isolated using Direct PCR-Cell Kit (PeqLab) and the region targeted by the gRNA was PCR amplified and analyzed by Sanger sequencing. Finally, clones with frameshift mutations were selected.

High-throughput Drug Screen

Fifty nL of compound per well was transferred into 384-well plates (Corning 3712) from DMSO stock plates using acoustic transfer (Labcyte Echo 520). Wildtype and XPA-deficient HAP1 cells at an amount of 1,000 cells were seeded in 50 μl media into the

compound-containing plates. After 24 hours of treatment, the cells were UV irradiated with 2,000 J/M^2. After 72 hours, cell viability was determined using Cell Titer-Glo (Promega). The screen was performed in duplicate. To analyse the data, the percentage of control was calculated and the signal of the DMSO negative control used to set the values to 0% and non-irradiated sample to 100%. Hits were defined based whether they alleviated the sensitivity by more than 40% and the signal was 3 standard deviation away from the DMSO treated conditions.

Genome-wide CRISPR-Cas9 screen

The virus production of GeCKO CRIPSR library comprising 122,411 gRNAs targeting 19,050 human genes was performed as reported by Shalem et al (Shalem, Sanjana et al., 2014). 100 million cells of XPA deficient HAP1 were infected with MOI of 0.37. Briefly, 1.5 x106 cells per well were plated into 12-well plate in IMDM with 10% FBS supplemented with 8 ug/ml polybrene (Sigma). The 12-well plate was centrifuged at 2,000 rpm for 2 h at 37°C. After the spin, media was aspirated and fresh media (without polybrene) was added. The following day, the cells were pooled and transferred into 15 cm dishes and selected with 2µg/ml puromycin for 4 days. After selection the cells were divided into 3 samples: representation sample (30x106 cells), UV irradiated sample (100x106 cells) and untreated condition (100x106 cells). The UV irradiated sample was challenged with 15 J/M2. Next, the UV treated cells were kept in culture for 10 days. Genomic DNA was extracted from 30 million cells using QIAamp DNA mini kit (Qiagen) according to the manufacture's protocol. The PCR reactions were performed as described by Shalem et al (Shalem et al., 2014). Barcoded samples were pooled and submitted to the Biomedical Sequencing Facility (BSF) for 61 base pair single read sequencing.

Karyogram Analysis

Metaphase preparation was carried out by standard methods. Dividing cells were blocked in metaphase stage by adding 0.1µg/ml Colcemid (Gibco, Thermo Fisher) for 30 - 60 minutes. Afterwards cells were treated for 20 minutes with hypotonic solution and fixed using Methanol /Acetic Acid mixture (one-part Acetic Acid and three parts Methanol). Then cells were dropped onto slides, dried at 42°C for about 20 minutes and then incubated at 60°C overnight. Chromosomes were digested in 2.5% Trypsin/NaCl solution for 30 seconds and incubated for about 5 seconds in ice-cold 0.9% NaCl solution. Finally, slides were stained in buffered Giemsa stain solution for 3 minutes. Karyotyping was done using the "MetaSystems Ikaros" software version

5.3.18.

Colony Formation Assay

Cells were treated with UV at different doses with or without drug pre-treatment and then seeded into 6-well plates, at a density of 1,000 cells/well, in duplicates for 2 weeks until visible colonies were formed. Then, the medium was removed, cells were washed with PBS and fixed using 3.7% PFA (paraformaldehyde) for 1 hour. Subsequently, the PFA was removed and 0.1% crystal violet in 5% ethanol solution was added for 1 hour. Next, the staining solution was removed and the wells were washed, imaged and quantified using CellProfiler.

Dose Responses and UV Treatment

Dose-response curves for the DNA damage agents including mitomycin C (MMC), methyl methanesulfonate (MMS), hydroxyurea (HU), neocarzinostatin (NCS) and illudin S were performed in 96-well plates by seeding 1,000 cells/well in triplicates. The next day, compounds at different concentrations were added and 3 days later, cell viability was assessed using Cell Titer-Glo (Promega).

For the UV irradiation the cells were washed with PBS, trypsinized, counted and distributed in equal number then irradiated with different doses of UV as indicated. Finally, 1,000 cells were re-distributed in 96 well plates. After 72 hours, survival was measured using Cell Titer-Glo (Promega). Cells were irradiated with UVC using the UVP CX-2000 device (254 nm, Fisher Scientific).

Cell Cycle Analysis

Cells were treated with either DMSO or acetohexamide as indicated. Cell cycle stages were marked using propidium iodide staining. Briefly, cells were harvested, resuspended in PBS and fixed overnight with cold 70% ethanol. After centrifugation, ethanol was removed and cells were resuspended in PBS containing 1 µg/mL RNase A and 1 µg/mL propidium iodide. Finally, cells were analyzed on a FACScalibur flow cytometer. Following cell acquisition, analysis was performed using FlowJo software (Tree Star).

Quantitative Reverse Transcription PCR (RT-PCR)

WT and ΔXPA HAP1 cells were harvested and RNA was isolated using phenol-chlorophorm extraction. After treatment with 1 µl DNase (Sigma), the cDNA was transcribed using SuperScript III Reverse Transcriptase (Invitrogen). An amount of 1 µg of cDNA template was used for the qRT-PCR using SYBR Green qPCR Mastermix (Qiagen). Analysis was performed in triplicates using GAPDH as a control gene. The

PCR was performed on a 7900HT Fast Real-Time PCR System (Applied Biosystems). The following primers were used:
SUR1: 5'-AGCTGAGAGCGAGGAGGATG -3'; 5'-CACTTGGCCAGCCAGTAGTC-3',
GAPDH: 5'- AGAACATCATCCCTGCATCC -3'; 5'- ACATTGGGGGTAGGAACAC-3'.

Protein Extracts and Immunoblotting

Cells were lysed in lysis buffer composed of RIPA lysis buffer supplemented with protease inhibitors (Sigma) and phosphatase inhibitors (Sigma, NEB). After sonication and centrifugation of the lysates, they were heated with reducing sample buffer. Protein samples were separated by SDS–PAGE (3-8% or 4-12% gradient gels; Invitrogen) and then transferred onto nitro-cellulose membranes. All primary antibodies were used at 1:1,000 dilution and secondary antibodies at 1:5,000. Antibodies used were: ATM 2C1 (Santa Cruz), P-S1981-ATM (10H11.E12; NEB), P-S824-KAP1 (Bethyl Laboratories, Inc), KAP1 (BethylLaboratories, Inc), P-S15-TP53 (16G8; NEB), P-S957-SMC1 (5D11G5; Millipore), P-S345-CHEK1 (2341S; Cell Signaling), CHEK1 (DCS-310; Santa Cruz), XPA (14607S; Cell Signaling), MUTYH (ab55551; Abcam), PARP (9532; Cell Signaling), TUBULIN (3873, Cell Signaling) P-S140-H2AX (07-164; Millipore) and ß-actin (A 5060A, Sigma).

Immunofluorescence for CPDs and Associated Microscopy

For CPDs measurement, cells were seeded onto coverslips (VWR) in 5 cm dish. On the following day, they were treated as indicated. Next, they were washed twice with PBS and fixed with 4% paraformaldehyde (PFA) for 10 min at room temperature (RT), then permeabilized with 0.5% Triton X-100 in PBS for 5 min at RT. After 3 steps of washing with PBS, DNA was denatured with 2M HCL for 30 minutes at room temperature, followed by blocking with 10% FBS in PBS for 30 minutes at 37°C. The primary anti-CPDs and secondary antibodies (anti-CPDs - TDM-2, Cosmo Bio; secondary antibody - Alexa Fluor 488 goat anti-mouse, Invitrogen) were diluted in PBS (1:1,000) and incubated on cells for 30 minutes at 37°C, with five washes (PBS) performed between individual steps. Finally, cells were stained with DAPI (Sigma-Aldrich) for 20 minutes at room temperature in the dark. Cell images were taken on a deconvolution microscope (Leica). Quantification was performed using CellProfiler.

Dot Blot for CPDs

The amount of CPDs in the DNA was quantified using immuno-Dot-blot assay with the CPD-specific monoclonal antibody TDM-2. Genomic DNA was extracted using QIAamp DNA mini kit (Qiagen), The genomic DNA was denatured in TE buffer (10 mM

Tris-CL and 1 mM EDTA, pH 7.5) by boiling for 5 minutes and subsequently 50ng of genomic DNA was dot-blotted in triplicate onto a nitrocellulose membrane. The DNA then was fixed by baking the membrane for 2 hours at 80°C. The membranes were blocked for 1 hour in TBS, 0.2% Tween 20 (TBS-T) containing 5% (w/v) milk. After washing in TBS-T for 15 minutes, the membranes were incubated overnight at room temperature at 4°C with the monoclonal antibody TDM-2 (anti CPD monoclonal antibody, Cosmo Bio) using a dilution of 1:1,500 in TBS-T. After washing 5 times for 15 minutes, membranes were incubated for 1 hour with anti-mouse secondary antibody diluted 1:2,500 in phosphate-buffered saline (Invitrogen). Signals were detected using Amersham ECL (GE Healthcare Life Sciences).

Statistical Analysis

Data are expressed as ± SEM unless otherwise stated.

AUTHOR CONTRIBUTIONS

Conceptualization, A.M. and J.I.L.; Methodology, A.M., S.C.M, M.W., C.-H.L., A.R. and B.W.; Data Curation, A.M. and C.-H.L.; Writing, A.M. and J.I.L.; Visualization, A.M., and J.I.L.; Supervision, J.N., S.K. and J.I.L.; Project Administration, S.K. and J.L.; Funding Acquisition, A.M., S.K. and J.I.L.

ACKNOWLEDGEMENTS

We would like to acknowledge Life Science Editors for editing this manuscript and also the Loizou lab for fruitful discussions. A.M. was funded by a DOC fellowship from the Austrian Academy of Sciences (24102). The J.I.L. lab is supported by a Marie-Curie Career Integration Grant (project no. 321602-NonCanATM). S.K. acknowledges support by the Austrian Federal Ministry of Science, Research and Economy and the National Foundation for Research, Technology, and Development. CeMM is funded by the Austrian Academy of Sciences.

FIGURE LEGENDS

Figure 1. Acetohexamide alleviates the UV sensitivity of NER deficient cells

A. Schematic representation of the experimental setup used for performing the high-throughput drug screen. B. Bubble plot displaying the used drugs plotted against cell viability. Blue bubbles indicate wildtype (WT) cells, red bubbles indicate XPA deficient cells (ΔXPA) and the green bubble highlights acetohexamide. The size of the bubbles

indicates the significance, as $-LOG_{10}$(p-value). C. Chemical structure of acetohexamide. D. Dose–response curve of WT and ΔXPA cells treated with or without 0,5 mM acetohexamide for 6 hours followed by UV irradiation. Survival was assessed after 3 days using CellTiter-Glo. Displayed is the relative viability by normalizing the raw data of the DMSO control to acetohexamide treated cells. Error bars indicate SEM (n = 3). E. Colony formation assay using the same conditions indicated in (D) where cells were kept in culture for 10 days following UV irradiation. F. Survival of WT and ΔXPC or ΔCSB HAP1 cells treated with or without 0.5 mM acetohexamide, followed by UV exposure. Survival was assessed after 3 days using CellTitre-Glo.

Figure 2: Acetohexamide enhances the clearance of CPDs in NER in deficient cells.

A. Dose–response curve of WT and ΔXPA cells treated with or without 0.5 mM acetohexamide for 6 hours followed by illudin S treatment. Survival was assessed after 3 days using CellTiter-Glo. B. Colony formation assay for WT (BJ, a human fibroblastoid cell line) and XPA-patient derived fibroblasts ($XPA^{\Delta/\Delta}$) treated with or without 0.5 mM acetohexamide for 6 hours followed by UV irradiation as indicated and kept in culture for 10 days following UV irradiation. C. WT BJ cells and $XPA^{\Delta/\Delta}$ were treated with 0.5 mM acetohexamide for 6 hours, irradiated with 15 J/M^2 and then fixed and immunostained with an anti-CPD antibody at the indicated times. Nuclear DNA was counterstained with DAPI. Scale bar, 10 μm. D: Scatter plot displaying the quantification of CPD intensities per nucleus of WT and $XPA^{\Delta/\Delta}$ cells in the presence or absence of 0.5 mM acetohexamide of more than 100 cells. Red lines within each column represent median intensities.

Figure 3: Acetohexamide functions through MUTYH degradation

A. Bubble plot displaying the percentage of rescue defined as the difference in survival of a given cell line treated with acetohexamide compared to untreated, following UV irradiation. The red, green and black bubbles highlight MUTYH, XPA-deficient and WT HAP1 cells respectively, and blue bubbles indicate the rest of the knockout cell lines. The size of the bubbles indicates the significance as $-LOG_{10}$(p-value). B. Survival of WT and MUTYH deficient (ΔMUTYH) cells with or without 0.5 mM acetohexamide treatment, following UV irradiation exposure as assessed after 3 days using CellTitre-Glo. Loss of MUTYH was confirmed by immunoblotting using an anti-MUTYH antibody.

C. Deletion of MUTYH in WT HAP1 or an XPA deficient background was confirmed by immunoblotting using an anti-MUTYH antibody. Tubulin was used as a loading control. D. Clonogenic survival of WT, ΔXPA or ΔXPA-MUTYH cells were irradiated with UV with the indicated dose or left untreated, then cells were incubated for 10 days. BER, base excision repair; NER, nucleotide excision repair; DSBR; double strand break repair; MMR, mismatch repair; FA, Fanconi anemia; DR, direct reversal; TLS, translesion DNA synthesis.

Figure 4: Deletion of MUTYH recapitulates the effect of acetohexamide in NER deficient cells: A. WT HAP1 cells were treated with or without 0.5 mM acetohexamide for 6 hours, then released into compound-free media for the indicated time points and immunoblotted with an anti-MUTYH antibody. Actin was used as a loading control. B. WT HAP1 cells were either treated with 0.5 mM acetohexamide alone or with 10 μM MG132 for 6 hours and analyzed by immunoblotting for MUTYH. C. Left panel: colony formation assay of the WT, ΔXPA or ΔXPA-MUTYH HAP1 cells treated with or without 0.5 mM acetohexamide for 6 hours followed by 15 J/M^2 UV irradiation and then kept in culture for 10 days. Macroscopic colonies were stained with crystal violet and quantified (Right panel). D. WT, ΔXPA or ΔXPA-MUTYH HAP1 cells treated with 15 J/M^2 UV or left untreated, and kept in culture at the indicated recovery time and analyzed by dot blot for the presence of CPDs within genomic DNA. E. Number of chromosome abnormalities per metaphase spreads of ΔXPA or ΔXPA-MUTYH HAP1 exposed at different doses of UV irradiation. Data in (E) represented as mean ± SEM. F. Survival of WT and ΔMULE HAP1 cells exposed to UV irradiation at different doses and assessed after 3 days using CellTitre-Glo. G. Model illustrating the proposed mechanism by which acetohexamide corrects NER deficiency via MUTYH degradation.

Figure S1: Generation of the XPA deficient HAP1 cell line and experimental optimization for the high-throughput drug screen. A. Immunoblots of whole cell extracts of WT and ΔXPA cells as well as XPA patient-derived fibroblasts (XPA$^{\Delta/\Delta}$). Tubulin was used as a loading control. (B) Survival of WT and ΔXPA cells and patient derived fibroblasts (XPA$^{\Delta/\Delta}$) following UV exposure assessed after 3 days using CellTitre-Glo. C. Colony formation assay of WT and ΔXPA cells irradiated with UV at different doses as indicated and kept in culture for 10 days. D. WT and ΔXPA cells were seeded in 384-well plates and irradiated at different UV doses, as indicated.

Figure S2: High-throughput drug screen reveals that acetohexamide alleviates the UV sensitivity of NER deficient cells. A. Spearman's rank correlation coefficient to determine the experimental reproducibility of the two biological replicates for the high-throughput drug screen performed on WT and ΔXPA cells after UV irradiation or under untreated conditions. B. Separation between DMSO control-treated samples after 2,000 J/M^2 UV irradiated or untreated. C. Top 10 drugs that showed an alleviation of cell death of ΔXPA more than 40% compared to wildtype cells.

Figure S3: Acetohexamide alleviates UV and illudin S sensitivity of ΔXPA cells due to enhanced clearance of CPDs

A. Dose–response curve of WT and ΔXPA cells treated with or without 0.5 mM acetohexamide for the indicated times, followed by UV irradiation. Survival was assessed after 3 days using CellTiter-Glo. Displayed is the relative viability obtained by normalizing the raw data of the DMSO control to acetohexamide treated cells. Error bars indicate SEM (n = 3). B. Clonogenic survival of WT and ΔXPA cells treated with 0.5 mM acetohexamide for 6 hours or left untreated, then challenged with illudin S for 10 days, as indicated. C-D. WT HAP1 and ΔXPA cells were treated with or without 0.5 mM Acetohexamide for 6 hours, followed by 15 J/M^2 irradiation and then released into compound-free media for the indicated time points and immunoblotted with the indicated antibodies. Actin was used as a loading control. E. WT and ΔXPA cells treated with or without 0.5 mM acetohexamide for the indicated time followed by 15 J/M^2 irradiation and analyzed by dot blot for the presence of CPDs in genomic DNA. F. Quantification of the intensities of the (E).

Figure S4: Acetohexamide does not function by altering the cell cycle, apoptosis or by quenching reactive oxygen species

A**.** WT and ΔXPA cells were either treated with DMSO or 0.5 mM acetohexamide for 6 hours. Cell cycle profiles were determined using propidium iodide staining followed by FACS analysis. B-E. Survival of WT HAP1 cells treated with either DMSO or 0.5 mM acetohexamide for 6 hours, followed by exposure to the indicated DNA damaging agents (MMC, HU, NCS, MMS and illudin S). Survival was assessed after 3 days using CellTitre-Glo. F. Cell viability of WT cells treated either with 0.5 mM acetohexamide or 30 μM N-acetylcysteine (NAC) for 6 hours, followed by 30 J/M^2 UV exposure.

Figure S5: Acetohexamide does not function via SUR1 inhibition in NER deficient cells. A. RPKM values from RNA sequencing of Sur1 expression in HAP1 WT cells compared to Gapdh expression. B. mRNA expression of Sur1 transcript assessed by

quantitative reverse transcription PCR in WT and ΔXPA cells with or without 0.5 mM acetohexamide treatment for 6 hours followed by 15 J/M^2 UV irradiation and recovered as indicated. Expression of Gapdh was used as a reference. Error bars indicate standard error of the mean "SEM" (n=3). C. Workflow for the identification of genetic rescue interactions for ΔXPA following UV irradiation using genome-wide CRISPR-Cas9 screen. D. Bubble plot displaying the rescue score of enriched DNA repair genes (rescue score: defined as the difference in survival of a given gRNAs in ΔXPA cell line compared to gRNAs control, following UV irradiation). The red bubble highlights MUTYH.

Figure S6: Not all sulfonylurea compounds correct the UV sensitivity of NER deficient cells: A-C. Cell viability of ΔXPA cells treated with different concentrations of acetohexamide, gliclazide and glimepiride following 10 J/M^2 of UV irradiation. D. Survival of WT and ΔXPA cells treated with or without 50 μM glibenclamide for 6 hours, followed by UV exposure. Survival was assessed after 3 days using CellTitre-Glo. E. Cell viability of ΔXPA cells treated with 10 μM of different derivatives of acetohexamide for 6 hours, followed by UV irradiation with 5 J/M^2.

Figure S7: Loss of MUTYH corrects CPD-induced UV sensitivity of XPA-deficient cells. A. ΔXPA (mCherry$^+$) and ΔXPA-MUTYH (GFP$^+$) were mixed equally and then UV irradiated with different doses, followed by FACS analysis after 10 days. B. WT, ΔMUTYH, ΔXPA ΔXPA-MUTYH HAP1 cells treated with 15 J/M^2, followed by recovery for the indicated times. Genomic DNA was analyzed for the presence of CPDs by dot blot. C. Bubble plot displaying the rescue score of enriched deubiquitin ligases in the genome-wide CRISPR-Cas9 screen.

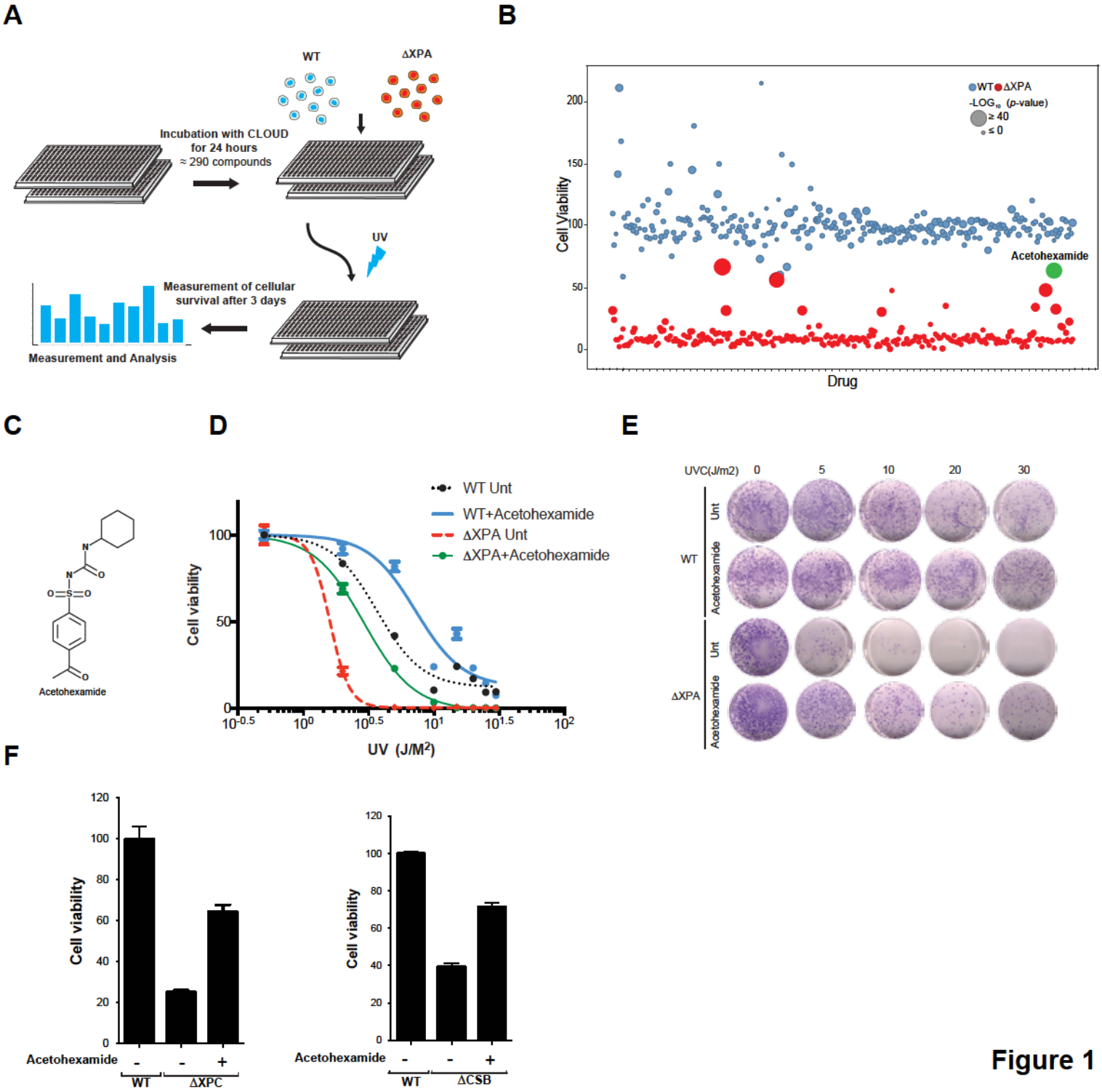
A
WT
ΔXPA
Incubation with CLOUD
for 24 hours
≈ 290 compounds
UV
Measurement of cellular
survival after 3 days
Measurement and Analysis
B
WT ΔXPA
-LOG10 (p-value)
≥ 40
≤ 0
Cell Viability
Drug
Acetohexamide
C
Acetohexamide
D
WT Unt
WT+Acetohexamide
ΔXPA Unt
ΔXPA+Acetohexamide
Cell viability
UV (J/M2)
E
UVC(J/m2) 0 5 10 20 30
WT
ΔXPA
Unt
Acetohexamide
F
Cell viability
Acetohexamide
WT
ΔXPC
ΔCSB

Figure 1

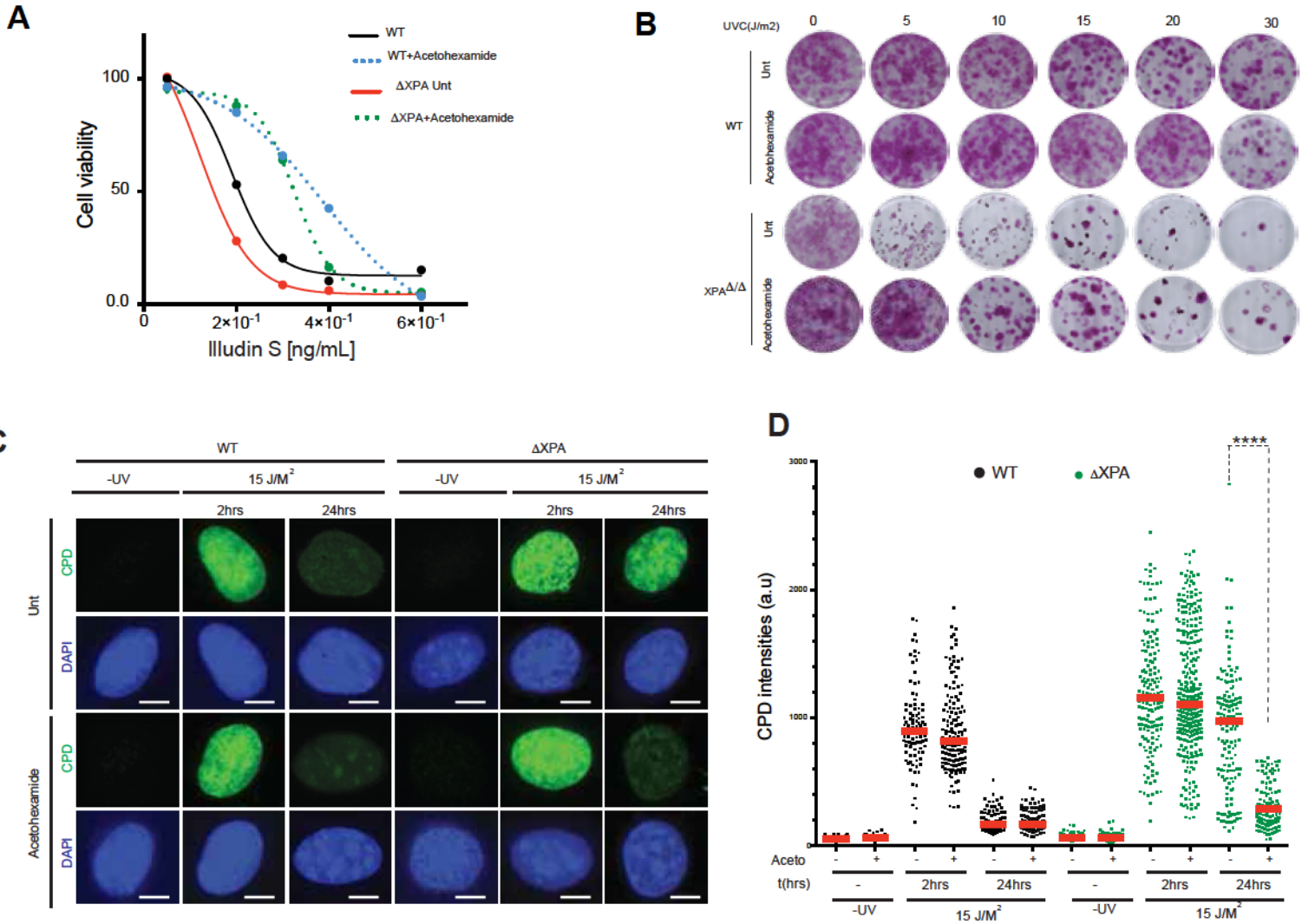
A
WT
WT+Acetohexamide
ΔXPA Unt
ΔXPA+Acetohexamide
Cell viability
100
50
0.0
0
2×10-1
4×10-1
6×10-1
Illudin S [ng/mL]
B
UVC(J/m2)
0
5
10
15
20
30
WT
XPAΔ/Δ
Unt
Acetohexamide
C
WT
ΔXPA
-UV
15 J/M2
2hrs
24hrs
Unt
Acetohexamide
CPD
DAPI
D
WT
ΔXPA
****
CPD intensities (a.u)
3000
2000
1000
0
Aceto
t(hrs)
-
2hrs
24hrs
-UV
15 J/M2

Figure 2

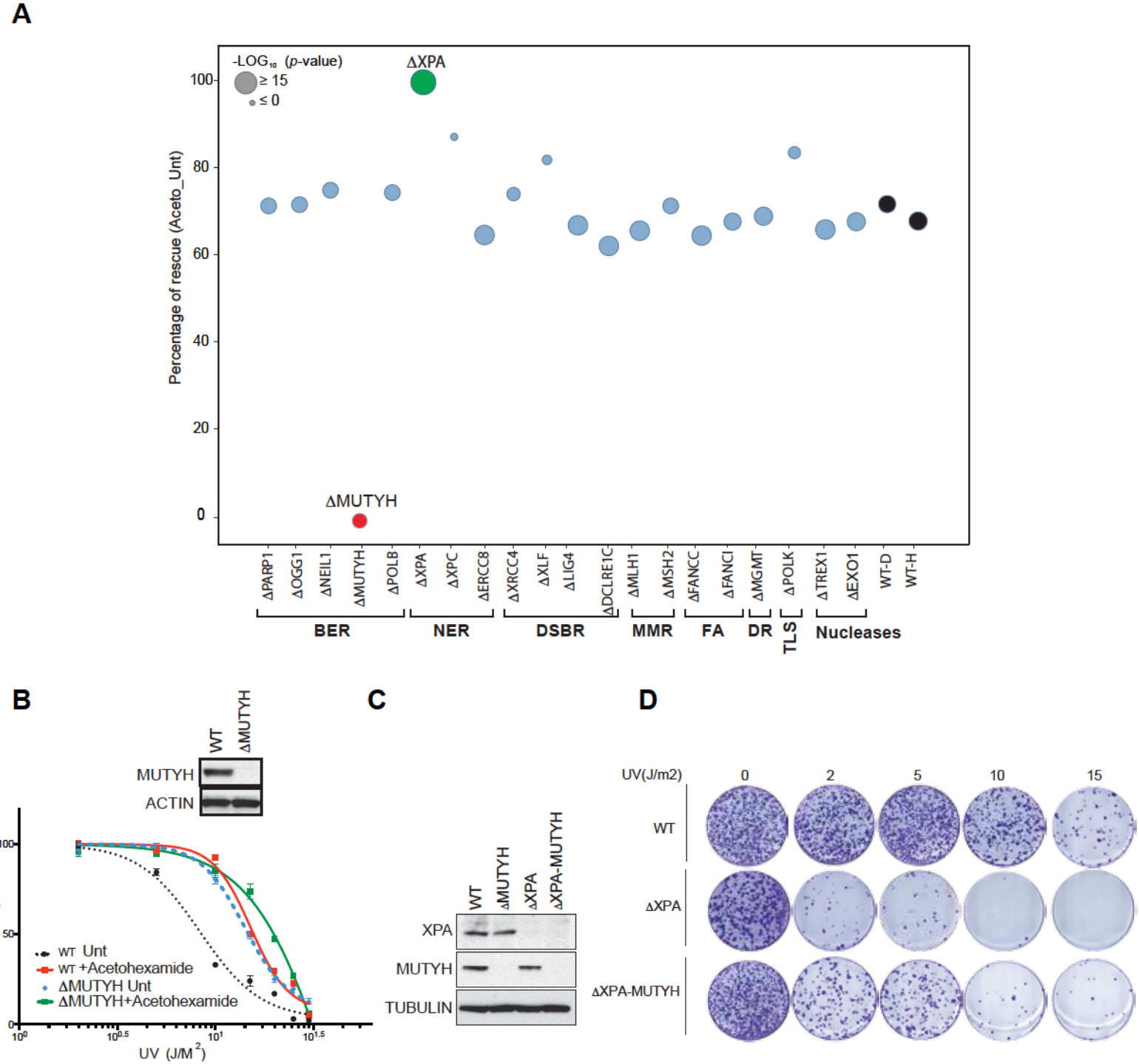
A
-LOG10 (p-value)
≥ 15
≤ 0
ΔXPA
ΔMUTYH
Percentage of rescue (Aceto_Unt)
100
80
60
40
20
0
ΔPARP1
ΔOGG1
ΔNEIL1
ΔMUTYH
ΔPOLB
ΔXPA
ΔXPC
ΔERCC8
ΔXRCC4
ΔXLF
ΔLIG4
ΔDCLRE1C
ΔMLH1
ΔMSH2
ΔFANCC
ΔFANCI
ΔMGMT
ΔPOLK
ΔTREX1
ΔEXO1
WT-D
WT-H
BER
NER
DSBR
MMR
FA
DR
TLS
Nucleases
B
WT
ΔMUTYH
MUTYH
ACTIN
Cell viability
100
50
0
WT Unt
WT +Acetohexamide
ΔMUTYH Unt
ΔMUTYH+Acetohexamide
10^0
10^0.5
10^1
10^1.5
UV (J/M^2)
C
WT
ΔMUTYH
ΔXPA
ΔXPA-MUTYH
XPA
MUTYH
TUBULIN
D
UV(J/m2)
0
2
5
10
15
WT
ΔXPA
ΔXPA-MUTYH

Figure 3

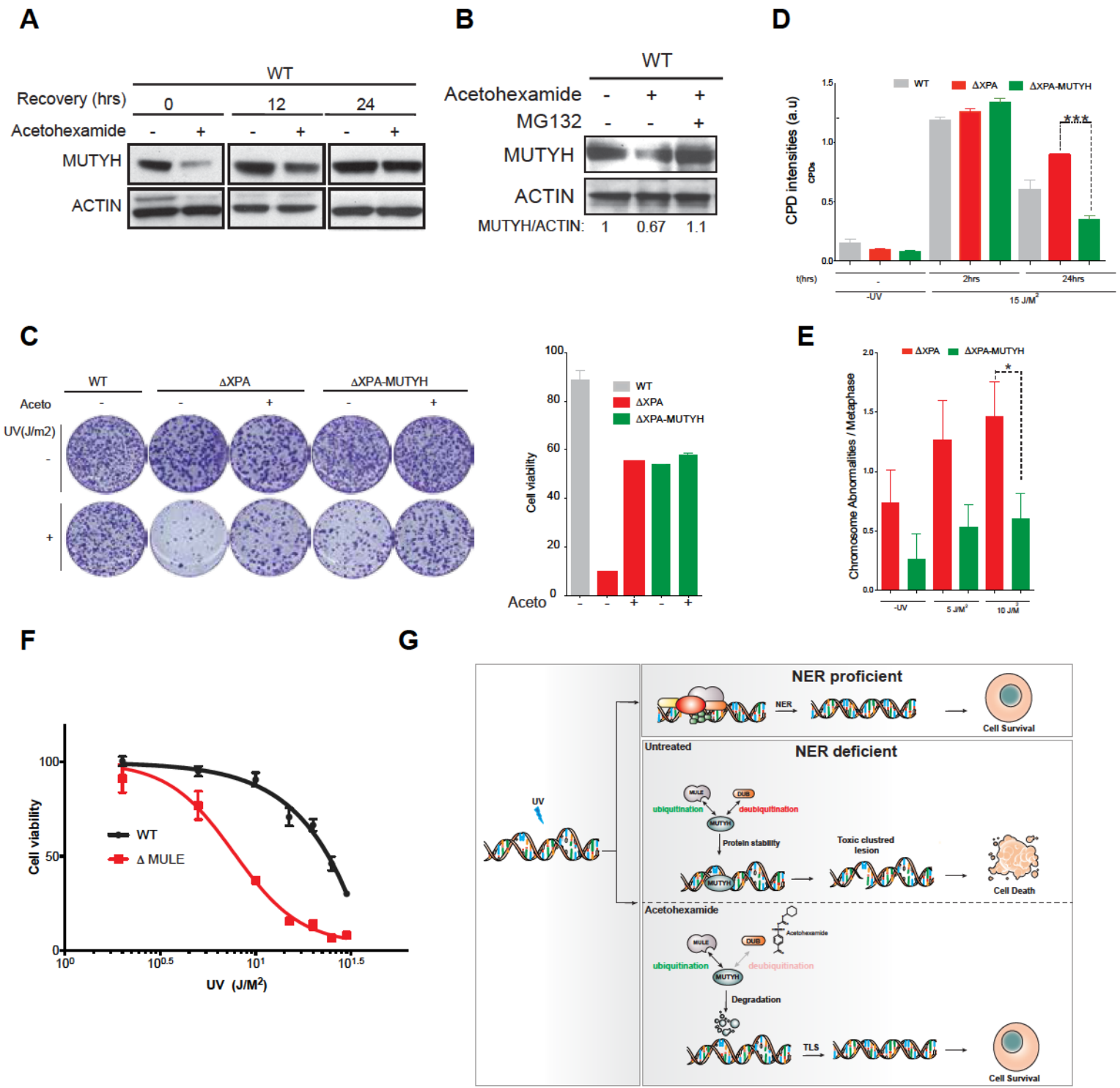
A
WT
Recovery (hrs)
0
12
24
Acetohexamide
MUTYH
ACTIN
B
WT
Acetohexamide
MG132
MUTYH
ACTIN
MUTYH/ACTIN:
1
0.67
1.1
D
WT
ΔXPA
ΔXPA-MUTYH
CPD intensities (a.u)
CPDs
t(hrs)
-UV
2hrs
24hrs
15 J/M²
C
WT
ΔXPA
ΔXPA-MUTYH
Aceto
UV(J/m2)
Cell viability
E
ΔXPA
ΔXPA-MUTYH
Chromosome Abnormalities / Metaphase
-UV
5 J/M²
10 J/M²
F
Cell viability
WT
Δ MULE
UV (J/M²)
G
NER proficient
NER
Cell Survival
Untreated
NER deficient
UV
MULE
DUB
ubiquitination
deubiquitination
MUTYH
Protein stability
Toxic clustred lesion
Cell Death
Acetohexamide
Degradation
TLS
Cell Survival

Figure 4

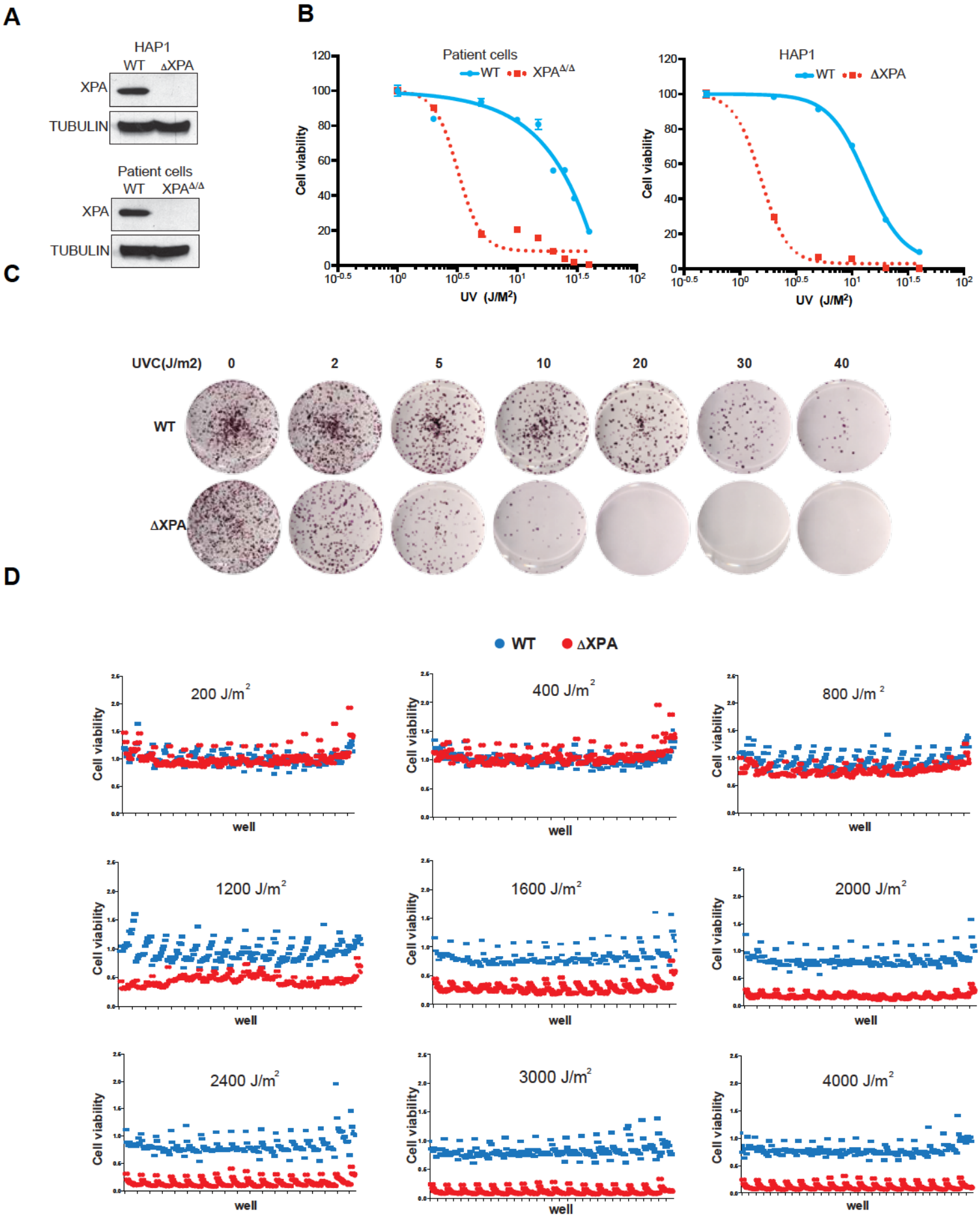
A
HAP1
WT
ΔXPA
XPA
TUBULIN
Patient cells
WT
XPA^Δ/Δ
XPA
TUBULIN
B
Patient cells
WT
XPA^Δ/Δ
Cell viability
UV (J/M2)
HAP1
WT
ΔXPA
Cell viability
UV (J/M2)
C
UVC(J/m2)
0
2
5
10
20
30
40
WT
ΔXPA
D
WT
ΔXPA
200 J/m2
400 J/m2
800 J/m2
1200 J/m2
1600 J/m2
2000 J/m2
2400 J/m2
3000 J/m2
4000 J/m2
Cell viability
well

Figure S1

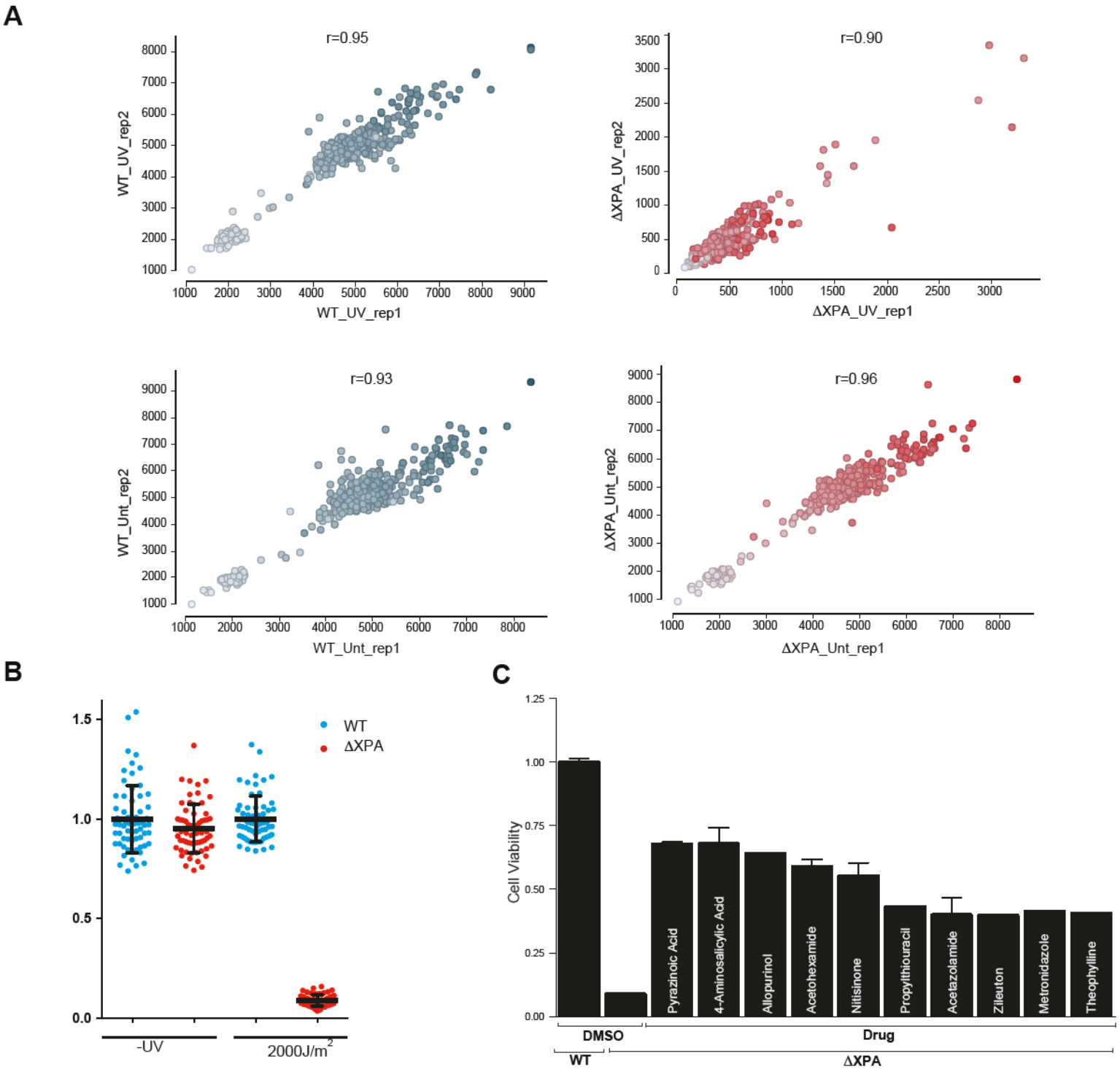
A
r=0.95
WT_UV_rep2
WT_UV_rep1
r=0.90
ΔXPA_UV_rep2
ΔXPA_UV_rep1
r=0.93
WT_Unt_rep2
WT_Unt_rep1
r=0.96
ΔXPA_Unt_rep2
ΔXPA_Unt_rep1
B
WT
ΔXPA
-UV
2000J/m2
C
Cell Viability
Pyrazinoic Acid
4-Aminosalicylic Acid
Allopurinol
Acetohexamide
Nitisinone
Propylthiouracil
Acetazolamide
Zileuton
Metronidazole
Theophylline
DMSO
Drug
WT
ΔXPA

Figure S2

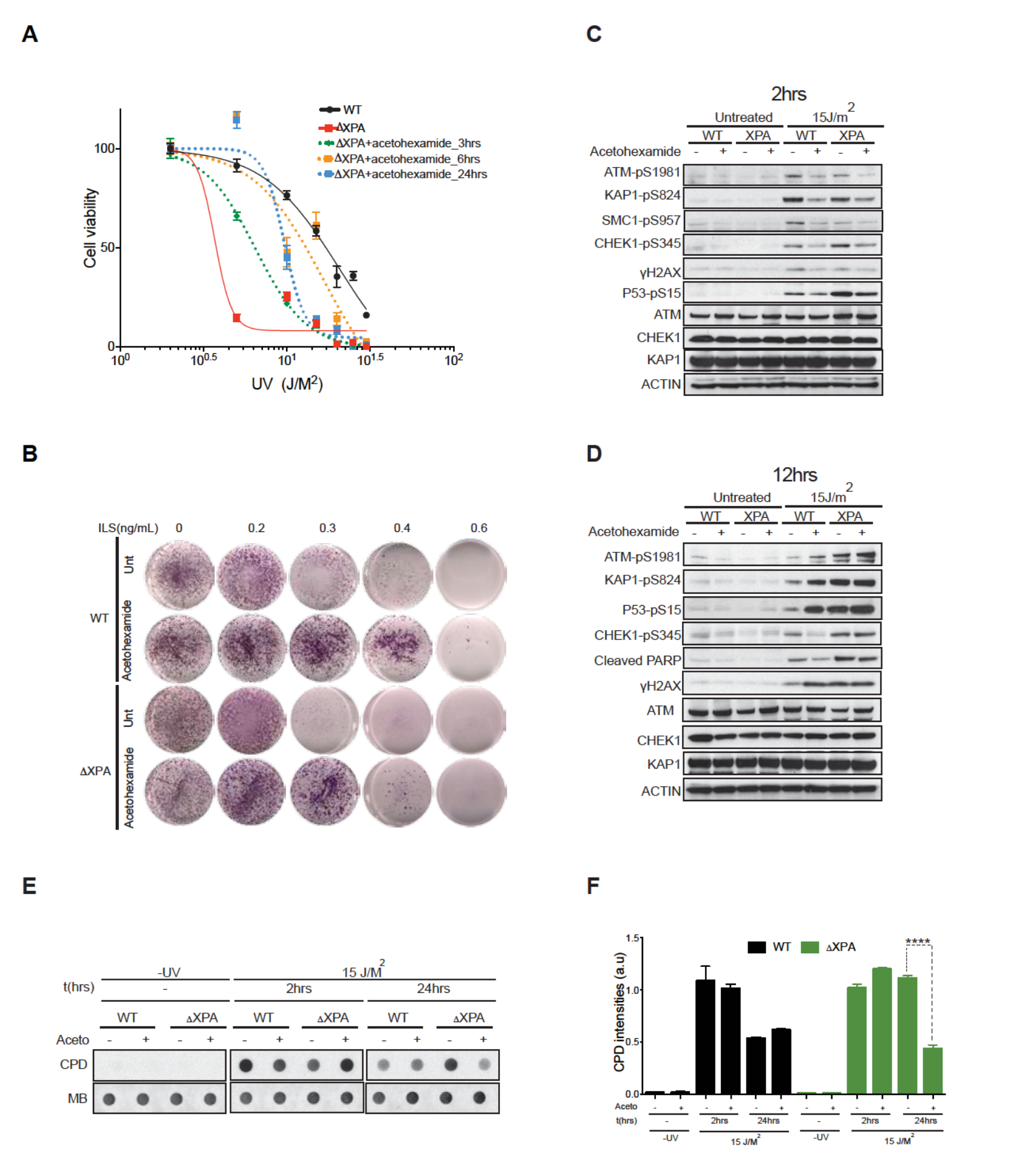
A
WT
ΔXPA
ΔXPA+acetohexamide_3hrs
ΔXPA+acetohexamide_6hrs
ΔXPA+acetohexamide_24hrs
Cell viability
UV (J/M2)
B
ILS(ng/mL)
0
0.2
0.3
0.4
0.6
WT
ΔXPA
Unt
Acetohexamide
C
2hrs
Untreated
15J/m2
WT
XPA
Acetohexamide
ATM-pS1981
KAP1-pS824
SMC1-pS957
CHEK1-pS345
γH2AX
P53-pS15
ATM
CHEK1
KAP1
ACTIN
D
12hrs
Cleaved PARP
E
-UV
15 J/M2
t(hrs)
2hrs
24hrs
Aceto
CPD
MB
F
CPD intensities (a.u)
****

Figure S3

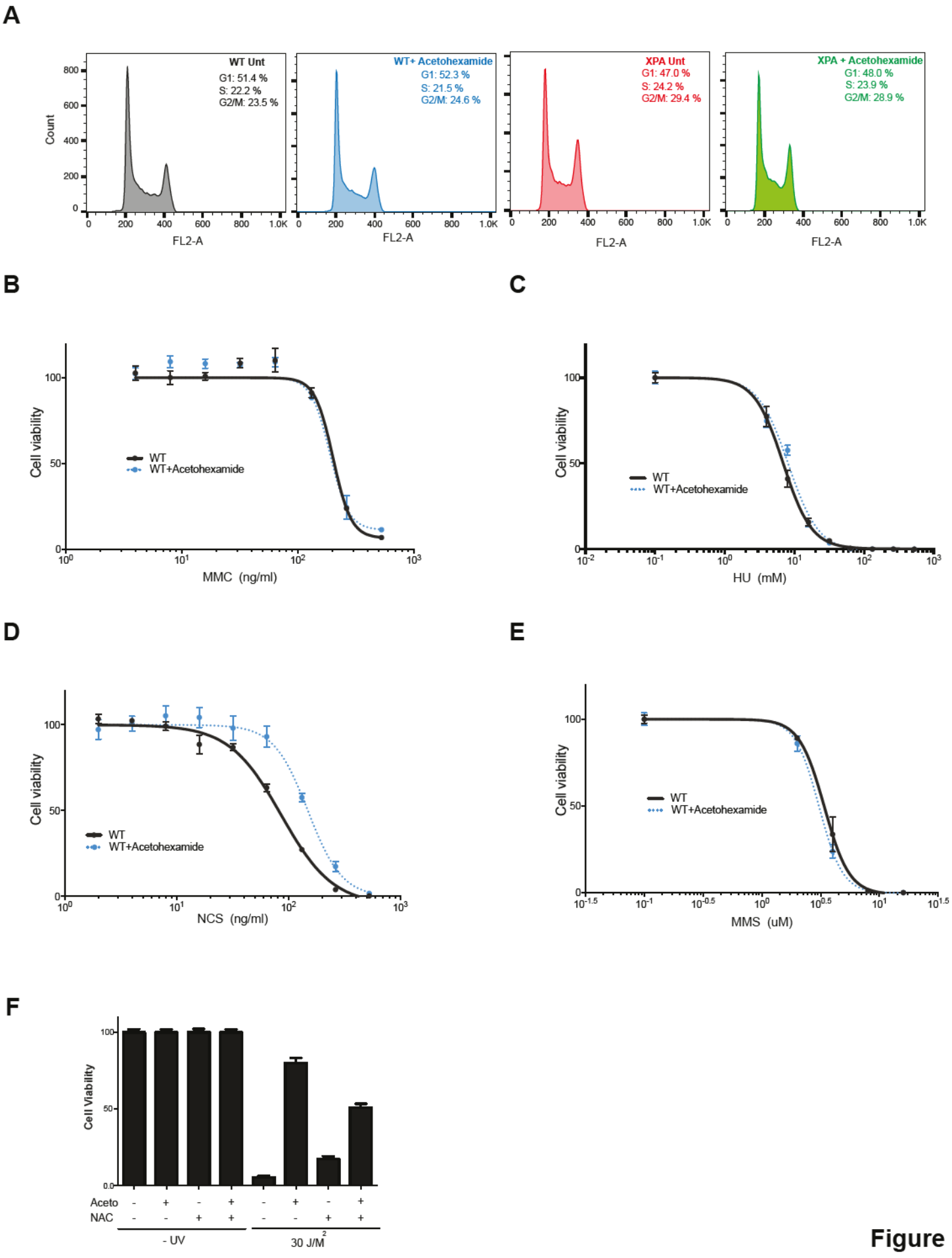
A
WT Unt
G1: 51.4 %
S: 22.2 %
G2/M: 23.5 %
WT+ Acetohexamide
G1: 52.3 %
S: 21.5 %
G2/M: 24.6 %
XPA Unt
G1: 47.0 %
S: 24.2 %
G2/M: 29.4 %
XPA + Acetohexamide
G1: 48.0 %
S: 23.9 %
G2/M: 28.9 %
Count
FL2-A
B
Cell viability
WT
WT+Acetohexamide
MMC (ng/ml)
C
HU (mM)
D
NCS (ng/ml)
E
MMS (uM)
F
Cell Viability
Aceto
NAC
- UV
30 J/M2

Figure S4

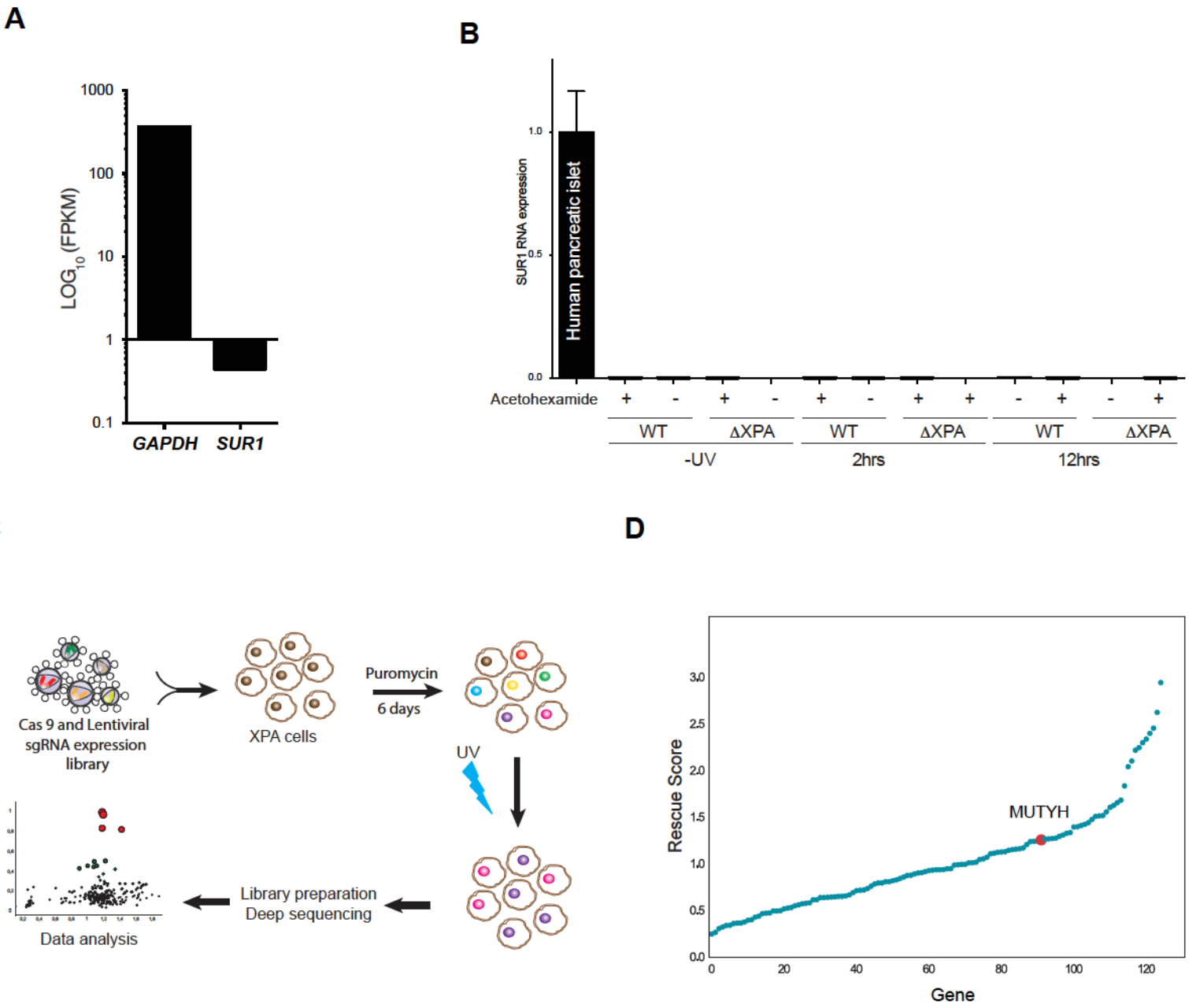
A
1000
100
10
1
0.1
LOG10 (FPKM)
GAPDH
SUR1
B
SUR1 RNA expression
1.0
0.5
0.0
Human pancreatic islet
Acetohexamide
+ - + - + - + + - + - +
WT
ΔXPA
WT
ΔXPA
WT
ΔXPA
-UV
2hrs
12hrs
C
Cas 9 and Lentiviral sgRNA expression library
XPA cells
Puromycin
6 days
UV
Library preparation
Deep sequencing
Data analysis
D
Rescue Score
3.0
2.5
2.0
1.5
1.0
0.5
0.0
MUTYH
0
20
40
60
80
100
120
Gene

Figure S5

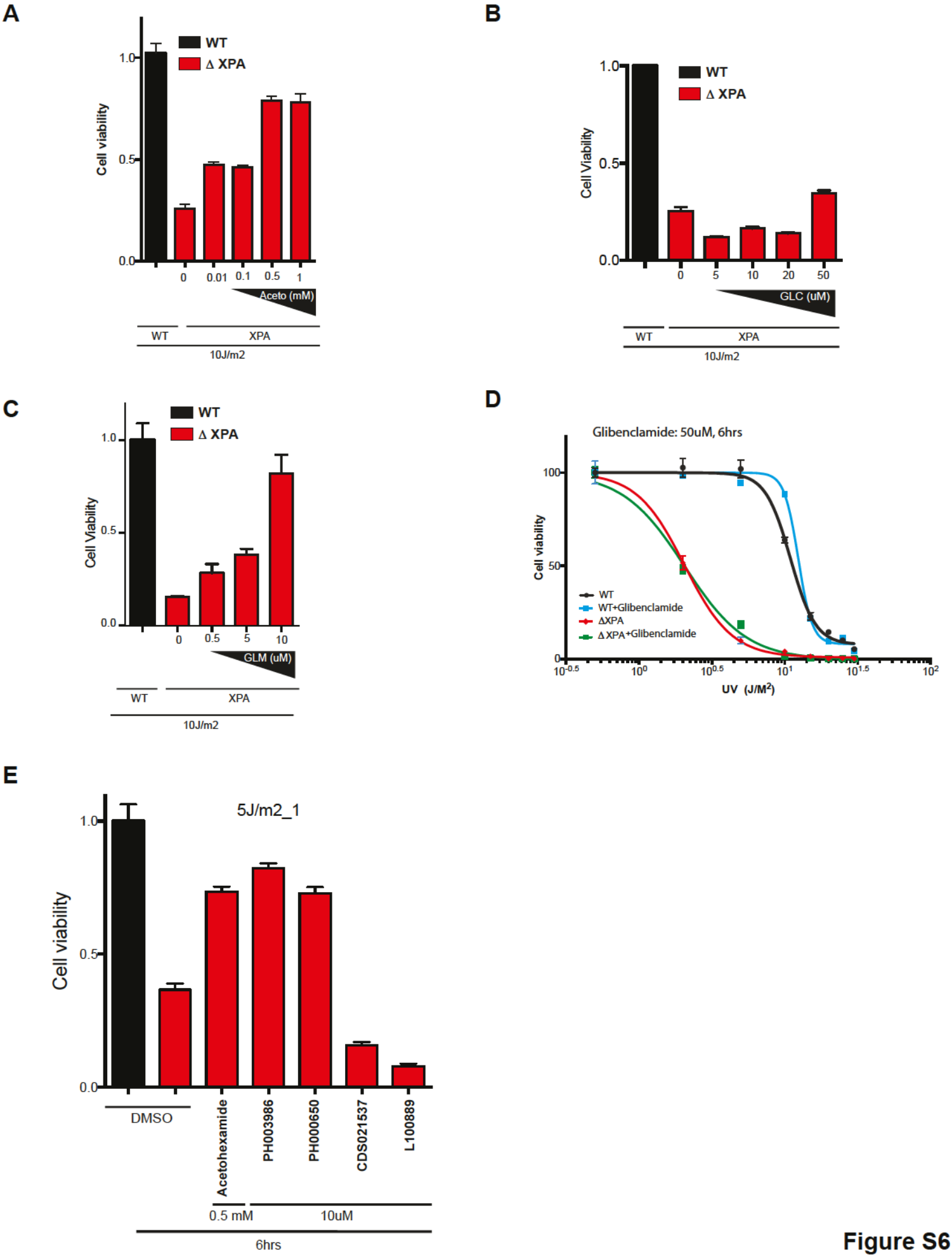
A
WT
Δ XPA
Cell viability
1.0
0.5
0.0
0
0.01
0.1
0.5
1
Aceto (mM)
WT
XPA
10J/m2
B
WT
Δ XPA
Cell Viability
1.0
0.5
0.0
0
5
10
20
50
GLC (uM)
WT
XPA
10J/m2
C
WT
Δ XPA
Cell Viability
1.0
0.5
0.0
0
0.5
5
10
GLM (uM)
WT
XPA
10J/m2
D
Glibenclamide: 50uM, 6hrs
Cell viability
100
50
0
WT
WT+Glibenclamide
ΔXPA
ΔXPA+Glibenclamide
$10^{-0.5}$
10^{0}
$10^{0.5}$
10^{1}
$10^{1.5}$
10^{2}
UV (J/M^2)
E
5J/m2_1
Cell viability
1.0
0.5
0.0
DMSO
Acetohexamide
PH003986
PH000650
CDS021537
L100889
0.5 mM
10uM
6hrs

Figure S6

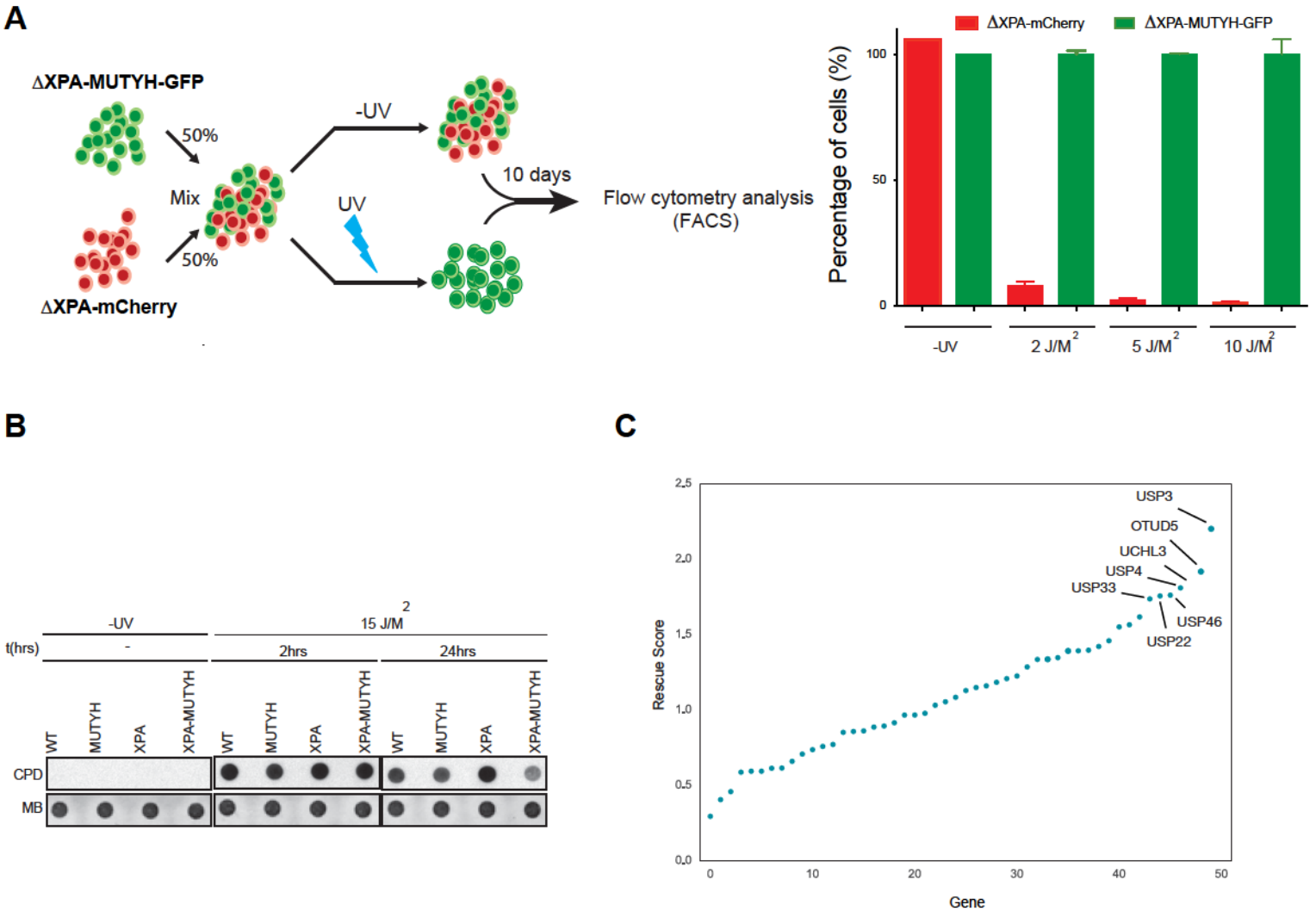
A
ΔXPA-MUTYH-GFP
50%
Mix
50%
ΔXPA-mCherry
-UV
UV
10 days
Flow cytometry analysis
(FACS)
ΔXPA-mCherry
ΔXPA-MUTYH-GFP
Percentage of cells (%)
100
50
0
-UV
2 J/M2
5 J/M2
10 J/M2
B
-UV
15 J/M2
t(hrs)
-
2hrs
24hrs
WT
MUTYH
XPA
XPA-MUTYH
CPD
MB
C
Rescue Score
Gene
USP3
OTUD5
UCHL3
USP4
USP33
USP46
USP22

Figure S7

4. CHAPTER THREE: CONCLUDING DISCUSSION

4.1. Replication stress-induced events dependent on ATM and ATMIN

To systematically examine the cellular response to replication stress, we have implemented an approach that relies on using transcriptomics and phosphoproteomics. Here, we show that replication stress induces time-dependent and widespread changes to gene expression and protein phosphorylation. These changes are clustered in to early and late responses, which are regulated to a great extent by ATM and/or its cofactor ATMIN. Furthermore, we reveal that in response to the cellular threat imposed by replication stress, the post-translational modification of proteins by phosphorylation is altered more dramatically than the expression profile.

The post-translational modifications (PTMs) induced by DNA double-strand breaks (DSBs), specifically the phosphorylation, are extensively investigated by numerous proteome-wide studies, however replication stress responses remains poorly investigated (Beli, Lukashchuk et al., 2012, Bensimon, Schmidt et al., 2010, Choi, Srivas et al., 2012, Matsuoka, Ballif et al., 2007). Therefore, we have applied high throughput mass spectrometry based proteomics and RNA sequencing to investigate for the first time the role of ATM and its cofactor ATMIN in signaling replication stress, in a time resolved manner. Our data reveal that ATM and ATMIN play crucial function in regulating several replication stress induced phosphorylation sites. We also show that ATM functions in the early replication stress signaling, which has not been previously reported. ATM is activated by various types of DNA damage, which requires the both co-factors ATMIN and NBS1 for its activity. The former is important for ATM signaling following DSBs, while ATMIN has a crucial function in ATM activation following replication stress and it binds to ATM in a manner similar to how NBS1 interacts to ATM utilizing a short carboxy-terminal motif (Kanu & Behrens, 2007, Kanu & Behrens, 2008, Schmidt, Wiedner et al., 2014, Wang, Yang et al., 2014, Zhang, Penicud et al., 2012). In light of the model suggested by these studies, we found that many of the replication stress induced phosphorylation sites are shared between ATM and ATMIN, revealing an important role of ATMIN as a cofactor to support the kinase activity of ATM. Our data also reveal that multiple phosphorylation sites induced by replication stress are regulated by ATMIN in an ATM independent manner, suggesting a general role for ATMIN in modulating phosphorylation events following replication stress.

Systematic construction of the networks involving the kinase-substrate and phosphatase-substrate dynamic relationship derived from our data propose that, in addition to ATM and DNA-PKcs, several other kinases respond to replication stress. This data indicates that replication stress induces substantially broader phosphorylation events than those associated with PIKK signaling. Moreover, our data postulates that ATMIN could operate as a general cofactor for many other kinases involved in replication stress signaling.

Interestingly, the transcriptomics data showed that several ATMIN dependent phosphorylation sites are not altered in gene expression upon ATMIN depletion, suggesting that ATMIN function in phosphorylation events is independent from its role in transcription as described previously (Jurado, Gleeson et al., 2012).

ATM is known to trigger a panoply of signaling pathways, in response to different cellular stresses, but predominantly to DNA double strand breaks. Here, we show that ATM additionally plays a crucial function in regulating early and late phosphorylation events in response replication stress. This is further confirmed by a large-scale study, demonstrating that ATM is indeed activated and recruited after replication stress to the nascent chromatin of stalled forks during initial steps of DNA synthesis (Alabert, Bukowski-Wills et al., 2014).

Our study also describes for the first time the modulation of H2AX phosphorylation at serine 140 known as γH2AX by ATMIN. This posttranslational modification that takes place on the chromatin to signal various stimuli to DNA damage, has also been shown previously to signal replication stress (Burhans & Weinberger, 2007, Flach, Bakker et al., 2014). This highlights the importance of ATMIN in signaling replication stress. Depletion of the histone variant H2AX has a strong effect in signaling DNA damage response (DDR), including failure to recruit several DDR factors to the DNA damage site such as MDC1 and 53BP1 (Celeste, Fernandez-Capetillo et al., 2003, Celeste, Petersen et al., 2002, Paull, Rogakou et al., 2000). Our data also suggest that the regulation of H2AX phosphorylation by ATMIN might affect the downstream signaling factors such as 53BP1. Indeed, ATMIN depletion reduced significantly 53BP1 localization to the site of DNA damage upon replication stress treatment, leading to increased errors during DNA replication and causing genomic instability (Kanu, Zhang et al., 2016, Schmidt et al., 2014).

Interestingly, our proteome-wide study also revealed a requirement of ATMIN in regulating the phosphorylation of one of the aminohydrolase enzymes CRMP2 at

S522. CRMP2 is well known to play a crucial function in remodeling the cytoskeleton by interacting with microtubules and also to be essential for class 3 semaphorins signaling. Phosphorylation of CRMP2 at S522, that is ensured by the kinase CDK5, is crucial for its binding to the mitotic spindle, which subsequently primes its phosphorylation at T501 and T514 by the kinase GSK3β during pro-metaphase (Oliemuller, Pelaez et al., 2013). We found that CRMP2 is a phosphoprotein induced by replication stress at the priming residue S522 after 24 hrs APH treatment, which coincided with cell arrest in S-phase. This suggests that the phosphorylation of CRMP2 (S522) has a novel function in signaling replication stress, besides its known role in mitosis, which is supported by the fact that cells with phospho-mutant CRMP2 are more sensitive to DNA damage triggered by replication stress. Based on this data we hypothesize that ATMIN may modulate the kinase activity of CDK5, thereby inducing CRMP2 phosphorylation (S522). CRMP2 is involved in several neuropathologic disorders, specifically in Alzheimer's disease (AD). This protein is highly phosphorylated at the priming site S522 within neurofibrillary tangles (NFTs) and peptide-rich plaques (Hensley, Venkova et al., 2011). This postulates the potential involvement of ATMIN in Alzheimer's disease, since it modulates CRMP2 phosphorylation. Moreover, the high phosphorylation levels of CRMP2 observed in the AD patients could originate from replication stress during abortive cell cycle re-entry in neuronal cells (Yang, Geldmacher et al., 2001).

In conclusion our study has charted for the first time the replication stress response and shown that this signaling pathway is modulated by differential protein phosphorylation more substantially than by gene expression. Moreover, we underlined the crucial role of ATM-ATMIN pathway in regulating a large number of phosphorylation sites, including sites in several DNA repair factors. Interestingly, ATMIN and ATM overlap in their substrates, suggesting ATMIN as ATM cofactor following replication stress. Furthermore, we found that ATMIN controls H2AX phosphorylation at serine, upon replication stress treatment.

We additionally identified a considerable number of proteins that have not been associated with DNA damage induced by replication stress. We also show that CRMP2 is a novel replication-induced phospho-protein that depends on ATMIN for its function and ensures chromosomal stability and cell survival. Finally, our study suggests that several other kinases, in addition to ATM, modulate the replication stress signaling by using ATMIN as a cofactor. Collectively, our data provide a systematic and

comprehensive analysis of the replication stress signaling in time-resolved manner, which may allow the identification of novel players in replication stress signaling and associated diseases.

4.2. MUTYH loss corrects nucleotide excision repair deficiency

Despite the advances that have been made in revealing the genetic mutations of various diseases associated with NER deficiency, the development of effective therapies has remained a challenge. Most of the medical interventions for patients suffering from NER deficiency are preventives rather than being curative. However, the concept of synthetic rescue represents a promising avenue for correcting defects in NER. Based on this concept, we aimed to search for compounds that may rescue the UV sensitivity of nucleotide excision repair (NER) deficient cells. We performed a high-throughput drug screen using a library of Food and Drug Administration (FDA) approved compounds to allow for potential drug repurposing.

Here, we have shown that an anti-diabetic drug, acetohexamide alleviates the sensitivity of NER deficient cells and enhances the repair of UV lesions. Independently from the canonical target SUR1, acetohexamide targets MUTYH for degradation in a proteasome dependent manner. However, the mechanism of this degradation remains still elusive. It has been reported that MUTYH is ubiquitinated by the E3 ubiquitin ligase Mule at the C terminal of the protein, changing its protein levels and recruitment to chromatin (Dorn et al., 2014). Furthermore, we found that Mule depletion sensitizes cells to UV irradiation due to alteration in MUTYH stability. Taking together these considerations, we hypothesize that acetohexamide is probably acting through inhibition of a deubiquitin ligase that opposes the effect of Mule, leading to an increase in MUTYH ubiquitination and hence triggering its degradation. Interestingly, a whole-genome CRISPR screen performed in XPA deficient cells after UV irradiation revealed several deubiquitin ligase enzymes to have a protective effect against UV irradiation including USP3 and OTUD5.

MUTYH is a DNA glycosylase enzyme that catalyzes the excision of the adenine mis-paired with 8-oxo-guanine in the base excision repair (BER) pathway. Thus, MUTYH is a particular DNA glycosylase since it removes an undamaged base situated opposite a DNA lesion, instead of removing the damaged base. Interestingly, MUTYH loss promotes cellular survival and clearance of UV-induced DNA damage without the

accumulation of chromosomal instability in NER deficient cells following UV irradiation. Therefore, we hypothesize that the toxicity observed in NER deficient cells upon UV irradiation is probably MUTYH dependent. This may be because MUTYH generates complex lesions containing DNA single breaks next to CPDs which can be dealt with in wildtype but not in NER deficient cells. Hence, removing MUTYH alleviates this toxicity and cellular death.

Mutations in the NER pathway are known to cause diverse clinical manifestations associated with several diseases including: Xeroderma pigmentosum (XP), Cockayne syndrome (CS), UV-sensitive syndrome (UVSS) and Trichothiodystrophy (TTD). All these patients display enhanced sensitivity to sunlight and UV irradiation. Therefore, the use acetohexamide or one of its derivatives may open a new approach for preventive and / or curative therapies for NER deficient patients. Since acetohexamide is an FDA-approved drug this may facilitate its repurposing for NER deficient patients because one of the biggest challenges that lengthen the process of drug development is the issues of toxicity and safety for human use.

The protective effect of acetohexamide in NER deficient cells can be also achieved by depleting MUTYH. This finding highlights the importance of developing specific inhibitors targeting the enzymatic activity of MUTYH, which could be potentially beneficial for NER deficient patients. The protective effect of MUTYH loss is also observed in mice lacking MUTYH or OGG1/MUTYH. These mice were protected against neurodegeneration under oxidative stress conditions compared to OGG1 deficient animals which exhibited striatal neurodegeneration (Sheng et al., 2012). Therefore, acetohexamide or small molecules targeting MUTYH may alleviate the neurological symptoms associated with NER deficiency observed in XP and CS patients. However, a few studies have highlighted the importance of MUTYH in protecting the intestinal tract from malignancies as well as lymphoma and adenoma (Russo et al., 2009, Sakamoto et al., 2007). Furthermore, loss-of-function mutations of MUTYH have been reported to occur in familial adenomatous polyposis (FAP), where the patients suffer from growth of adenomatous polyps in the colons and rectums (Al-Tassan et al., 2002), indicating that MUTYH plays an important role in clearing oxidative lesions in highly proliferative tissues such as the intestinal tract. Therefore, developing small molecule inhibitors for MUTYH in the brain or the skin tissues may provide additional opportunities for alleviating NER deficiency in certain diseases such as XP and CS.

Overall, our data reveal a novel synthetic viable interaction between acetohexamide or MUTYH and UV-induced cell death that could be used to develop new therapeutic approaches for a variety of diseases including those associated with NER deficiency.

REFERENCES

Adamo A, Collis SJ, Adelman CA, Silva N, Horejsi Z, Ward JD, Martinez-Perez E, Boulton SJ, La Volpe A (2010) Preventing nonhomologous end joining suppresses DNA repair defects of Fanconi anemia. Mol Cell 39: 25-35

Al-Tassan N, Chmiel NH, Maynard J, Fleming N, Livingston AL, Williams GT, Hodges AK, Davies DR, David SS, Sampson JR, Cheadle JP (2002) Inherited variants of MYH associated with somatic G:C-->T:A mutations in colorectal tumors. Nat Genet 30: 227-32

Alabert C, Bukowski-Wills JC, Lee SB, Kustatscher G, Nakamura K, de Lima Alves F, Menard P, Mejlvang J, Rappsilber J, Groth A (2014) Nascent chromatin capture proteomics determines chromatin dynamics during DNA replication and identifies unknown fork components. Nat Cell Biol 16: 281-93

Beli P, Lukashchuk N, Wagner SA, Weinert BT, Olsen JV, Baskcomb L, Mann M, Jackson SP, Choudhary C (2012) Proteomic investigations reveal a role for RNA processing factor THRAP3 in the DNA damage response. Mol Cell 46: 212-25

Bensimon A, Aebersold R, Shiloh Y (2011) Beyond ATM: the protein kinase landscape of the DNA damage response. FEBS Lett 585: 1625-39

Bensimon A, Schmidt A, Ziv Y, Elkon R, Wang SY, Chen DJ, Aebersold R, Shiloh Y (2010) ATM-dependent and -independent dynamics of the nuclear phosphoproteome after DNA damage. Sci Signal 3: rs3

Blomen VA, Majek P, Jae LT, Bigenzahn JW, Nieuwenhuis J, Staring J, Sacco R, van Diemen FR, Olk N, Stukalov A, Marceau C, Janssen H, Carette JE, Bennett KL, Colinge J, Superti-Furga G, Brummelkamp TR (2015) Gene essentiality and synthetic lethality in haploid human cells. Science

Bouwman P, Aly A, Escandell JM, Pieterse M, Bartkova J, van der Gulden H, Hiddingh S, Thanasoula M, Kulkarni A, Yang Q, Haffty BG, Tommiska J, Blomqvist C, Drapkin R, Adams DJ, Nevanlinna H, Bartek J, Tarsounas M, Ganesan S, Jonkers J (2010) 53BP1 loss rescues BRCA1 deficiency and is associated with triple-negative and BRCA-mutated breast cancers. Nat Struct Mol Biol 17: 688-95

Bunting SF, Callen E, Wong N, Chen HT, Polato F, Gunn A, Bothmer A, Feldhahn N, Fernandez-Capetillo O, Cao L, Xu X, Deng CX, Finkel T, Nussenzweig M, Stark JM, Nussenzweig A (2010) 53BP1 inhibits homologous recombination in Brca1-deficient cells by blocking resection of DNA breaks. Cell 141: 243-54

Burhans WC, Weinberger M (2007) DNA replication stress, genome instability and aging. Nucleic Acids Res 35: 7545-56

Burke MA, Mutharasan RK, Ardehali H (2008) The sulfonylurea receptor, an atypical ATP-binding cassette protein, and its regulation of the KATP channel. Circ Res 102: 164-76

Camenisch U, Dip R, Schumacher SB, Schuler B, Naegeli H (2006) Recognition of helical kinks by xeroderma pigmentosum group A protein triggers DNA excision repair. Nat Struct Mol Biol 13: 278-84

Cappelli E, Taylor R, Cevasco M, Abbondandolo A, Caldecott K, Frosina G (1997) Involvement of XRCC1 and DNA ligase III gene products in DNA base excision repair. J Biol Chem 272: 23970-5

Ceccaldi R, Sarangi P, D'Andrea AD (2016) The Fanconi anaemia pathway: new players and new functions. Nat Rev Mol Cell Biol 17: 337-49

Celeste A, Fernandez-Capetillo O, Kruhlak MJ, Pilch DR, Staudt DW, Lee A, Bonner RF, Bonner WM, Nussenzweig A (2003) Histone H2AX phosphorylation is dispensable for the initial recognition of DNA breaks. Nat Cell Biol 5: 675-9

Celeste A, Petersen S, Romanienko PJ, Fernandez-Capetillo O, Chen HT, Sedelnikova OA, Reina-San-Martin B, Coppola V, Meffre E, Difilippantonio MJ, Redon C, Pilch DR, Olaru A, Eckhaus M, Camerini-Otero RD, Tessarollo L, Livak F, Manova K, Bonner WM, Nussenzweig MC et al. (2002) Genomic instability in mice lacking histone H2AX. Science 296: 922-7

Chen R, Shi L, Hakenberg J, Naughton B, Sklar P, Zhang J, Zhou H, Tian L, Prakash O, Lemire M, Sleiman P, Cheng WY, Chen W, Shah H, Shen Y, Fromer M, Omberg L, Deardorff MA, Zackai E, Bobe JR et al. (2016) Analysis of 589,306 genomes identifies individuals resilient to severe Mendelian childhood diseases. Nat Biotechnol 34: 531-8

Choi S, Srivas R, Fu KY, Hood BL, Dost B, Gibson GA, Watkins SC, Van Houten B, Bandeira N, Conrads TP, Ideker T, Bakkenist CJ (2012) Quantitative proteomics reveal ATM kinase-dependent exchange in DNA damage response complexes. J Proteome Res 11: 4983-91

Cleaver JE (2005) Cancer in xeroderma pigmentosum and related disorders of DNA repair. Nat Rev Cancer 5: 564-73

Coin F, Oksenych V, Egly JM (2007) Distinct roles for the XPB/p52 and XPD/p44 subcomplexes of TFIIH in damaged DNA opening during nucleotide excision repair. Mol Cell 26: 245-56

Crossan GP, Patel KJ (2012) The Fanconi anaemia pathway orchestrates incisions at sites of crosslinked DNA. J Pathol 226: 326-37

de Boer J, Hoeijmakers JH (2000) Nucleotide excision repair and human syndromes. Carcinogenesis 21: 453-60

de Laat WL, Appeldoorn E, Sugasawa K, Weterings E, Jaspers NG, Hoeijmakers JH (1998) DNA-binding polarity of human replication protein A positions nucleases in nucleotide excision repair. Genes Dev 12: 2598-609

Deans AJ, West SC (2011) DNA interstrand crosslink repair and cancer. Nat Rev Cancer 11: 467-80

Demple B, Herman T, Chen DS (1991) Cloning and expression of APE, the cDNA encoding the major human apurinic endonuclease: definition of a family of DNA repair enzymes. Proc Natl Acad Sci U S A 88: 11450-4

Dianov G, Price A, Lindahl T (1992) Generation of single-nucleotide repair patches following excision of uracil residues from DNA. Mol Cell Biol 12: 1605-12

Dietz HC (2010) New therapeutic approaches to mendelian disorders. N Engl J Med 363: 852-63

DiGiovanna JJ, Kraemer KH (2012) Shining a light on xeroderma pigmentosum. J Invest Dermatol 132: 785-96

Ding X, Ray Chaudhuri A, Callen E, Pang Y, Biswas K, Klarmann KD, Martin BK, Burkett S, Cleveland L, Stauffer S, Sullivan T, Dewan A, Marks H, Tubbs AT, Wong N, Buehler E, Akagi K, Martin SE, Keller JR, Nussenzweig A et al. (2016) Synthetic viability by BRCA2 and PARP1/ARTD1 deficiencies. Nat Commun 7: 12425

Dorn J, Ferrari E, Imhof R, Ziegler N, Hubscher U (2014) Regulation of human MutYH DNA glycosylase by the E3 ubiquitin ligase mule. J Biol Chem 289: 7049-58

Drummond JT, Li GM, Longley MJ, Modrich P (1995) Isolation of an hMSH2-p160 heterodimer that restores DNA mismatch repair to tumor cells. Science 268: 1909-12

Dubaele S, Proietti De Santis L, Bienstock RJ, Keriel A, Stefanini M, Van Houten B, Egly JM (2003) Basal transcription defect discriminates between xeroderma pigmentosum and trichothiodystrophy in XPD patients. Mol Cell 11: 1635-46
Fan L, Fuss JO, Cheng QJ, Arvai AS, Hammel M, Roberts VA, Cooper PK, Tainer JA (2008) XPD helicase structures and activities: insights into the cancer and aging phenotypes from XPD mutations. Cell 133: 789-800
Flach J, Bakker ST, Mohrin M, Conroy PC, Pietras EM, Reynaud D, Alvarez S, Diolaiti ME, Ugarte F, Forsberg EC, Le Beau MM, Stohr BA, Mendez J, Morrison CG, Passegue E (2014) Replication stress is a potent driver of functional decline in ageing haematopoietic stem cells. Nature 512: 198-202
Flannick J, Thorleifsson G, Beer NL, Jacobs SB, Grarup N, Burtt NP, Mahajan A, Fuchsberger C, Atzmon G, Benediktsson R, Blangero J, Bowden DW, Brandslund I, Brosnan J, Burslem F, Chambers J, Cho YS, Christensen C, Douglas DA, Duggirala R et al. (2014) Loss-of-function mutations in SLC30A8 protect against type 2 diabetes. Nat Genet 46: 357-63
Forment JV, Herzog M, Coates J, Konopka T, Gapp BV, Nijman SM, Adams DJ, Keane TM, Jackson SP (2017) Genome-wide genetic screening with chemically mutagenized haploid embryonic stem cells. Nature chemical biology 13: 12-14
Fousteri M, Mullenders LH (2008) Transcription-coupled nucleotide excision repair in mammalian cells: molecular mechanisms and biological effects. Cell Res 18: 73-84
Fousteri M, Vermeulen W, van Zeeland AA, Mullenders LH (2006) Cockayne syndrome A and B proteins differentially regulate recruitment of chromatin remodeling and repair factors to stalled RNA polymerase II in vivo. Mol Cell 23: 471-82
Friedberg EC (2001) How nucleotide excision repair protects against cancer. Nat Rev Cancer 1: 22-33
Friend SH, Schadt EE (2014) Translational genomics. Clues from the resilient. Science 344: 970-2
Frosina G, Fortini P, Rossi O, Carrozzino F, Raspaglio G, Cox LS, Lane DP, Abbondandolo A, Dogliotti E (1996) Two pathways for base excision repair in mammalian cells. J Biol Chem 271: 9573-8
Garinis GA, van der Horst GT, Vijg J, Hoeijmakers JH (2008) DNA damage and ageing: new-age ideas for an age-old problem. Nat Cell Biol 10: 1241-7
Hartlerode AJ, Scully R (2009) Mechanisms of double-strand break repair in somatic mammalian cells. Biochem J 423: 157-68
Hashimoto S, Egly JM (2009) Trichothiodystrophy view from the molecular basis of DNA repair/transcription factor TFIIH. Hum Mol Genet 18: R224-30
Hensley K, Venkova K, Christov A, Gunning W, Park J (2011) Collapsin response mediator protein-2: an emerging pathologic feature and therapeutic target for neurodisease indications. Mol Neurobiol 43: 180-91
Hoeijmakers JH (2009) DNA damage, aging, and cancer. N Engl J Med 361: 1475-85
Hoffman EP, Brown RH, Jr., Kunkel LM (1987) Dystrophin: the protein product of the Duchenne muscular dystrophy locus. Cell 51: 919-28
Hombauer H, Campbell CS, Smith CE, Desai A, Kolodner RD (2011) Visualization of eukaryotic DNA mismatch repair reveals distinct recognition and repair intermediates. Cell 147: 1040-53
Jackson SP, Bartek J (2009) The DNA-damage response in human biology and disease. Nature 461: 1071-8
Jacobs AL, Schar P (2012) DNA glycosylases: in DNA repair and beyond. Chromosoma 121: 1-20

Jing Y, Kao JF, Taylor JS (1998) Thermodynamic and base-pairing studies of matched and mismatched DNA dodecamer duplexes containing cis-syn, (6-4) and Dewar photoproducts of TT. Nucleic Acids Res 26: 3845-53
Joenje H, Patel KJ (2001) The emerging genetic and molecular basis of Fanconi anaemia. Nat Rev Genet 2: 446-57
Joseph KS, Anguizola J, Jackson AJ, Hage DS (2010) Chromatographic analysis of acetohexamide binding to glycated human serum albumin. J Chromatogr B Analyt Technol Biomed Life Sci 878: 2775-81
Jurado S, Gleeson K, O'Donnell K, Izon DJ, Walkley CR, Strasser A, Tarlinton DM, Heierhorst J (2012) The Zinc-finger protein ASCIZ regulates B cell development via DYNLL1 and Bim. J Exp Med 209: 1629-39
Kanu N, Behrens A (2007) ATMIN defines an NBS1-independent pathway of ATM signalling. EMBO J 26: 2933-41
Kanu N, Behrens A (2008) ATMINistrating ATM signalling: regulation of ATM by ATMIN. Cell Cycle 7: 3483-6
Kanu N, Zhang T, Burrell RA, Chakraborty A, Cronshaw J, DaCosta C, Gronroos E, Pemberton HN, Anderton E, Gonzalez L, Sabbioneda S, Ulrich HD, Swanton C, Behrens A (2016) RAD18, WRNIP1 and ATMIN promote ATM signalling in response to replication stress. Oncogene 35: 4009-19
Kottemann MC, Smogorzewska A (2013) Fanconi anaemia and the repair of Watson and Crick DNA crosslinks. Nature 493: 356-63
Kraemer KH, Patronas NJ, Schiffmann R, Brooks BP, Tamura D, DiGiovanna JJ (2007) Xeroderma pigmentosum, trichothiodystrophy and Cockayne syndrome: a complex genotype-phenotype relationship. Neuroscience 145: 1388-96
Larrieu D, Britton S, Demir M, Rodriguez R, Jackson SP (2014) Chemical inhibition of NAT10 corrects defects of laminopathic cells. Science 344: 527-32
Laugel V (2013) Cockayne syndrome: the expanding clinical and mutational spectrum. Mech Ageing Dev 134: 161-70
Li SK, Martin A (2016) Mismatch Repair and Colon Cancer: Mechanisms and Therapies Explored. Trends Mol Med 22: 274-89
Li W, Xu H, Xiao T, Cong L, Love MI, Zhang F, Irizarry RA, Liu JS, Brown M, Liu XS (2014) MAGeCK enables robust identification of essential genes from genome-scale CRISPR/Cas9 knockout screens. Genome Biol 15: 554
Lieber MR (2008) The mechanism of human nonhomologous DNA end joining. J Biol Chem 283: 1-5
Liu H, Rudolf J, Johnson KA, McMahon SA, Oke M, Carter L, McRobbie AM, Brown SE, Naismith JH, White MF (2008) Structure of the DNA repair helicase XPD. Cell 133: 801-12
Lo JA, Fisher DE (2014) The melanoma revolution: from UV carcinogenesis to a new era in therapeutics. Science 346: 945-9
Long DT, Raschle M, Joukov V, Walter JC (2011) Mechanism of RAD51-dependent DNA interstrand cross-link repair. Science 333: 84-7
Markkanen E, Dorn J, Hubscher U (2013) MUTYH DNA glycosylase: the rationale for removing undamaged bases from the DNA. Front Genet 4: 18
Marteijn JA, Lans H, Vermeulen W, Hoeijmakers JH (2014) Understanding nucleotide excision repair and its roles in cancer and ageing. Nat Rev Mol Cell Biol 15: 465-81
Matsumoto Y, Kim K (1995) Excision of deoxyribose phosphate residues by DNA polymerase beta during DNA repair. Science 269: 699-702
Matsuoka S, Ballif BA, Smogorzewska A, McDonald ER, 3rd, Hurov KE, Luo J, Bakalarski CE, Zhao Z, Solimini N, Lerenthal Y, Shiloh Y, Gygi SP, Elledge SJ (2007)

ATM and ATR substrate analysis reveals extensive protein networks responsive to DNA damage. Science 316: 1160-6
Mazouzi A, Stukalov A, Muller AC, Chen D, Wiedner M, Prochazkova J, Chiang SC, Schuster M, Breitwieser FP, Pichlmair A, El-Khamisy SF, Bock C, Kralovics R, Colinge J, Bennett KL, Loizou JI (2016) A Comprehensive Analysis of the Dynamic Response to Aphidicolin-Mediated Replication Stress Uncovers Targets for ATM and ATMIN. Cell reports
Mazouzi A, Velimezi G, Loizou JI (2014) DNA replication stress: causes, resolution and disease. Exp Cell Res 329: 85-93
Mitchell DL, Adair GM, Nairn RS (1989) Inhibition of transient gene expression in Chinese hamster ovary cells by triplet-sensitized UV-B irradiation of transfected DNA. Photochem Photobiol 50: 639-46
Modrich P (2006) Mechanisms in eukaryotic mismatch repair. J Biol Chem 281: 30305-9
Motter AE, Gulbahce N, Almaas E, Barabasi AL (2008) Predicting synthetic rescues in metabolic networks. Molecular systems biology 4: 168
Nash RA, Caldecott KW, Barnes DE, Lindahl T (1997) XRCC1 protein interacts with one of two distinct forms of DNA ligase III. Biochemistry 36: 5207-11
Nishi R, Alekseev S, Dinant C, Hoogstraten D, Houtsmuller AB, Hoeijmakers JH, Vermeulen W, Hanaoka F, Sugasawa K (2009) UV-DDB-dependent regulation of nucleotide excision repair kinetics in living cells. DNA Repair (Amst) 8: 767-76
O'Driscoll M (2012) Diseases associated with defective responses to DNA damage. Cold Spring Harb Perspect Biol 4
Oliemuller E, Pelaez R, Garasa S, Pajares MJ, Agorreta J, Pio R, Montuenga LM, Teijeira A, Llanos S, Rouzaut A (2013) Phosphorylated tubulin adaptor protein CRMP-2 as prognostic marker and candidate therapeutic target for NSCLC. Int J Cancer 132: 1986-95
Pace P, Mosedale G, Hodskinson MR, Rosado IV, Sivasubramaniam M, Patel KJ (2010) Ku70 corrupts DNA repair in the absence of the Fanconi anemia pathway. Science 329: 219-23
Papamichos-Chronakis M, Peterson CL (2013) Chromatin and the genome integrity network. Nat Rev Genet 14: 62-75
Paull TT, Rogakou EP, Yamazaki V, Kirchgessner CU, Gellert M, Bonner WM (2000) A critical role for histone H2AX in recruitment of repair factors to nuclear foci after DNA damage. Curr Biol 10: 886-95
Philpott S, Burger H, Charbonneau T, Grimson R, Vermund SH, Visosky A, Nachman S, Kovacs A, Tropper P, Frey H, Weiser B (1999) CCR5 genotype and resistance to vertical transmission of HIV-1. J Acquir Immune Defic Syndr 21: 189-93
Podlutsky AJ, Dianova, II, Podust VN, Bohr VA, Dianov GL (2001) Human DNA polymerase beta initiates DNA synthesis during long-patch repair of reduced AP sites in DNA. EMBO J 20: 1477-82
Proks P, Reimann F, Green N, Gribble F, Ashcroft F (2002) Sulfonylurea stimulation of insulin secretion. Diabetes 51 Suppl 3: S368-76
Ray Chaudhuri A, Callen E, Ding X, Gogola E, Duarte AA, Lee JE, Wong N, Lafarga V, Calvo JA, Panzarino NJ, John S, Day A, Crespo AV, Shen B, Starnes LM, de Ruiter JR, Daniel JA, Konstantinopoulos PA, Cortez D, Cantor SB et al. (2016) Replication fork stability confers chemoresistance in BRCA-deficient cells. Nature 535: 382-7
Robson CN, Hickson ID (1991) Isolation of cDNA clones encoding a human apurinic/apyrimidinic endonuclease that corrects DNA repair and mutagenesis defects in E. coli xth (exonuclease III) mutants. Nucleic Acids Res 19: 5519-23

Russo MT, De Luca G, Casorelli I, Degan P, Molatore S, Barone F, Mazzei F, Pannellini T, Musiani P, Bignami M (2009) Role of MUTYH and MSH2 in the control of oxidative DNA damage, genetic instability, and tumorigenesis. Cancer Res 69: 4372-9

Sakamoto K, Tominaga Y, Yamauchi K, Nakatsu Y, Sakumi K, Yoshiyama K, Egashira A, Kura S, Yao T, Tsuneyoshi M, Maki H, Nakabeppu Y, Tsuzuki T (2007) MUTYH-null mice are susceptible to spontaneous and oxidative stress induced intestinal tumorigenesis. Cancer Res 67: 6599-604

Scharer OD (2013) Nucleotide excision repair in eukaryotes. Cold Spring Harb Perspect Biol 5: a012609

Schmidt L, Wiedner M, Velimezi G, Prochazkova J, Owusu M, Bauer S, Loizou JI (2014) ATMIN is required for the ATM-mediated signaling and recruitment of 53BP1 to DNA damage sites upon replication stress. DNA Repair (Amst) 24: 122-30

Schwertman P, Lagarou A, Dekkers DH, Raams A, van der Hoek AC, Laffeber C, Hoeijmakers JH, Demmers JA, Fousteri M, Vermeulen W, Marteijn JA (2012) UV-sensitive syndrome protein UVSSA recruits USP7 to regulate transcription-coupled repair. Nat Genet 44: 598-602

Scrima A, Konickova R, Czyzewski BK, Kawasaki Y, Jeffrey PD, Groisman R, Nakatani Y, Iwai S, Pavletich NP, Thoma NH (2008) Structural basis of UV DNA-damage recognition by the DDB1-DDB2 complex. Cell 135: 1213-23

Shalem O, Sanjana NE, Hartenian E, Shi X, Scott DA, Mikkelsen TS, Heckl D, Ebert BL, Root DE, Doench JG, Zhang F (2014) Genome-scale CRISPR-Cas9 knockout screening in human cells. Science 343: 84-7

Sheng Z, Oka S, Tsuchimoto D, Abolhassani N, Nomaru H, Sakumi K, Yamada H, Nakabeppu Y (2012) 8-Oxoguanine causes neurodegeneration during MUTYH-mediated DNA base excision repair. J Clin Invest 122: 4344-61

Sobol RW, Horton JK, Kuhn R, Gu H, Singhal RK, Prasad R, Rajewsky K, Wilson SH (1996) Requirement of mammalian DNA polymerase-beta in base-excision repair. Nature 379: 183-6

Sugasawa K, Okamoto T, Shimizu Y, Masutani C, Iwai S, Hanaoka F (2001) A multistep damage recognition mechanism for global genomic nucleotide excision repair. Genes Dev 15: 507-21

Sugasawa K, Okuda Y, Saijo M, Nishi R, Matsuda N, Chu G, Mori T, Iwai S, Tanaka K, Tanaka K, Hanaoka F (2005) UV-induced ubiquitylation of XPC protein mediated by UV-DDB-ubiquitin ligase complex. Cell 121: 387-400

Toledo LI, Altmeyer M, Rask MB, Lukas C, Larsen DH, Povlsen LK, Bekker-Jensen S, Mailand N, Bartek J, Lukas J (2013) ATR prohibits replication catastrophe by preventing global exhaustion of RPA. Cell 155: 1088-103

Tornaletti S, Reines D, Hanawalt PC (1999) Structural characterization of RNA polymerase II complexes arrested by a cyclobutane pyrimidine dimer in the transcribed strand of template DNA. J Biol Chem 274: 24124-30

van Leeuwen J, Pons C, Mellor JC, Yamaguchi TN, Friesen H, Koschwanez J, Usaj MM, Pechlaner M, Takar M, Usaj M, VanderSluis B, Andrusiak K, Bansal P, Baryshnikova A, Boone CE, Cao J, Cote A, Gebbia M, Horecka G, Horecka I et al. (2016) Exploring genetic suppression interactions on a global scale. Science 354

Vermeij WP, Dolle ME, Reiling E, Jaarsma D, Payan-Gomez C, Bombardieri CR, Wu H, Roks AJ, Botter SM, van der Eerden BC, Youssef SA, Kuiper RV, Nagarajah B, van Oostrom CT, Brandt RM, Barnhoorn S, Imholz S, Pennings JL, de Bruin A, Gyenis A et al. (2016) Restricted diet delays accelerated ageing and genomic stress in DNA-repair-deficient mice. Nature 537: 427-431

Vermeulen W, Fousteri M (2013) Mammalian transcription-coupled excision repair. Cold Spring Harb Perspect Biol 5: a012625

Vieira NM, Elvers I, Alexander MS, Moreira YB, Eran A, Gomes JP, Marshall JL, Karlsson EK, Verjovski-Almeida S, Lindblad-Toh K, Kunkel LM, Zatz M (2015) Jagged 1 Rescues the Duchenne Muscular Dystrophy Phenotype. Cell 163: 1204-13

Wang T, Birsoy K, Hughes NW, Krupczak KM, Post Y, Wei JJ, Lander ES, Sabatini DM (2015) Identification and characterization of essential genes in the human genome. Science 350: 1096-101

Wang Z, Yang X, Mazouzi A, Ramotar D (2014) The long N-terminus of the C. elegans DNA repair enzyme APN-1 targets the protein to the nucleus of a heterologous system. Gene 553: 151-7

Wiederhold L, Leppard JB, Kedar P, Karimi-Busheri F, Rasouli-Nia A, Weinfeld M, Tomkinson AE, Izumi T, Prasad R, Wilson SH, Mitra S, Hazra TK (2004) AP endonuclease-independent DNA base excision repair in human cells. Mol Cell 15: 209-20

Winter GE, Radic B, Mayor-Ruiz C, Blomen VA, Trefzer C, Kandasamy RK, Huber KV, Gridling M, Chen D, Klampfl T, Kralovics R, Kubicek S, Fernandez-Capetillo O, Brummelkamp TR, Superti-Furga G (2014) The solute carrier SLC35F2 enables YM155-mediated DNA damage toxicity. Nature chemical biology 10: 768-73

Wright WE, Sassoon DA, Lin VK (1989) Myogenin, a factor regulating myogenesis, has a domain homologous to MyoD. Cell 56: 607-17

Yakala GK (2014) Protein truncating variants of SLC30A8 reduce type 2 diabetes mellitus risk in humans. Clin Genet 86: 121-2

Yang Y, Geldmacher DS, Herrup K (2001) DNA replication precedes neuronal cell death in Alzheimer's disease. J Neurosci 21: 2661-8

Zeman MK, Cimprich KA (2014) Causes and consequences of replication stress. Nat Cell Biol 16: 2-9

Zhang T, Penicud K, Bruhn C, Loizou JI, Kanu N, Wang ZQ, Behrens A (2012) Competition between NBS1 and ATMIN controls ATM signaling pathway choice. Cell reports 2: 1498-504

CURRICULUM VITAE

Personal Data

Name:	Abdelghani Mazouzi
Date of birth:	26.01.1987
City of birth:	Bouandas, Algeria
Address:	Ce-M-M, Lazarettgasse 14 AKH BT 25.3, A 1090 Vienna
Telephone:	004366.02.85.75.13
E-Mail:	amazouzi@cemm.oeaw.ac.at
Current position: (since 2012)	PhD student at CeMM Research Center for Molecular Medicine of the Austrian Academy of Sciences

Dissertation / PhD Thesis

2012 - present: PhD student at CeMM Research Center for Molecular Medicine of the Austrian Academy of Sciences, Vienna, Austria.

Title of thesis: Identification of novel proteins required for the DNA damage response.

Education

Academic studies:

2009 - 2011: Master Research in Biochemistry and Structural Biology at the Joseph Fourier University (UJF) in Grenoble, France.

2005- 2009: Engineer in Bioengineering at the University of Science and Technology Houari Boumediene (USTHB) Algiers, Algeria.

2005: Bachelor in Natural and Life Sciences in high school Tahar El-ARGHIB in Bouandas, Algeria.

Internships:

2012: Internship at Research Center of Maisonneuve-Rosemont Hospital, Montreal, Canada.

Topic: DNA Repair and Genomic Stability in the Cellular Response to Anticancer Agents Laboratory.

2011: Master internship at the Gustave Roussy Institute of cancerology (IGR) in Villejuif, Paris, France

Topic: DNA Repair and Genomic Stability in the DNA Repair Laboratory.

2009: Internship in Biochemistry and Hormonology Laboratory of Pierre and Marie Curie Cancer Center (CPMC) in Algiers, Algeria.

Topic: Biochemistry and Endocrinology.

Fellowships

2015 - 2017: PhD fellowship (DOC-Stipendium) granted by the Austrian Academy of Sciences.

Publications and Conferences

Publications

- **Mazouzi A**., Moser, SC., Wiedner, M., Lardeau, CH., Ringler, A., Neesen J., Kubicek, S and Loizou JI. UV sensitivity and genomic instability due to defective nucleotide excision repair is alleviated by MUTYH loss. Molecular Cell. Submitted.

- Smida, M., Fece de la Cruz, F., Kerzendorfer C., Uras, IZ., Mair, B., **Mazouzi, A**, Suchankova T., Konopka, T., Katz, AM., Paz, K., Nagy-Bojarszky, K., Muellner, MK., Bago-Horvath, Z., Haura, EB., Loizou, JI., Nijman, SM (2016) MEK inhibitors block growth of lung tumours with mutations in ataxia-telangiectasia mutated. Nat Commun 7: 13701.

- **Mazouzi, A**., Stukalov, A., Müller, A., Wiedner, M., Chen,D., Prochazkova,J., Schuster,M., Breitwieser,FP., Chiang,C., Pichlmair,A., El-Khamisy,S., Bock,C, Kralovics,R., Colinge,J., Bennett, K and Loizou, JI. (2016) A Comprehensive Analysis of the Dynamic Response to Aphidicolin-Mediated Replication Stress Uncovers Targets for ATM and ATMIN. Cell Reports 15: 893-908.

- Prochazkova, J., Sakaguchi, S., Owusu, M., **Mazouzi, A**., Wiedner, M., Velimezi, G., Moder, M., Turchinovich, G., Hladik, A., Gurnhofer, E., et al. (2015). DNA Repair Cofactors ATMIN and NBS1 Are Required to Suppress T Cell Activation. PLoS genetics 11, e1005645.

- **Mazouzi, A**., Velimezi, G., and Loizou, J.I. (2014). DNA replication stress: causes, resolution and disease. Experimental cell research 329, 85-93.

- Wang, Z., Ayoub, E., **Mazouzi, A**., Grin, I., Ishchenko, A.A., Fan, J., Yang, X., Harihar, T., Saparbaev, M., and Ramotar, D. (2014a). Functional variants of human APE1 rescue the DNA repair defects of the yeast AP endonuclease/3'-diesterase-deficient strain. DNA repair 22, 53-66.

- Wang, Z., Yang, X., **Mazouzi, A**., and Ramotar, D. (2014b). The long N-terminus of the C. elegans DNA repair enzyme APN-1 targets the protein to the nucleus of a heterologous system. Gene 553, 151-157.

- **Mazouzi, A**., Vigouroux, A., Aikeshev, B., Brooks, P.J., Saparbaev, M.K., Morera, S., and Ishchenko, A.A. (2013). Insight into mechanisms of 3'-5' exonuclease activity and removal of bulky 8,5'-cyclopurine adducts by apurinic/apyrimidinic endonucleases. PNAS.110, E3071-3080.

- Redrejo-Rodriguez, M., Saint-Pierre, C., Couve, S., **Mazouzi, A**., Ishchenko, A.A., Gasparutto, D., and Saparbaev, M. (2011). New insights in the removal of the hydantoins, oxidation product of pyrimidines, via the base excision and nucleotide incision repair pathways. PLoS One 6, e21039.

Conferences

- 10th Quinquennial Conference on Responses to DNA damage: from molecule to disease. Egmond aan Zee, The Netherlands (17-22/04/2016, poster presentation).
- PTMs in Cell Signaling of Copenhagen Bioscience Conferences. Copenhagen, Denmark (14-17/09/2014, poster presentation).
- 9th YSA PhD Symposium of the Medical University of Vienna (MUV). Vienna, Austria (19-20/06/2013, poster presentation).
- PTMs in Cell Signaling of Copenhagen Bioscience Conferences. Copenhagen, Denmark (3-5/12/2012, poster presentation).
- 19e Journée de la recherche at research Center of Maisonneuve-Rosemont Hospital, Montreal, Canada (22/06/2012, poster presentation)
- The annuel Meeting in the leading European Cancer Center Gustave Roussy Institute of cancerology (IGR) in Villejuif, Paris, France (07/05/2011, oral presentation).

Lab experience

Biochemistry, Molecular and Cell Biology Techniques:

Western blotting, immunoprecipitation (IP), TAP/MS (Tandem Affinity Purification coupled with Mass Spectrometry), cell culture, immunoflerescence and confocal microscopy, PCR, RT-PCR, Q-PCR, enzymatic tests in vitro (DNA radioactive labeling), ChIP seq (Chromatin Immunoprecipitation assay coupled with NGS), gene editing (siRNA, shRNA, CRISPR), FACS analysis, global phospho-proteomics (pS,T and Y), RNA seq.

High throughput screening:

Haploid genetic screens (insertional mutagenesis), Whole-genome CRISPR screens (loss of function), drug screens.

Computer skills:

Standard and specialized software for analyzing, presenting experimental and quantitative data and scientific graphic design and animation (R, run commands in Terminal and LINUX, CellProfiler, Statistica, Photoshop, Adobe illustrator, ImageQuant, Image J, CorelDraw, Cytoscape, yEd, GraphPad Prism, ChemSketch).

Teaching and supervision:

Supervision of an undergraduate student.

Languages

Berber: mother tongue
French: fluent
Arabic: fluent
English: fluent
German: beginner